AD_____

Award Number: W81XWH-07-1-0281

TITLE: Cell Therapy to Obtain Spinal Fusion

PRINCIPAL INVESTIGATOR:
Principal Investigator: Elizabeth A. Olmsted-Davis, Ph.D.
Co-Investigators: Alan R. Davis, Ph.D., Michael Heggeness, M.D., Ph.D., Francis Gannon M.D., Ronke Olabisi Ph.D., and Jennifer West, Ph.D.

CONTRACTING ORGANIZATION:
Baylor College of Medicine
Houston, Texas 77030

REPORT DATE: July, 2010

TYPE OF REPORT: Annual

PREPARED FOR: U.S. Army Medical Research and Materiel Command
Fort Detrick, Maryland 21702-5012

DISTRIBUTION STATEMENT:

x Approved for public release; distribution unlimited

REPORT DOCUMENTATION PAGE

Form Approved
OMB No. 0704-0188

1. REPORT DATE *(DD-MM-YYYY)*	2. REPORT	3. DATES COVERED *(From - To)*
01-07-*2010*	Annual	1 JUL 2009 - 30 JUN 2010

4. TITLE AND SUBTITLE

Cell Therapy to Obtain Spinal Fusion

5a. CONTRACT NUMBER

5b. GRANT NUMBER
W81XWH-07-1-0281

5c. PROGRAM ELEMENT NUMBER

6. AUTHOR(S)
Elizabeth A. Olmsted-Davis, Ph.D., Alan R. Davis, Ph.D, Michael Heggeness

Jennifer West, Ph.D., Ronke Olabisi Ph.D, John Hipp, Ph.D, ZaWaunyka Lazard. edavis@bcm.tmc.edu

5d. PROJECT NUMBER

5e. TASK NUMBER

5f. WORK UNIT NUMBE

7. PERFORMING ORGANIZATION NAME(S) AND ADDRESS(ES)

Baylor College of Medicine

Houston, Texas 77030

8. PERFORMING ORGANIZATION REPORT NUMBER

9. SPONSORING / MONITORING AGENCY NAME(S) AND ADDRESS(ES)

US ARMY MEDICAL RESEARCH AND MATERIEL COMMAND
504 SCOTT STREET
FORT DETRICK, MD 21702-5012

10. SPONSOR/MONITOR'S ACRONYM(S)

11. SPONSOR/MONITOR'S REPORT NUMBER(S)

12. DISTRIBUTION / AVAILABILITY STATEMENT

Approved for public release; distribution unlimited

13. SUPPLEMENTARY NOTES

14. ABSTRACT

Surgery of the spine to fuse the vertebral bones is one of the most commonly performed operations with an estimated 350,000 Americans undergoing this surgery annually with estimated costs of $60 billion. Current procedures are highly invasive with limited success. The goal of this study is to develop a safe efficacious system for inducing spine fusion which will eliminate the need for invasive surgery. We have currently developed a cell based gene therapy system that can induce rapid bone formation at a targeted location which is independent of immune status of the model. This system relies on adenovirus transduced cells expressing bone morphogenetic protein 2 to induce bone formation leading to vertebral fusion after delivery into the paraspinous musculature. To prolong cell survival and insure cells are maintained at the target site, we have encapsulated them in a non-degradable hydrogel material. This provides additional safety by eliminating direct injection of the virus through cell delivery, and prevention of cell diffusion, through encapsulation. Here we provide preliminary data; demonstrating spine fusion using this system at 6 weeks after induction. This is the first step in demonstrating efficacy, a critical component of preclinical testing. Thus with validation of our hypothesis, this approach can now be developed as a safe and efficacious gene therapy system for spine fusion, thus circumventing the need for costly invasive surgery.

15. SUBJECT TERMS
BMP2, Spine fusion, Hydrogel, Gene Therapy, Adenovirus.

16. SECURITY CLASSIFICATION OF:			17. LIMITATION OF ABSTRACT	18. NUMBER OF PAGES	19a. NAME OF RESPONSIBLE PERSON
a. REPORT	b. ABSTRACT	c. THIS PAGE			USAMRMC
U	U	U	UU	140	19b. TELEPHONE NUMBER *(include area code)*

Table of Contents

Introduction: Surgery of the spine to fuse the vertebral bones is one of the most commonly performed operations with some 400,000 Americans undergoing this type of surgery annually in the United States. The estimated cost associated with such procedures exceeding $60 billion annually demonstrating this to be a significant problem. In the most common form, posterolateral fusion, the paraspinous musculature is stripped and the bone decorticated, resulting in significant pain, reduced stability afforded by these muscles, and disruption of the blood supply to both bone and muscle. Further, success rates for fusion range from 50-70% depending on how many levels are fused and the number and types of attendant complications. We recently demonstrated that transduced cells expressing high levels of bone morphogenetic protein 2 (BMP2) in skeletal muscle could rapidly recruit and expand endogenous cell populations to initiate all stages of endochondral bone formation, with mineralized bone forming within one week of implantation. The central hypothesis of this application is that posterolateral spine fusion can be successfully achieved with only minimally invasive percutaneous techniques and without a scaffold, by collecting cells from patient's, transducing them to express BMP2, encapsulating the cells with hydrogel material, and then delivering them to the fusion site. If added structural stability is required, the injectable hydrogel will be crosslinked *in vivo* with a small fiber-optic light source. Successful completion of this project would advance the current state of gene therapy in this field by eliminating the search for an optimal osteoprogenitor cell and scaffolding.

Body: The central hypothesis of this application is that posterolateral spine fusion can be successfully achieved with a novel and simple minimally invasive percutaneous technique. We propose that this can be done by transducing human fibroblasts to express an osteoinductive factor (bone morphogenetic protein 2 or BMP2), encapsulating the cells with hydrogel material, and then delivering them to the fusion site. This injectable material will be a liquid, but once in place can be crosslinked with a small fiber-optic light source. We have developed three specific tasks to accomplish our goals.

*** The experiments highlighted in blue are still being conducted as described in the original application, however, these were in overlap with another application and therefore no funds from this award were used or will be used for their completion.**

Task 1: *To determine the optimal levels of BMP2 for efficient rapid production of endochondral bone from human bone marrow mesenchymal stem cells (hBM-MSCs) transduced with a tetracycline regulated Ad5F35tet-BMP2 adenovirus carrying a red luciferase reporter gene.*

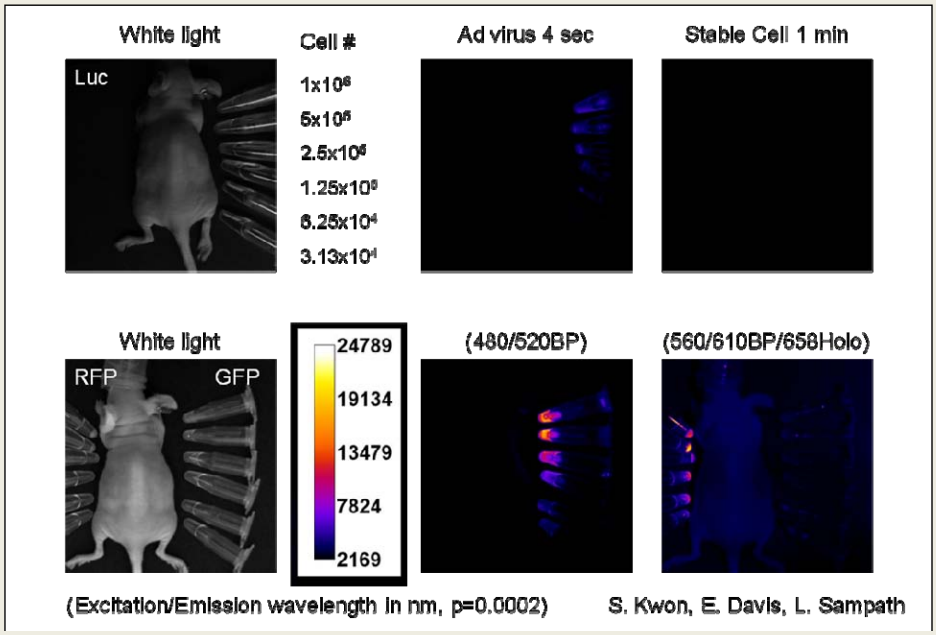

Figure 1: Detection of a red luciferase reporter in live animal imaging. Expression of a red shifted luciferase reporter was compared both in cells, and in live animals after subcutaneous intramuscular injection.Two types of cells were tested, one which was a cell line that had the reporter stably integrated, and the other cells which had been transduced with an AdCRBluc virus.

a. To determine if sustained expression of BMP2 is more efficient at inducing rapid bone formation than a pulse of expression using the tetracycline regulated vectors. **(Months 0-12)**

Comparison studies were performed to determine the optimal method for tracking transgene expression *in vivo*. As seen in figure 1, the originally described methodology using red luciferase reporter gene expression was compared to other red-shifted reporters to determine if we could obtain

something more sensitive which would allow us to image the expression of the transgene during bone formation. In original experiments using luciferase (figure 1) we were unable to readily detect the reporter after intramuscular injection of our transduced cells at the levels routinely used for induction of bone formation. However, as seen in figure 2, when this was compared to dsRED, a red fluorescent protein, we could readily detect dsRED. Therefore we initiated studies using dsRED in place of the red luciferase.

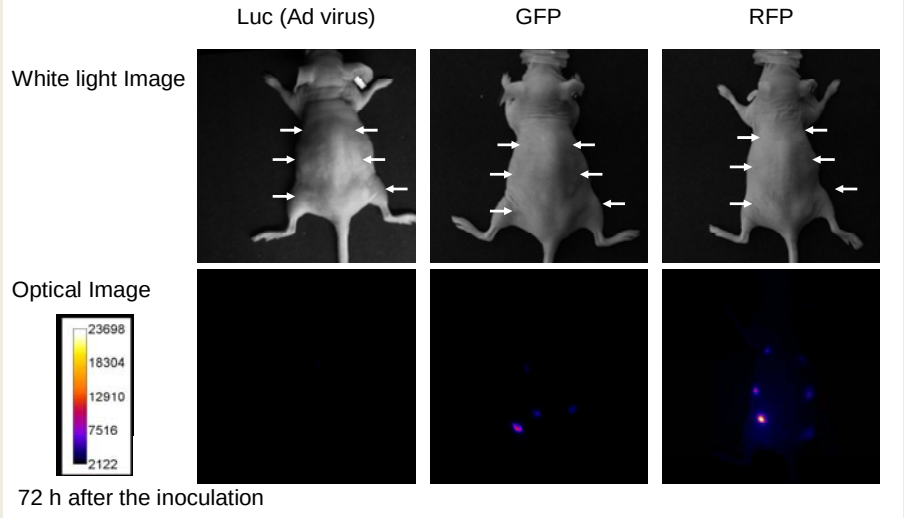

Figure 2: Comparison of reporter expression after intramuscular injection of dsRED, GFP, and CRBluc in live animals, through optical imaging.

In these studies, cells were transduced with Ad5dsRED (2500 vp/cell) and were encapsulated into microbead structures using PEGDA hydrogel (nondegradable). The microbeads were then injected into the hindlimbs of the animal, and transgene expression compared to animals receiving the same Ad5dsRED transduced cells which have not been encapsulated.

Two days after the initial injection of cells, dsRED expression was readily detected whether cells were encapsulated or not and in no cases were cells or microspheres detected migrating from the injection site (Figure 3A). The dsRED expression, as measured by fluorescence intensity at 590 ± 10 nm, was significantly elevated in microencapsulated Ad5dsRED-transduced cells compared to other groups (Figure 3B). Microencapsulated control cells transduced with AdEmpty cassette had no fluorescent signal at 590 ± 10 nm, demonstrating that neither the cells nor the PEGDA were autofluorescing. Fluorescent intensity in animals receiving Ad5dsRED-transduced cells directly injected was substantially reduced after seven days and was indistinguishable from control. In microencapsulated Ad5dsRED-transduced cells, this 590 ± 10 nm dsRED fluorescent signal was significantly elevated over that of microencapsulated control cells for 15 days (Figure 3B). After 15 days, these levels dropped; however, signal was still detectable (Figure 3A, arrows) in some animals, suggesting that the microencapsulated cells remained viable to express the dsRED transgene. Statistical power to detect intensity over control ranged from 100% in microencapsulated cells to 99.7% in directly injected cells, and power to detect the difference between microencapsulated and unencapsulated cells was 88%.

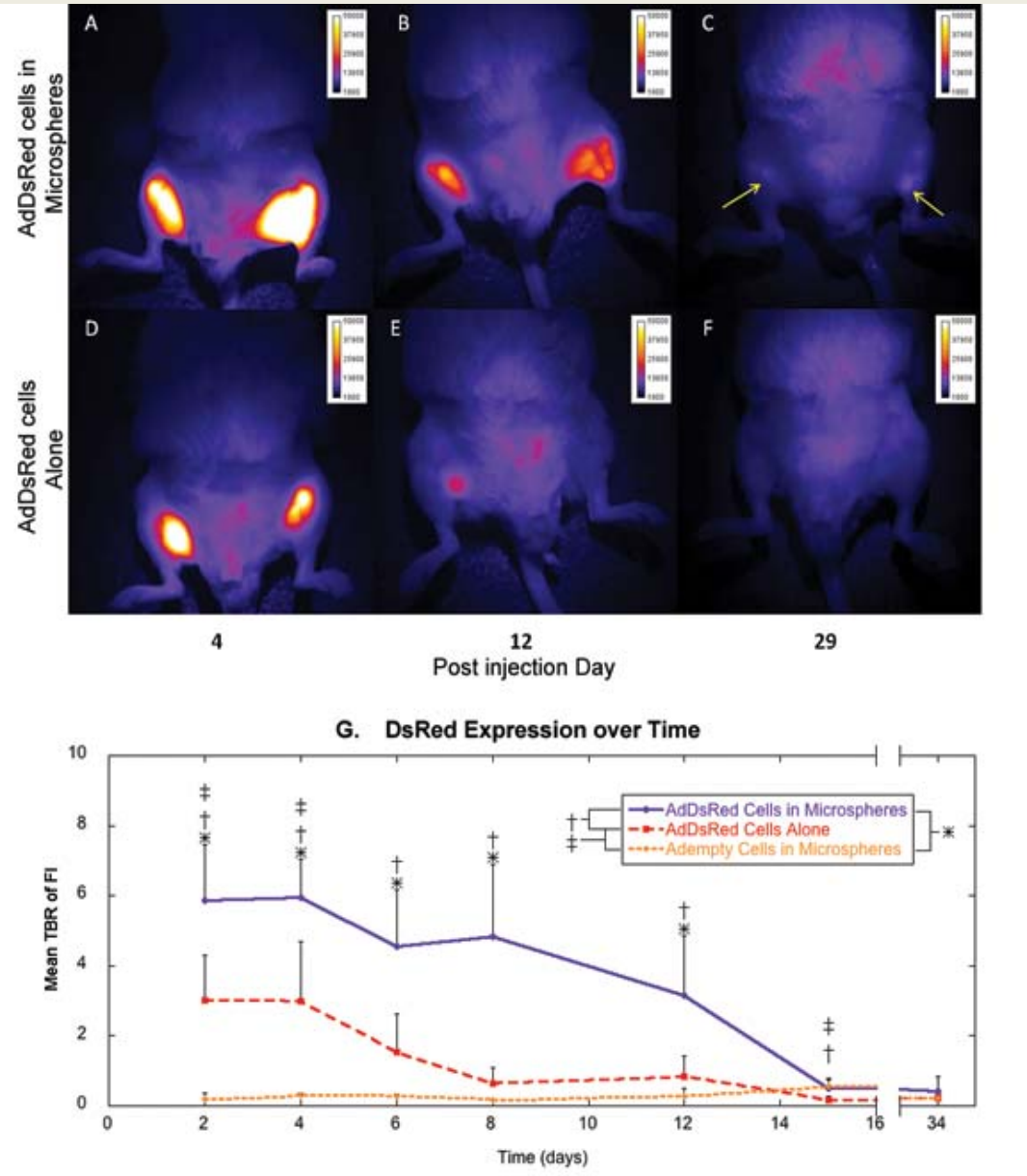

Figure 3: Optical fluorescence imaging of mice injected with cells expressing dsRed. Top panels (A through C) are images of a representative mouse (n=4) injected with dsRed-expressing cells encapsulated in microspheres and bottom panels (D through F) are of a mouse injected with dsRed-expressing cells directly, without microspheres. The images were taken at day 4, 12 and 29 post-injection of cells. By day 29, the fluorescent signal is at background levels or undetectable for the mouse given dsRed-expressing cells without microspheres (F). Whereas, the signal remains detectable in the mouse given dsRed-expressing cells encapsulated in microspheres (C).
G. Mean Target-to-Background Ratio (TBR) of Fluorescence Intensity (FI) in mice given unencapsulated dsRed cells, microencapsulated dsRed cells or microencapsulated control cells. * $p \leq 0.05$ for microencapsulated dsRed cells versus microencapsulated control cells; † $p \leq 0.05$ for microencapsulated dsRed cells versus unencapsulated dsRed cells; ‡ $p \leq 0.05$ for unencapsulated dsRed cells versus microencapsulated control cells.

b. To determine the optimal expression time of BMP2 from cells embedded in hydrogel for the production of rapid bone formation. **(Months 9-12)**

We next set up similar experiments to track the dsRED in live animals during heterotopic ossification. In these experiments, we transduced the cells with an Ad5BMP2-dsRED virus, which was not tetracycline regulated. In these studies we look at the ability to detect the signal through the bone matrix that is forming. As seen in figure 4, dsRED could readily be detected above background for up to 16 days. Interestingly, the cells directly injected appeared to be readily detected, and stronger than the cells within the microbeads. Both the microbeads and directly injected cells were tracked up to 16 days, again which is odd, considering all previous experiments appeared to remove the cells rapdily after 6 -8 days. The data does suggest that we can track the reporter even in the presence of bone formation. Further, the signal is stronger in the directly injected cells, mist likely because the microbeads, and bone itself that is forming, shield the signal as compared to the directly injected cells that are not necessarily encapsulated within the bone. Further, the bone formation as determined by microCT was not as robust in the samples receiving the cells directly, thus less shield would also occur. The results suggest that we can somewhat follow the input cells within the newly forming bone. We are currently working on continuing these experiments with the regulated vector. However, it is highly unlikely that reducing the expression of BMP2 would provide a benefit to bone formation. Alternatively, we have data that suggests that the enhanced BMP2 expression does not appear to greatly enhance the bone formation either. **We are currently working on completing this aim and the first publication of this work, has been accepted in Tissue Engineering.**

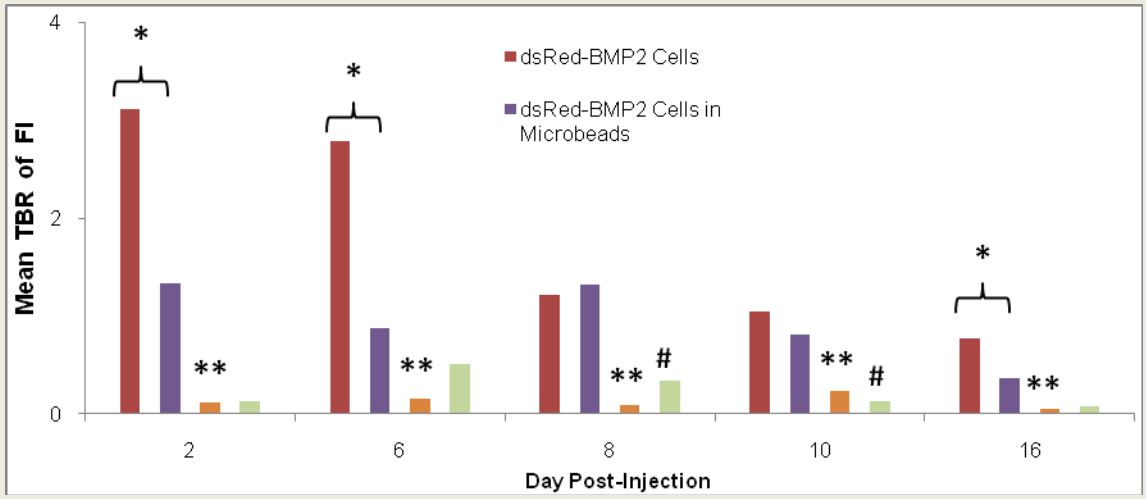

Figure 4: Mean Target-to-Background Ratio (TBR) of Fluorescence Intensity (FI) in mice given unencapsulated dsRed cells, microencapsulated dsRed cells or microencapsulated control cells.
*P < 0.05 for Ad5dsRED-BMP2 transduced cells versus Ad5dsRED-BMP2 cells in microbeads at days 2, 6, and 16 post-injection.
**P < 0.05 for Ad5dsRED-BMP2 cells transduced cells versus Ad5dsRED-BMP2 cells in microbeads at all time points.
# P < 0.05 for dsRED-BMP2 cells in microbeads versus Ad5empty cassette transduced cells (Control) in microbeads at days 8 and 10 after injection.

b. To demonstrate spine fusion using Ad5F35tet-BMP2 transduced cells encapsulated in hydrogel can effectively lead to spine fusion **(Months 0-12).**

We have been working on spine fusion in the mice using the directly injected cells (see task 3 and appendix). **This work is completed for mice.** We are now focused on completing fusion studies with the microspheres, and we have been focused on both mouse and rat. We have noted that genetic inbreeding within the mice makes them somewhat unique from other eukaryotes. Cells isolated from any animal of a specific strain, will function as autologous in the mice, whereas in rats, only cells from the animal itself can be used as autologous, all other cells including those from a littermate will be rejected. Thus it is a more representative model, which is why we are testing the materials in this model as well. See task 3 for details.

c. To demonstrate regulated expression of BMP2 in spine fusion studies using an Ad5F35tet-BMP2-IRESCBRLuc vector in which expression can be tracked through live animal imaging. **(Months 12-24)**

We have not been tracking transgene expression through spine fusion, because the resultant bone formation appears to start to shield the signal after a few days, further, there appears to be no benefit to terminating the expression early in the process. Finally we are able to track the bone so readily that there is no additional

optimization at this point that we can make from tracking the expression. We also have a caspase system available that can not only shut down expression of the transgene but it actually send the cells into apoptosis, so that at times when the materials start to degrade we can effectively kill off any viable cells. Since the caspase can be turned on, by delivery of a small molecule; degradation of the cells, can be timed to occur with bone formation and removal of the hydrogel materials.

d. To track the BMP2 delivery cells *in vivo* during spine fusion by following the luciferase expression via live animal imaging. **(Months 24-48). See above section.**

Task 2: To design an optimal hydrogel material that will rapidly promote endochondral bone formation and be capable of removal through bone remodeling processes. In addition to BMP2 transduced cells, we propose to include peptides essential to the recruitment and migration of osteoprogenitors for bone and cartilage. Selective protease sites will also be introduced into the hydrogel to allow for osteoclast selective degradation during bone remodeling. We propose to do this by incorporation of calcium into the material and inclusion of cathepsin K protease cleavage sites into the material. Inclusion of these factors in the hydrogel will provide a mechanism for removal of the hydrogel once bone has formed by using the normal bone remodeling process.

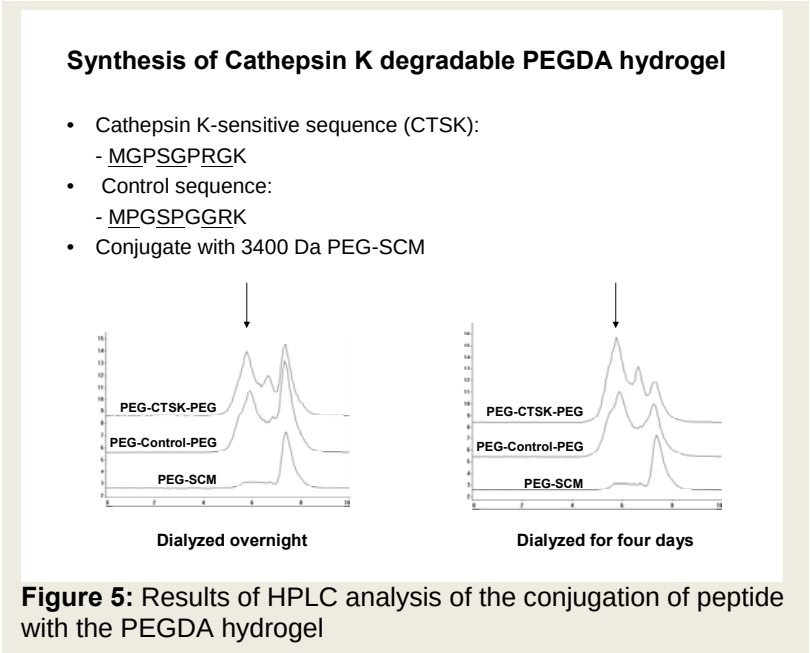

Figure 5: Results of HPLC analysis of the conjugation of peptide with the PEGDA hydrogel

a. Optimize and develop a hydrogel that can be specifically degraded by osteoclasts. **(Months 0-24)**

We have synthesized the peptide MGPSGPRG (Gowen et a;1999) using a 431A solid-phase peptide synthesizer (Applied Biosystems, Foster City, CA). In order to make degradable PEG, we start with PEG-DA-SMC (succinimidyl carbonate). The PEG-SMC is conjugated with our peptide in order to get PEG-PEPTIDE-PEG. So, we expect to obtain three peaks representing the completely conjugated product: PEG-PEPIDE-PEG, incompletely conjugated product: PEG-PEPTIDE and unconjugated product: PEG-SMC (Figure 5). We have run GPC tests on it and the results indicate that there is still unconjugated PEG, ie: we have PEG-Peptide or free PEG in the preparations. We have tried changing the ratio of peptide to PEG, changing the length of conjugation time, increasing the pore size of the dialysis membrane and changing the length we dialyze the conjugation products. These have led to a higher concentration of PEG-PEPTIDE-PEG as indicated by the GPC results (Figure 5). We have cathepsin K (Calbiochem; Cathepsin K, His•Tag®, Human, Recombinant, *E. coli*). Degradation tests have found that the material did not degrade as expected. Analysis of the materials suggested that the protease site may be too confined to actually bind enzyme for digestion, thus, the protease site was redesigned to have a longer amino acid sequence linker to allow for better digestion. Thus the modified peptide sequence is GGGMGPSGPWGGK, see figure 6.

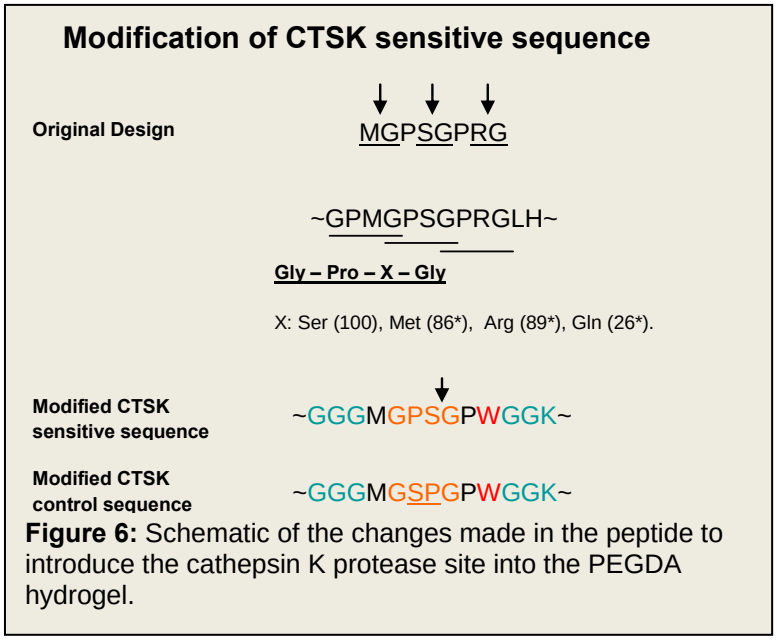

Figure 6: Schematic of the changes made in the peptide to introduce the cathepsin K protease site into the PEGDA hydrogel.

We next examined the ability of the cathespin K sensitive hydrogels to dergade in the presence of the enzyme. The hydrogels with the cathepsin K sensitive peptide GGGMGPSGPWGGK were designed to carry a cathepsin K sensitive cleavage site between serine and proline [25]. Proteinase K was used as a positive control. While the gel degrades, the peptide that was incorporated into the hydrogel structure will be cleaved by enzymes and gradually release into solution. The degradation profiles of GPSG hydrogels were measured by monitoring the concentration change of tryptophan in solution at UV absorbance of 280 nm. Crosslinkable GPSG hydrogels were polymerized in microcuvettes and incubated with enzyme solutions. After equilibilium swelling in TBS overnight, hydrogels were treated with different enzymes to evaluate the degradation profiles (Figure 7). After incubation with different enzyme solutions for 24 hours, hydrogels in cathepsin K and proteinase K solutions has similar degradation profiles, both indicating a rapid tryptophan concentration increase within the first hour and reaching about 80% release of total tryptophan at 24 hours. No degradation was observed when hydrogels were incubated in TBS buffer, NaOAc buffer, and plasmin. Hydrogels incubated in nonspecific collagenase I and collagenase III solutions also released 40% of incorporated tryptophan after a 24 hour incubation (figure 7).

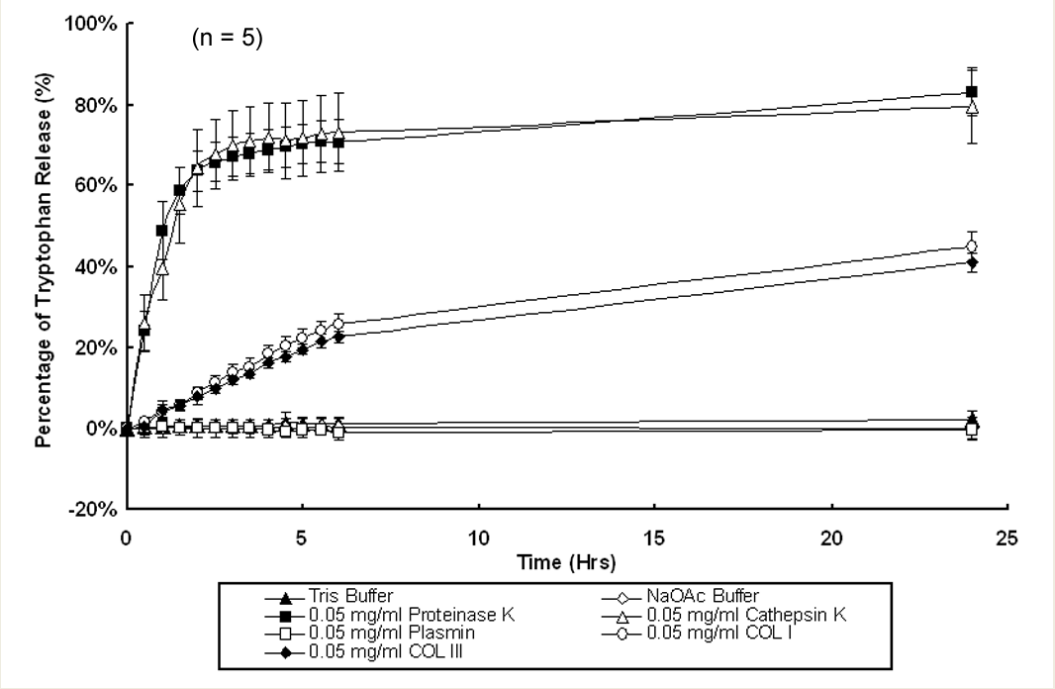

Figure 7: Degradation profiles of cathepsin K-sensitive GPSG hydrogels. Hydrogel droplets (3 µl) were polymerized in each micro-cuvette and swelled overnight with 250 µl of TBS buffer. Each hydrogel was incubated in buffer or enzyme solution at 0.05 mg/ml at 37^{O}C. UV absorbance at 280 nm was measured over 24 hours to monitor tryptophan release corresponding to the degradation of the GPSP hydrogels.

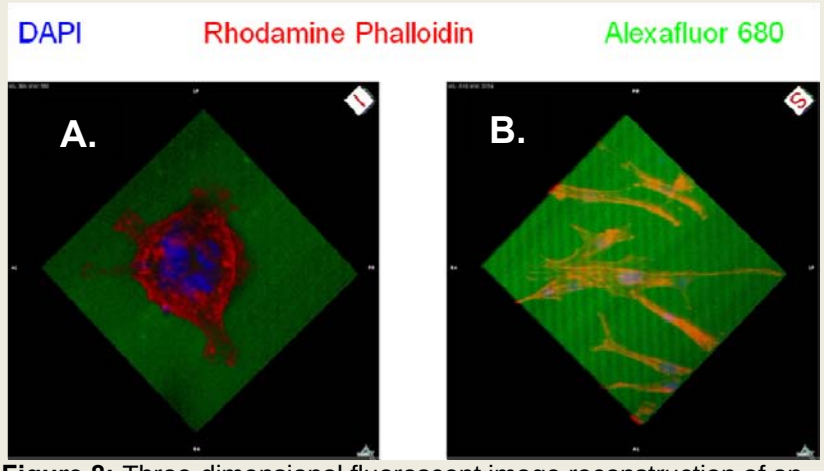

Figure 8: Three-dimensional fluorescent image reconstruction of an active osteoclast on the GPSG hydrogel surface. The GPSG hydrogel was labeled with Alexafluor 680 fluorophore (green), which is conjugated with the acryloyl-PEG-RGDS and incorporated into the hydrogel by photo-polymerization. The cells were fixed and permeabilized before staining the nuclei with DAPI (blue) and F-actin by rhodamine phalloidin (red) 48 hours after seeding. (A) Composed z-stack images of the osteoclast on hydrogel. (B) Composed z-stack images of osteoblasts on hydrogel. Osteoblasts did not appear to leave any pits.

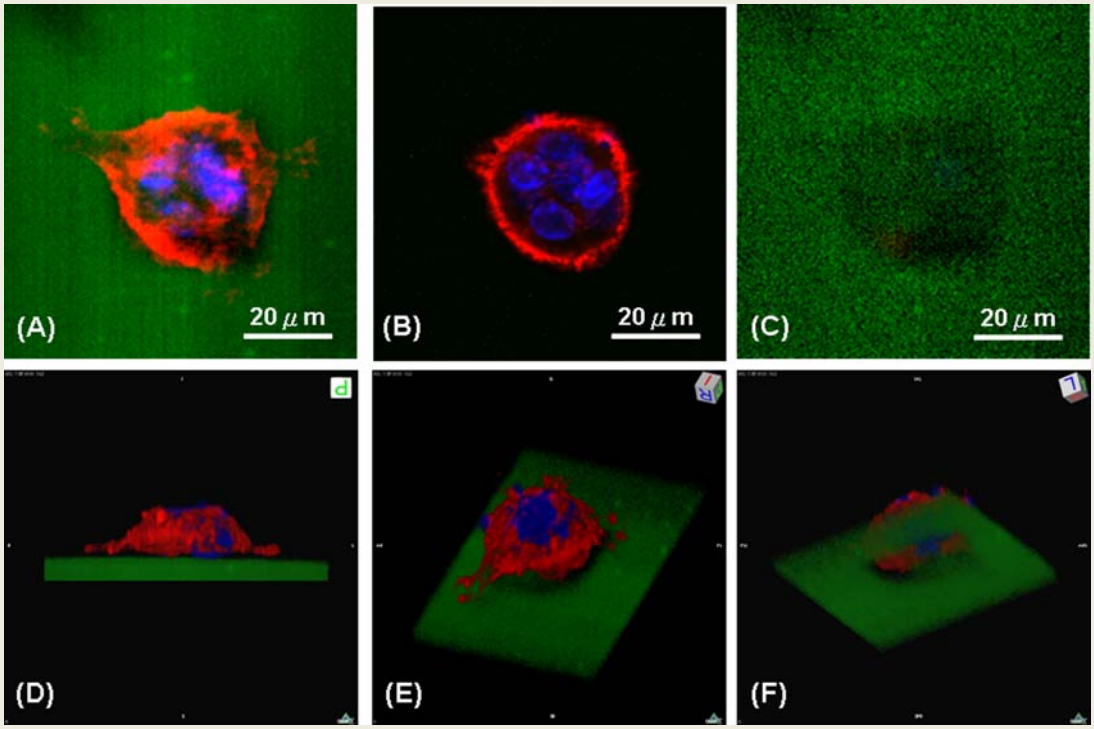

Figure 9: Three-dimensional fluorescent image reconstruction of an active osteoclast on the GPSG hydrogel surface. The GPSG hydrogel was labeled with Alexafluor 680 fluorophore (green), which is conjugated with the acryloyl-PEG-RGDS and incorporated into the hydrogel by photo-polymerization. The cells were fixed and permeabilized before staining the nuclei with DAPI (blue) and F-actin by rhodamine phalloidin (red) 48 hours after seeding. (A) Composed z-stack images of the osteoclast and hydrogel. (B) Sealing ring and multiple nuclei of the osteoclast. (C) GPSG hydrogel with fluorescent signal lost at middle. Z-stack Images were reconstructed using the volume renderings algorithm and presented from (D) side view, (E) orthogonal view from above, and (F) from bottom. The resorption site is located underneath the osteoclast, which was can be observed in the loss of the fluorescent intensity of Alexafluor 680. The resorption pit on the hydrogel surface can be clearly seen from different angles, suggesting that the GPSG hydrogel has been degraded by cathepsin K secreted by osteoclasts.

We next tested the degradable hydrogel to determine if it could be selectively degraded by osteoclasts. Raw 264.7 cells were differentiated in culture medium containing 30 ng/ml RANKL for 4 days. Cells collected through gradient centrifugation and placed in culture where they were enzymatically stained for tartrate acid phosphatase activity (TRAP). Multinucleated cells in the culture appeared to stain positive for TRAP suggesting that they had ungoing osteoclast differentiaiton. The majority of cells at the bottom fraction of the gradient contained the TRAP+ dRAW 264.7 osteoclasts were then used for hydrogel degradation studies. To demonstrate the ability of the cells to both adhere to the hydrogel material so a normal substrate for growth, as well as have the selectivity in degradation, we next plated both primary osteoblasts and the TRAP+ dRAW264.7 osteoclasts onto GPSG hydrogel sheets containing the RGD binding sites which were preformed, to provide a smooth surface to ensure they do not possess imperfections other than those introduced by degradation from the cell populations.

As can be seen in figure 8, both cell types readily adhered to the material, and formed normal cell structures observed in tissue culture. The degradable or GPSG hydrogels possessing Alexafluor 680 (green color) were fixed and stained with DAPI (blue color) for nuclei and rhodamine (red color) phalloidin for F-actin in the cytoplasm. As can be seen in figure 8 and 9, observed on hydrogel surface were actual resorption pits generated by RAW264.7 osteoclasts which were absent on the GPSG hydrogels which had been seeded with osteoblasts. Hydrogels-osteoclasts interactions were examined under confocal microscopy at higher magnification. Multinuclear and polarized cells RAW264.7 osteoclasts were identified on the hydrogel surface, (Figure 9A). A sealing ring of F-actin and multiple nuclei were clearly observed (Figure 9B). On the hydrogel surface where the osteoclast was located, a decrease in the fluorescent signal was observed (Figure 9C). The z-stack images were then examined closely by three-dimensional reconstructions using a volume rendering method. Figure 9D is the side view, showing the osteoclast attached to the hydrogel. From the three-dimensional perspective of the image from the top (Figure 9E) and bottom (Figure 9F) of the hydrogel, the loss in fluorescent signal of the hydrogel reveals a hole in the hydrogel through which the cell can be seen. This signal loss is indicative of activity by the differentiated RAW264.7 osteoclasts, degrading the underlying

hydrogel and creating a pit, resulting in the fluorescent intensity loss. No signal loss was observed on the gels seeded with dMC3T3-E1 cells. Therefore it appears that the osteoclasts may be selectively able to remodel the hydrogel material as predicted.

We next tested the material *in vivo* to determine if we observed degradation, and replacement of the microspheres with bone. We injected the microspheres, and then approximately 3 weeks after injection harvested the tissues, processed, and sectioned through the newly formed heterotopic ossification to detect the microspheres. Figure 10 shows a representative photomicrograph of a hematoxylin and eosin stained section of heterotopic bone and bone marrow. Intact microspheres can be detected within this section; however, there are also microspheres within the maturing bone that appear to be degrading. Further, the yellow rectangle encompasses a region which appears to be newly formed heterotopic bone, in the shape of a microsphere, suggesting that the removal of that material may be complete at this time. We are currently completing this *in vivo* analysis for

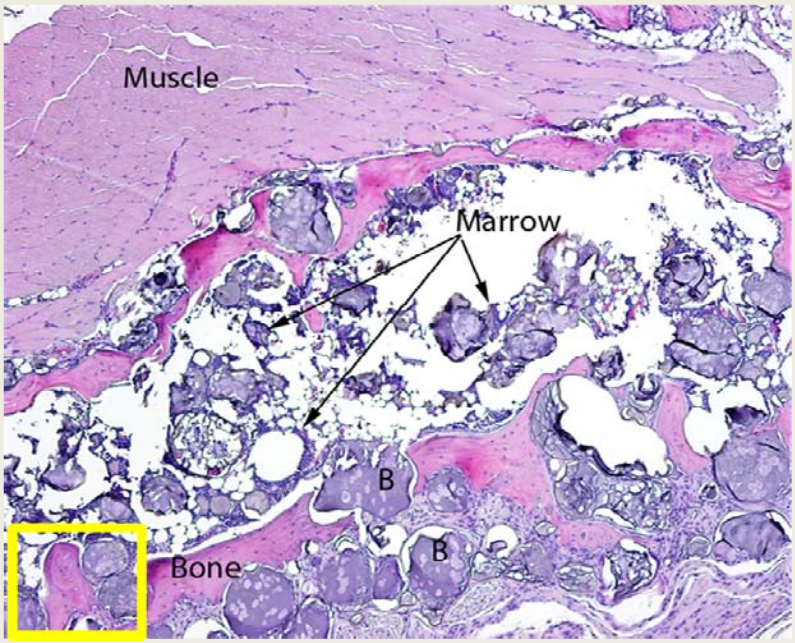

Figure 10: Photomicrograph of a hematoxylin and eosin stained tissue section depicting the degradation of the microbeads *in vivo.*

b. *Engineer cellular binding sights within the hydrogel to determine if this improves, cell viability of the transduced cells, and in turn BMP2 expression, and to tentatively enhance the migration of mesenchmyal stem cells to the sight of bone formation.* **(Months 24-36)**

We have introduced RGD binding sites within and throughout the hydrogel to enhance binding of the osteoclasts (see above section) as well as other cell migration. This has been very effective in allowing cells to bind to the material, during bone formation. Additionally, inclusion of the RGD binding sites within the material has appeared to greatly enhance cell viability, allowing for the cells to remain viable. However, the most optimal improvement for BMP2 expression and cell viability has come from altering the structures to be microspheres, rather than larger beads (Bikram ***et al***). Comparison of the BMP2 secretion from larger hydrogel structures to the microbead structures, showed a significant improvement. Figure 11 shows the BMP2 expression from larger bead structures, in comparison to the cells which were not encapsulated (Plated cells). As seen in Figure 11, the BMP2 expression is reduced by 50% in culture supernatants isolated from the encapsulated cells within the bead structures, as compared to the plated cells.

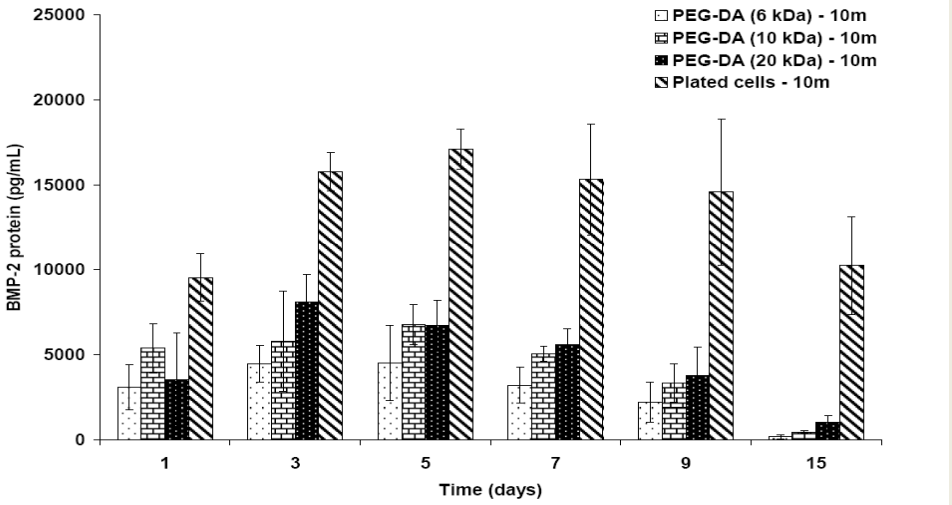

Figure 11: Western blot analysis for the detection of secreted BMP-2 protein. (a) Human recombinant BMP2 (lane 1), conditioned medium from PEG-DA (10 kDa) hydrogels only (lane 2), conditioned medium from 10 million MRC-5 cells encapsulated within PEGDA (10 kDa) hydrogels (lanes 3 and 4), conditioned medium from 10 million transduced fibroblasts control (lanes 5–8), human recombinant BMP-2 (lane 9), conditioned medium containing secreted BMP-2 protein from 10 million transduced fibroblasts encapsulated within PEG-DA (10 kDa) hydrogels (lanes 10–17). (b) Alkaline phosphatase activity in W20-17 cells without the addition of conditioned medium (W20-17) and after addition of conditioned media from PEG-DA (10 kDa) hydrogels with 10 million transduced fibroblasts and control plated transduced fibroblasts (Days 1–15). Data reported as mean ± SD, n = 5.

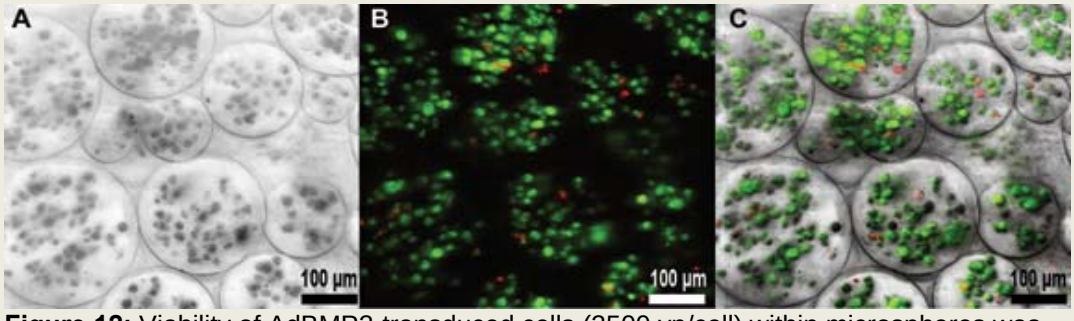

Figure 12: Viability of AdBMP2-transduced cells (2500 vp/cell) within microspheres was assessed at day 7 using a LIVE/DEAD® Viability/Cytotoxicity Kit for mammalian cells (Invitrogen, Molecular Probes, Eugene, OR). **A.** Minimum intensity projection of a differential interference contrast (DIC) Z-stack. **B.** Maximum intensity projection of fluorescent Z-stack merge of red and green channels. The red channel was thresholded to eliminate diffuse virus staining. Dead cells appear red and live cells appear green. **C.** Overlay of panels A and B. Living cells accounted for 95.08% ± 0.47% of total cells encapsulated.

We chose to next re-engineer the encapsulated structures, into microspheres, which hold between 0-100 cells. As seen in figure 12, within the microspheres, live cells converted the non-fluorescent calcein AM into green fluorescent calcein while ethidium homodimer freely passed through the permeable membranes of dead cells to bind the DNA and fluoresce red. Encapsulated cells showed high viability 95 ± 0.5 %, suggesting that they were not adversely affected by the microencapsulation process.

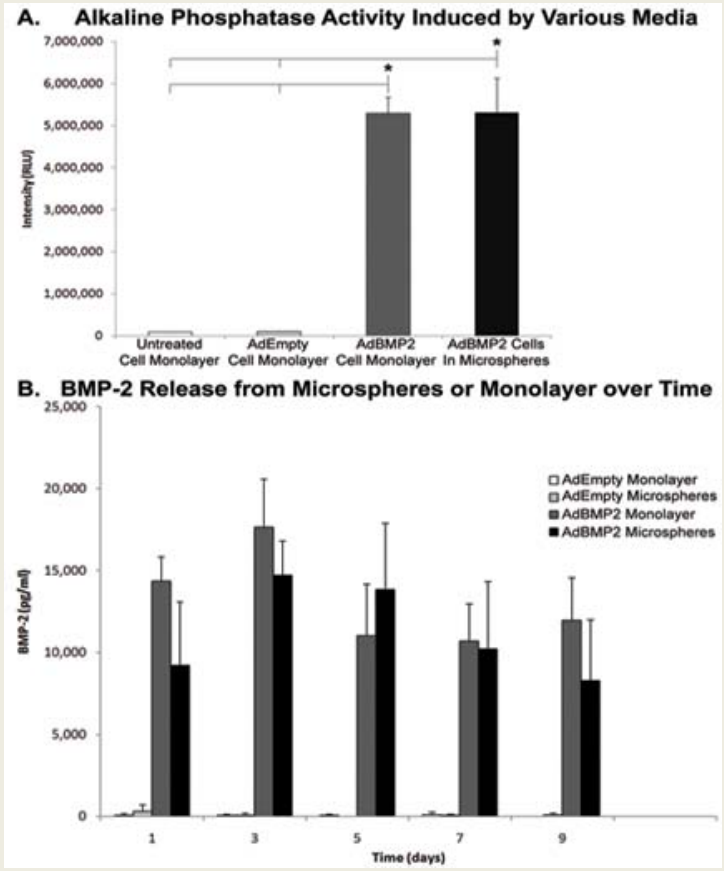

Figure 13: Comparison of BMP-2 expression, secretion and activity after PEGDA encapsulation. **A.** BMP-2 protein in culture supernatant taken from AdBMP2- or AdEmpty cassette-transduced cells (25000 vp/cell) (monolayer), or those encapsulated in PEGDA microspheres was quantified by sampling every other day for 9 days and evaluated using an ELISA. **B.** Alkaline phosphatase activity in W20-17 cells after addition of conditioned media from AdBMP2- or AdEmpty cassette-transduced cells (25000 vp/cell) (monolayer), or AdBMP2-transduced cells encapsulated in PEGDA microspheres. As a negative control, we also included culture supernatant from untransduced cells. Alkaline phosphatase activity is depicted as the average relative chemiluminescence units (RLU), where n=3. Error bars represent means ± SD for n=3. A Student t-Test was applied to demonstrate significance. AdBMP2-transduced monolayer and microsphere groups had significantly greater alkaline phosphatase activity and BMP-2 concentration levels ($p < 0.05$) when compared against other groups, but no differences when compared to each other. In other words, microencapsulation had no effect on BMP-2 release and function.

We also compared the level of BMP2 in culture supernatant taken from both cells directy plated and cells encapsulated in microspheres. BMP2 activity was quantified by measuring alkaline phosphatase (AP) activity in W20-17 cells exposed for 72 hours to the culture supernatants from AdBMP2-transduced cells directly plated or encapsulated in microspheres was significantly elevated over control cells but there was no difference between these groups, indicating the BMP-2 released is functionally active (Figure 13A). A 9 day time course of BMP-2 levels in culture supernatant was quantified by ELISA to be approximately 17,500 pg/ml and 15,000 pg/ml for directly plated and microencapsulated cells, respectively (Figure 13B). No BMP-2 was detected in either culture supernatant from AdEmpty cassette-transduced cells, or control cells. The results suggest that the smaller structures, may allow for both greater cell viability and diffusion of BMP2.

MicroCT analysis of bone formation showed a significantly greater volume of heterotopic ossification in tissues receiving microspheres (Figure 14A, C) than those receiving directly injected cells (Figure 13B, D). Statistical power to detect differences between volumes formed in these groups was 72.5%. Cross-sectional microCT analysis of the newly formed bone revealed a similar architecture between the groups. Heterotopic bone formed by both the microencapsulated cells and directly injected cells had a pattern of dense bone surrounding a hollow interior (Figures 14C and D); however the circumference of bone within the directly injected cells was significantly smaller. Microencapsulated AdBMP2-transduced cells produced approximately twice the bone volume of unencapsulated cells (Figure 15B). Despite the volumetric increase, the bone tissue mineral content was statistically similar between these groups, although trending towards an elevation in samples that received the microspheres (Figure 15A). This corresponds with the change in tissue mineral density of the new bone surrounding the microspheres (Figure 15C). The newly formed bone appears to be slightly less dense, leading to the overall similarity in mass between the two groups. Statistical power to detect differences between bone densities in these groups was 76.7%.

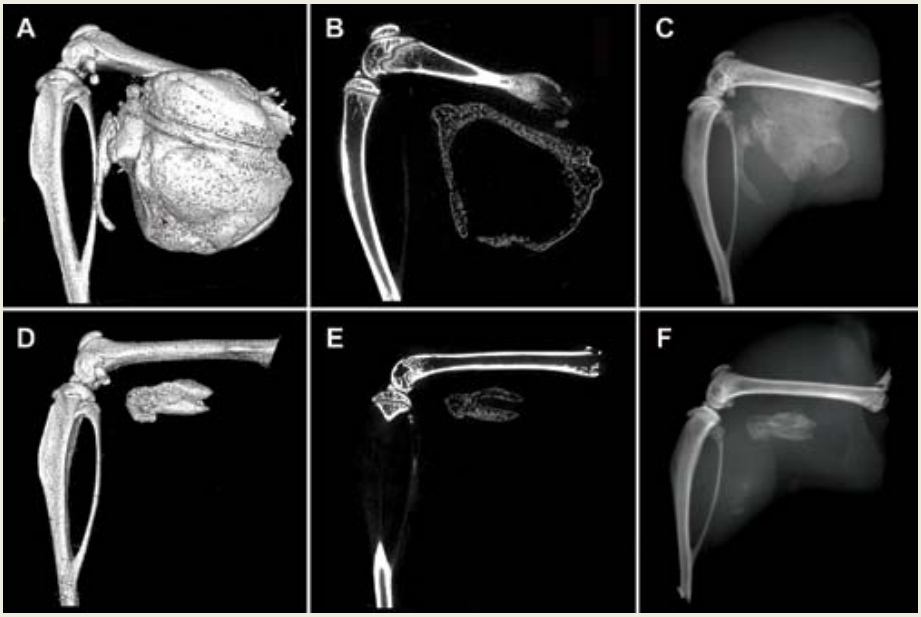

Figure 14: Micro computational analysis of the resultant heterotopic bone formation. Left images (**A, D**) are 3D surface renderings of the resultant heterotopic bone, while middle images (**B, E**) are cross-sectional slices through the new bone. Right images (C, F) show corresponding radiograms. Panels A - F show the resultant mineralization of the muscle tissues after injection of AdBMP2-transduced cells (2500 vp/cell) encapsulated into PEGDA microspheres (**A - C**) or direct injection of unencapsulated AdBMP2-transduced cells (**D - F**). Both have a denser rim of bone, with a hollow interior structure, suggesting that the biomaterial did not alter bone patterning.

From histological analysis, both groups had significant new bone formation within the muscle (Figure 16). In tissues that had received the direct injection of AdBMP2-transduced cells, there was a small compact piece of bone forming a ring-like structure encircling what appears to be blood and tentative stroma, and just exterior to this structure was significant adipose (Figure 16A). A similar structure was observed in tissues that had received microspheres (Figure 16B). Since the microspheres did not degrade, they appear histologically as gaps or holes within the matrix (Figure 16B). Thus, despite the presence of nondegradable microspheres, both structures were patterned to have a denser bone structure with a bone marrow-like cavity on the interior.

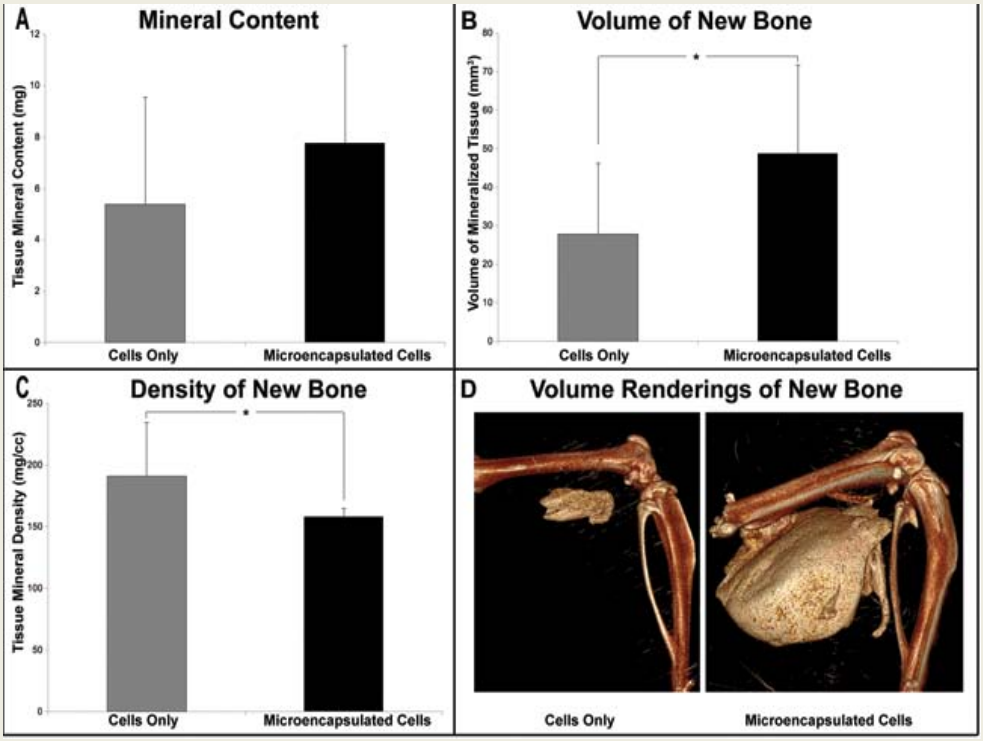

Figure 15: Quantification of the heterotopic ossification using microcomputational analysis. Cells were transduced with AdBMP2 and either directly injected or encapsulated into microspheres prior to injection, and the resultant heterotopic bone was analyzed two weeks later. Tissue parameters: **A.** bone tissue mineral content, **B.** bone volume of mineralized tissue, and **C.** bone tissue mineral density were calculated for the newly formed bone (n=6 per group). The means and standard deviations for each group were calculated and compared using a one-way analysis of variance. Results indicate that mineral content is statistically equivalent (p=0.2) between the groups, whereas the AdBMP2-transduced cells in microspheres had a significantly greater volume (p=0.038) than the AdBMP2-transduced cells directly injected. Alternatively, the bone tissue mineral density was significantly denser for the group receiving the cells directly as compared to those in microspheres (p=0.029). Panel **D.** shows a 3D volume rendering of new bone formed in cell only and microencapsulated cell groups, respectively.

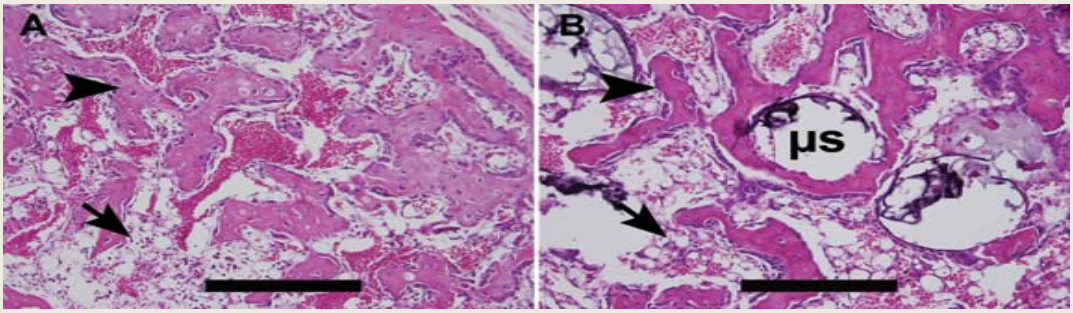

Figure 16: Photomicrographs of heterotopic ossification. Hematoxylin and eosin stains of new bone formation by: **A.** directly injected and **B.** microsphere (μs) encapsulated cells. Both groups show small compact pieces of bone (arrowheads) forming ring-like structures, encircling what appears to be blood and tentative stroma in the inner region, with significant adipose (arrows) just exterior to the new bone. Scale bars are 500 μm.

c. *Engineer proteins that may enhance the BMP2 bone inductive response, such as VEGF-A or -D and compare with gels without additional proteins.* ***(Months 36-48)***

We have demonstrated that the BMP2 rapidly induced new vessel formation, and elevates expression of VEGFs within the localized region of bone formation. Addition of the proteins to the material does not rapidly enhance the bone formation. As mentioned in the previous section, analysis of the newly forming bone shows a strong patterning of the bone formation even with the microspheres. The inside of the bone possesses a normal vascularized bone marrow cavity, amongst the microbeads.

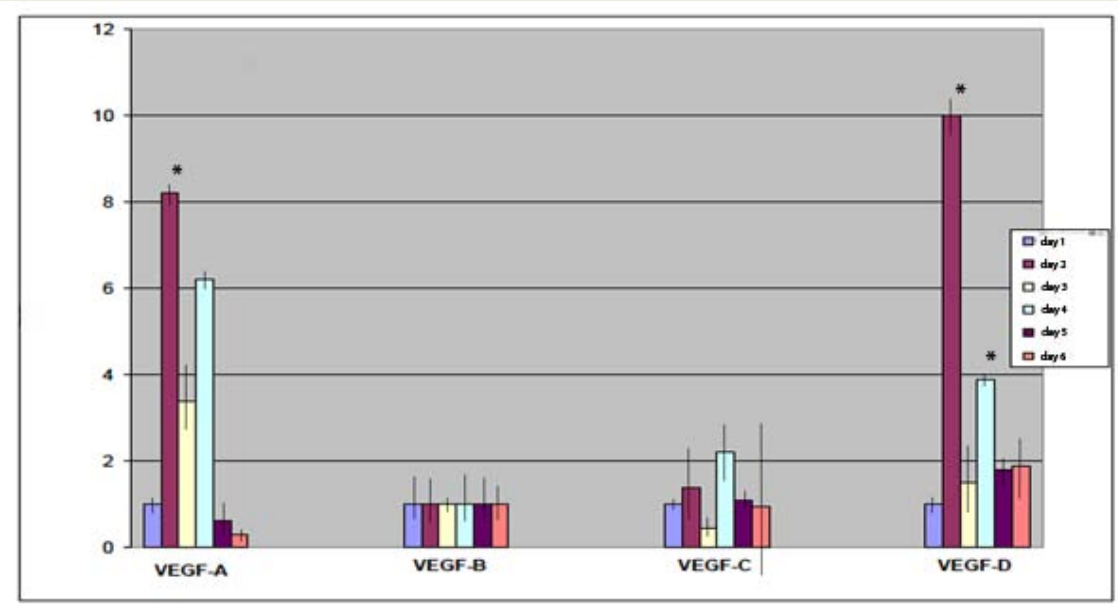

Figure 17: Quantitative RT-PCR of mRNA of VEGF family members within tissues isolated surrounding the site of new bone formation over daily intervals. n=8 biological replicates, and n=4 experimental replicates). The data is represented as a ΔΔ Ct.

We recently demonstrated the rapid increase of VEGD and A, within 48 hours of delivery of the BMP2. Interestingly this gene expression of these proteins within the localized site of bone formation appeared to be biphasic with a second elevation in expression at 4 days after delivery of the adBMP2 transduced cells (figure 17). This was not seen in the tissues receiving the Adempty transduced cells. We then quantified whether this led to new vessel formation, and found a 2 fold enhancement in new vessels in tissues receiving the BMP2 transduced cells (see appendix, J Bone Mineral Res). We also demonstrated that cells expressing the VEGFs were the brown adipose (Am J Path see appendix), and that the adipose appears to be generated rapidly, and involved in patterning of the newly forming bone. From these studies we have identified a novel mechanism which shows the molecular pathway induced directly by BMP2, which leads to production of brown adipose, new vessels, peripheral nerve ingrowth, and ultimately cartilage and bone. We are currently assembling the manuscript to connect the BMP2 protein directly to peripheral nerve signaling, and production of adipose. We have also been asked by the president of the American Society of Bone and Mineral Research, to submit a review article to demonstrate the molecular model.

d. *Test these gels in vivo. (Months 36-48)*

Please see previous sections (figure 10). We are currently testing the materials in rat models, through injection of the microspheres into the paraspinous musculature, similar to the rat studies, performed for the transduced cells.

Task 3: To achieve posterolateral spine fusion by percutaneous injection of the encapsulated Ad5F35BMP2 transduced senchymal stem cells into the paraspinous musculature of both rats and mice. Spine fusion will be assessed in both a rat and mouse model by both histological and radiological

analyses over time and confirmed by both microCT and biomechanical testing. The results will also be compared to a parallel murine system which is immunocompetent. These experiments will provide essential preclinical data in two different animal models.

a. Obtain approvals through the DOD institutional review board for approval to work with the human mesenchymal stem cells. **(Months 0-12)**

This was completed within the first few months of the award.

b. Once approved we will start to utilize these cells in all hydrogel formulation experiments as described in Task 2. **(Months 12-36)**

We chose to test the system in two different murine models: immune competent and immune compromised. One major reason for testing both is that the proposed clinical system will utilize human mesenchymal stem cells transduced with an Ad5F35BMP2 vector for the production of BMP2 *in vivo* for spine fusion. Thus the immune compromised NOD/Scid mouse will allow us to test this system directly. However, we wished to demonstrate similar efficacy in a mouse model which is not immune compromised since presumably this system would be developed for the general population. Thus we also chose to test the system in C57BL/6 wild type mice, which require us to use a matched C57BL/6 derived cell line (MC3T3-E1). The latter system also requires the inclusion of the polyamine compound gene jammer (Fouletier-Dilling et al, 2005). However, the gene jammer is not proposed to be a component of the final gene therapy system.

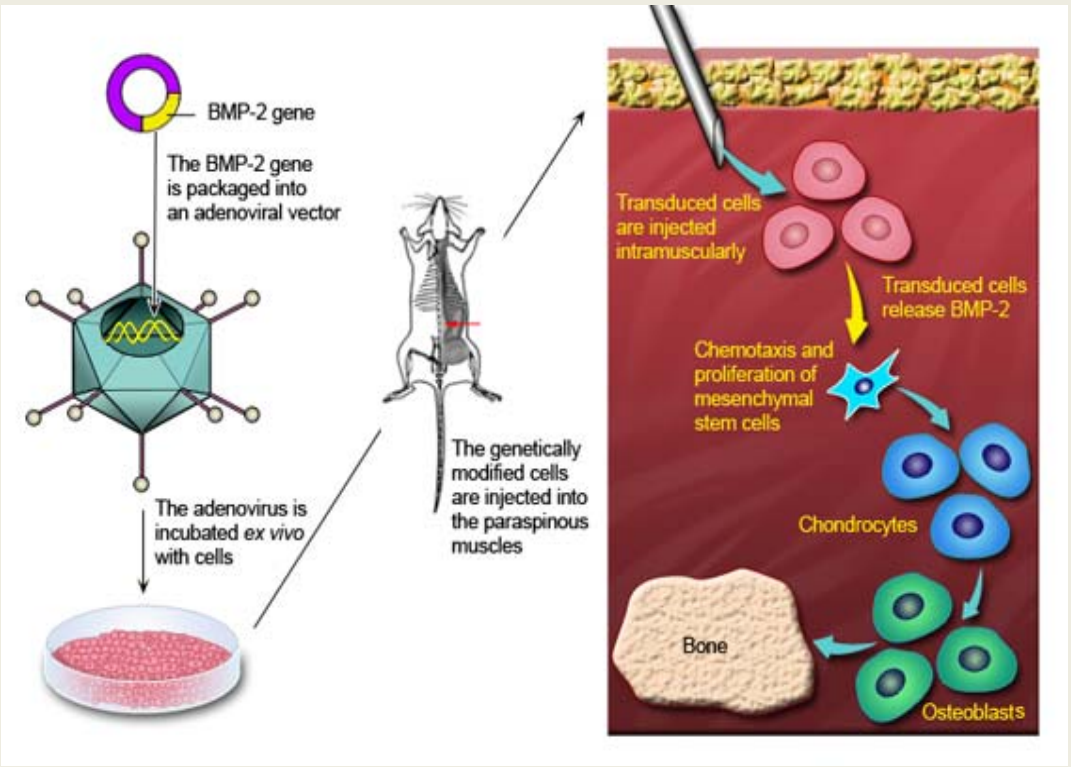

Figure 18: Schematic depiction of spine fusion using the cell based gene therapy system. AdBMP2 transduced cells injected into the muscle, rapidly recruit host cells to undergo all stages of endochondral ossification. Within one week mineralized osteoid can be detected in photomicrographs and radiographs.

Therefore we next tested the ability of the system to fusion multiple vertebra in both systems. For the NOD/Scid mice human fibroblasts, were directly transduced with an E1-E3 replication defective adenovirus vector which possesses a human BMP2 cDNA, in E1 and an altered fiber gene in which Ad5 fiber has been replaced with an Ad5F35 fiber, which we refer to as Ad5F35BMP2 vector (5000 vp/cell) whereas in the second model, MC3T3-E1 cells were transduced by addition of the gene jammer compound to the cells at time of infection with a standard E1-E3 deleted replication defective adenovirus type 5 vector possessing the same human BMP2 cDNA in E1, Ad5BMP2 virus (5000 vp/cell). Both systems routinely provide ≤90% transduction efficiency (Fouletier-Dilling et al, 2005). Next 5 x 10^6 transduced cells were injected into the parapsinous musculature of the mice (n=10 Nod/Scid and n=3 C57BL/6). To insure proper placement the material was injected under anesthesia into the mouse, along the length of the paraspinous muscle in the lumbar spine adjacent to the desired fusion point, to allow the transduced cells to track the entire muscle region (Figure 18). The mice were then euthanized at various time points and the bone was analyzed by various criteria to ensure

fusion. With this system, heterotopic ossification is generated rapidly, fused and remodeled into two or more of the adjacent vertebra, reducing spine motion.

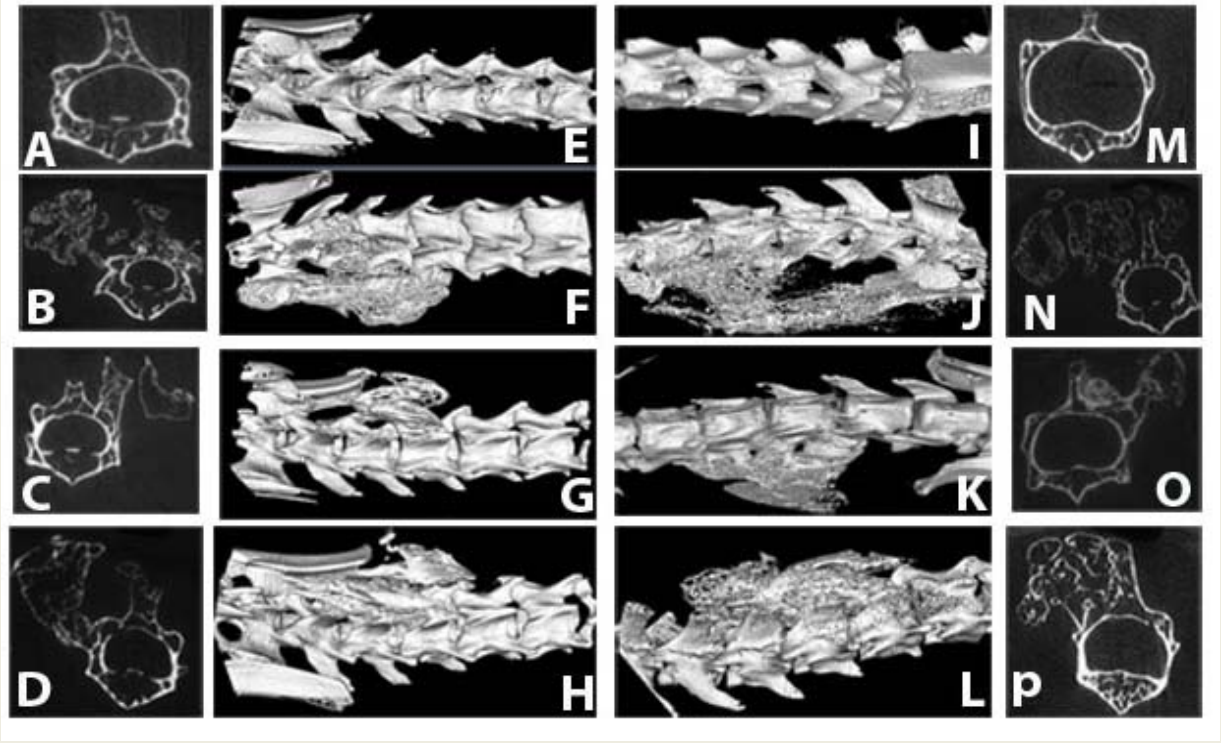

Figure 19: Radiographs of C57BL/6 (panels A-H) and NOD/Scid (panels I-P) spines imaged after intramuscular injection into the paraspinous musculature of cells transduced with Adempty cassette control virus (panels A, E, I, and M) or AdBMP2 (panels B-D, F-H, J-L, and N-P). Control animals injected with Ad5HM4 were scanned 6 weeks after delivery of the transduced cells (panels A, E, I and M). Mice receiving the AdBMP2 transduced cells, were scanned 2 weeks (panels B, F, J, N); 4 weeks (panels C, G, K, O); and 6 weeks (D, H, L, P) after the initial induction of heterotopic ossification. Two dimensional x-rays (panels A-D; C57BL/6 and panels M-P; NOD/Scid) show a cross section through the three dimensional reconstructions (panels E-H; C57BL/6 and I-L; NOD/Scid) of tentative fusions between the heterotopic ossification and the vertebral bone.

Radiological and microCT analysis of spine fusion: Accordingly heterotopic bone formation was allowed to progress for 2, 4 and 6 weeks, after initial injection of the AdBMP2 or empty cassette transduced cells. Spines were removed and analyzed for the presence of heterotopic bone, and spinal arthrodesis. In all AdBMP2 injections, heterotopic bone formation occurred along the injection site, adjacent to the spine, with greater than 90% bridging and fusing to the skeletal bone. (figure 19, three dimensional reconstructions E-L). Two dimensional radiographs (figure 19, panels A-D and M-P) show the cross sections through the tentative fusion. The radiographs and three dimensional reconstructions demonstrate that both the immune incompetent system, NOD/Scid mice receiving human cells transduced with AdBMP2 (panels I-P), and immune competent system, C57BL/6, receiving AdBMP2 transduced allogeneic murine cells (panels A-H); appear to produce similar bone within 4 to 6 weeks. This new bone appears to be remodeled with a contiguous cortical bone exterior. Although we did observe 40% of the samples in the NOD/Scid animals with potential points of fusion, panel N shows a scenario in which the heterotopic bone, although extensive, has not yet fused into the vertebrae. It appears in panel J, that the heterotopic bone occurred slightly distal to the vertebral bodies. Interestingly, we did not see similar findings in wild type mouse models, as seen in panel B even at two weeks the substantial bone has fused to the adjacent vertebra.

In the cross-sectional radiographs, vertebral cortical bone appears to be integrated with the heterotopic one (figure 19, panel B-D, O-P). The points of fusion appear to be in the laminae region of the vertebra, with the majority of cases encompassing the entire spinous and transverse processes, suggesting significant fusion. In this case although the location of the fusion is unchanged, only limited portions of the spinous and transverse process are actually integrated. In no case did we observe bone formation or bridging in the

samples receiving the Adempty cassette transduced cells. The apparent fusion appeared to be rapid, within two weeks, and limited in size and scale, to region of muscle which received the cells. Further, at no time did we observe bone formation within the spinal canal.

To confirm that the apparent mineralized bone observed on the radiographs is true osteoid, and that it has integrated at these tentative points of fusion, we isolated the spine and adjacent tissues for histological analysis using techniques. The spines were embedded in paraffin blocks, five micron sections cut, and every fifth section was stained with hematoxylin and eosin to identify the tentative point of fusions. Representative photomicrographs (2X and 4X) of samples from either model, taken 2, 4 and 6 weeks after induction of heterotopic ossification are shown in figure 20. In all cases we observed structures of mature bone, such as osteoclasts, osteocytes and tentative bone marrow elements in the heterotopic bone, as well as cartilage, analogous to the growth plate structures in the normal long bone. However the heterotopic bone appeared to grow in a direction towards the skeletal bone, with the most mature bone being distal to the skeletal bone in the 2 week samples. Figure 20, panel A-B, shows that there is substantial new bone, adjacent and fused with the more mature vertebral bone, along the transverse process, and laminae region of the vertebra. Although mature bone with tentative marrow elements was observed at 2 weeks; this structure was always distal to the vertebral bone (data not shown), suggesting that the original heterotopic ossification started *de novo*, in the muscle and grew towards the vertebrae to encompass the bone. By four weeks, (figure 20, panel C-D), the heterotopic bone is much more mature, and at the point of fusion, a very cellular reaction, that appears to be rapidly removing the mature cortex of the skeletal bone was noted. It is unclear whether the large number of cells is recruited to this boundary or is expanding from the vertebral periosteum, but as noted in panel G, the mature cortical bone of the vertebra appears to be pitted and undergoing removal by the maturing heterotopic bone. By 6 weeks, this boundary is completely remodeled (figure 20; panel E-F) with the two bones now contiguous as one integrated structure with a well defined cortex and trabecular interior, which houses the bone marrow. Interestingly, the only evidence remaining of the newly formed heterotopic ossification is the presence of substantial amounts of adipose tissue, which is found within heterotopic regions, in contrast to the mature marrow within the vertebra (panel F). Figure 20, all cases show what appears to be fusion with the transverse process within the laminae region of the vertebra, which was the target region for fusion. Depending on the depth of the section, more or less of this region was involved in the fusion site. In many cases the fusion actually encompassed both the spinous process through the laminae to the transverse process. In all tissues analyzed, the vertebral body did not appear to undergo growth, and there was no evidence of new bone formation within the spinal canal, similar to our observed radiological findings.

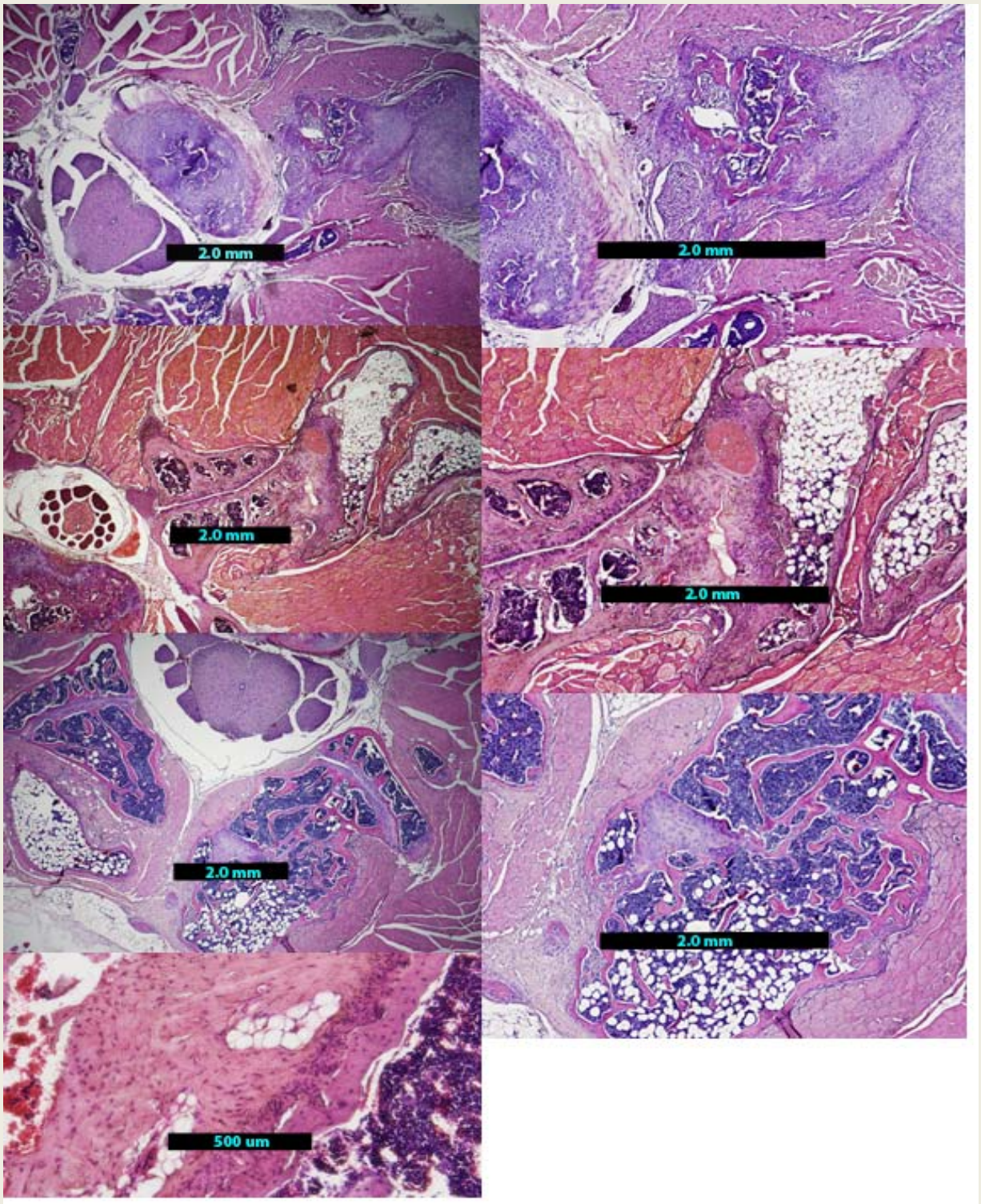

Figure 20: Representative photomicrographs of tentative vertebral fusion with the heterotopic bone, taken 2 (panels A-B; 2X and 4X respectively), 4 (panels C-D; 2X and 4X respectively), and 6 (panels E-F; 2X and 4X respectively) weeks after initial injection of the AdBMP2 transduced cells. The slides were stained with hematoxylin and eosin for viewing. Panel E is a representative photomicrograph (10X) of a sample taken 4 weeks after the initial injection of AdBMP2 transduced cells. As can be seen in this sample, there are a significant number of cells associated with the boundary between the new heterotopic and old vertebral bone.

The clinical goal of spine fusion is to reduce motion within the vertebral column; therefore, we developed a method for measuring flexion-extension of the spine. In this analysis spines were x-rayed before and after bending, and intervertebral motion was quantified using KIMAX QMA software (Medical Metrics, Inc.). This software has been validated to measure intervertebral motion with an accuracy of better than 0.5° of rotation and 0.5 mm of translation. Results of this analysis are shown in Table 1. In no cases did tissues receiving the Adempty cassette transduced cells, show a reduction in motion or spine stiffening. Whereas in NOD/Scid animals that received the human cells transduced with AdBMP2, approximately 40% of the spines at 2 weeks and 90% of those at 4 and 6 weeks had reduced movement, consistent with fusion of at least one level. Interestingly, the C57BL/6 group receiving AdBMP2 transduced cells, at all time points, consistently showed a reduction in motion within the lumbar spine correlating with fusion (Table 1).

Table 1: Spinal fusion in injected animals

Group	N	Strain	Time	Spines with 2 or more vertebrae fused (%)
Adempty cassette transduced cells	9	NOD/Scid	6 weeks	0 %
AdBMP2 transduced cells	9	NOD/Scid	2 weeks	44 %
AdBMP2 transduced cells	9	NOD/Scid	4 weeks	90 %
AdBMP2 transduced cells	9	NOD/Scid	6 weeks	90 %
Adempty cassette transduced cells	8	C57BL/6	6 weeks	0%
AdBMP2 transduced cells	8	C57BL/6	2 weeks	100%
AdBMP2 transduced cells	4	C57BL/6	4 weeks	100%
AdBMP2 transduced cells	8	C57BL/6	6 weeks	100%

To further confirm spine fusion, the isolated spines used for mechanical testing were bleached to remove soft tissues, and analyzed on a gross level to see if the bone was contiguous. Figure 21, panel A, a representative 6 week spine shows that in this fusion, 5 vertebrae of the lumbar spine are actually remodeled into a single structure. In all cases with biomechanical constraint of the spine after the induction of bone formation, there was also integration of the vertebra with heterotopic bone, which was observed after removal of the soft tissues. In cases that did not meet our criteria for fusion (several NOD/Scid animals at 2 weeks) in that they did not appear to be constrained after induction of bone formation, there was heterotopic bone that was not integrated with the vertebrae but rather individual bones, confirming our biomechanical findings.

Further, in both immune copentent and incompetent models the radiomicrographs show a distinct scoliosis in 6 month old growing mice, which received the Ad5BMP2 transduced cells injected into one side of the paraspinous musculature that parallels the spine. Figure 21, panel C, representative radiographs show a distinct curvature of the spine towards the area of new bone formation and tentative fusion. This was observed in a large number of animals with heterotopic bone and tentative fusion, but absent in animals that received the control cells (panel B).

Figure 21: Spine fusion was observed in bones isolated from the mouse after induction of targeted heterotopic ossification (panel A). Associated soft tissues were removed by bleaching, leaving only the bone. A wire was threaded through the spinal column, to preserve the orientation of the vertebra. Unfused vertebrae hang free; fused vertebrae remain joined and rigid. Ruler is in millimeters. Radiographs of mouse spines 6 weeks after induction of spine fusion Adempty cassette (panel B) or AdBMP2 (panel C) transduced cells. Panel C, shows obvious curvature of the spine suggesting a significant scoliosis, as compared to the normal mouse spine, shown in panel B.

Again this is from a simple injection of the material into the paraspinous musculature. Within 4 weeks we observed 100% fusion in all the spines, and between 30-100% in just 2 weeks after injection of the material. At this point we are rapidly repeating these experiments in the rat model, using the microbeads to complete the goals of this application.

c. Once the gels have been modified to offer optimal properties for bone formation and removal, we will test these in a murine model of spine fusion. **(24-36 months) These studies are ongoing and should be completed in the next 3-4 months. We will be using the degradable hydrogel materials in the mouse spine to repeat the above experiments.**

d. Since we have substantial knowledge of the mouse model, we will initially start to collect data with this system. We will demonstrate the ability to induce spine fusion in the presence of tetracycline. **(Months 24-**

40) We most likely will not attempt these, since we have an alternative method for looking at gene expression that may be more effective at removing the cells, and transgene expression. This relies on the caspase gene which can induce apoptosis in cells when provided an activator compound that can readily pass through the PEG-DA hydrogel.

e. Analyze the modified injectable hydrogel for optimal volume, *in vivo* crosslinking, design, selective degradation, and inflammatory reaction using both live animal imaging and histology. **(Months 24-48)**

We will no longer be crosslinking *in vivo* since we are actually attempting to perform the specific microbead structures for optimal cell viability and BMP2 secretion. These structures are actually injectable, and thus will be utilized similarly to the direct injection of the cells. Preliminary data suggests that these structures will provide for even more rapid and reliable fusion of the spine. In this next phase of the grant, we will be encapsulating human mesenchymal stem cells that possess a caspase gene, which will provide a method for timed cell removal. In this case we will add the activator of caspase to send the BMP2 transduced cells through apoptosis, paralleling the timing of remodeling of the PEG-DA hydrogel microbead structures. Thus we will ensure that we destroy the cells within the PEG-DA hydrogel microbead structures, prior to potential degradation of the polymer. These studies with the human mesenchymal stem cells will also be tested using the dsRED reporter so that we can track their viability in the presence of the drug, as well as determine the optimal timing of BMP2 secretion for bone formation. This is actually the final phase of the proposed set of studies, and should allow us to arrive at a final product for testing.

f. All fusions will be tested both biomechanically as well as radiologically using microCT to confirm the fusion. **(Months 40-48)**

This aim is complete! A method to reliably determine if newly mineralized tissue adjacent to the spine has formed a structurally competent bridge between vertebrae is needed to assess new spine fusion technologies in small animal models. Micro-computed tomography can be used to visualize any newly formed mineralized tissue adjacent to the spine, but it can be difficult in some cases to determine if the mineralized tissue is actually integrated with the vertebrae or if it is only overlying the vertebrae. Micro-CT exams also require expensive equipment and long-

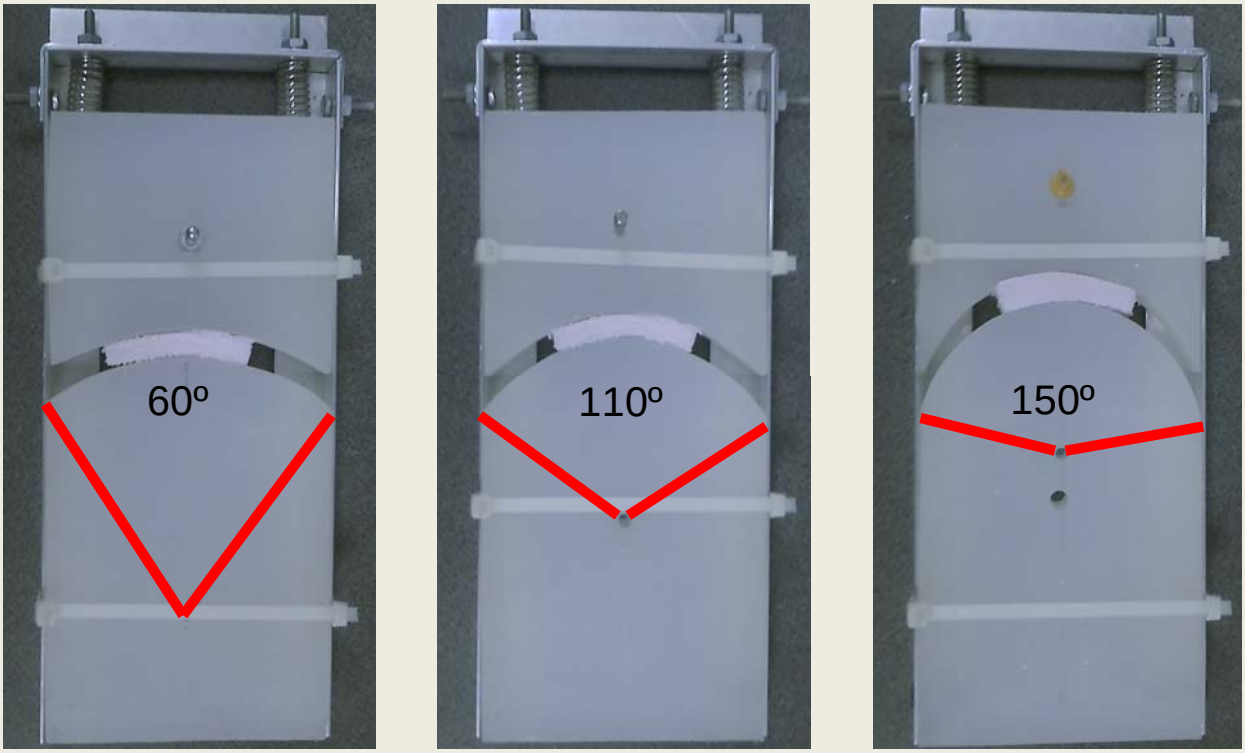

Figure 22: Angles and apparatus to flex and extend the spines after fusion, to determine if the degree of motion has been restricted in the murine model, to a similar extent to what would need to be achieved to reduce pain in a human clinical setting.

scan and post-processing times. To provide a simple and rapid method to directly test whether a fusion was mechanically successful, a mechanical device was developed that creates controlled flexion and extension in a mouse spine, so that spine fusions could be assessed using the same computer-assisted methods that are now widely used to assess spine fusions in human patients. This device was validated in a mouse spine fusion model. Utilization of the device involves embedding the spine and surrounding tissues, after removal from the body, in mold using rapid setting alginate. The embedded spine is then flexed using the device and a micro-radiograph is obtained with a digital Faxitron system. The embedded spine is then placed in extension and a second radiograph is obtained. These two radiographs are then imported into a workstation and analyzed using previously validated computer-assisted technology (Zhao KD, *et al*.2005). The software allows intervertebral motion to be accurately quantified. A successful spine fusion is intended to stop any significant motion between vertebrae. In the human spine, intervertebral motion under 1.5 degrees at any level is considered to be reliable evidence of a solid spine fusion (Hipp JA et al, 2008) using this image processing technology.

To test whether the tentative fusions were actually capable of reducing motion within the spine, we set up some experiments to look at flexion/tension under bending at specific angles. Briefly, three groups of NOD/Scid mice were given an injection of MRC5 cells transduced with 1) Ad5F35BMP2 (2 week analysis), 2) Ad5F35BMP2 (6 weeks), and 3) Ad5F35empty cassette all at 2500 vp/cell. The cells were transplanted into the paraspinous musculature of through direct injection. Group 1 animals were isolated at 2 weeks, while groups 2 and 3 were harvested at 6 weeks after initial induction. The spines were then embedded in an agarose gel material, and placed between two plates for bending analysis (figure 22).

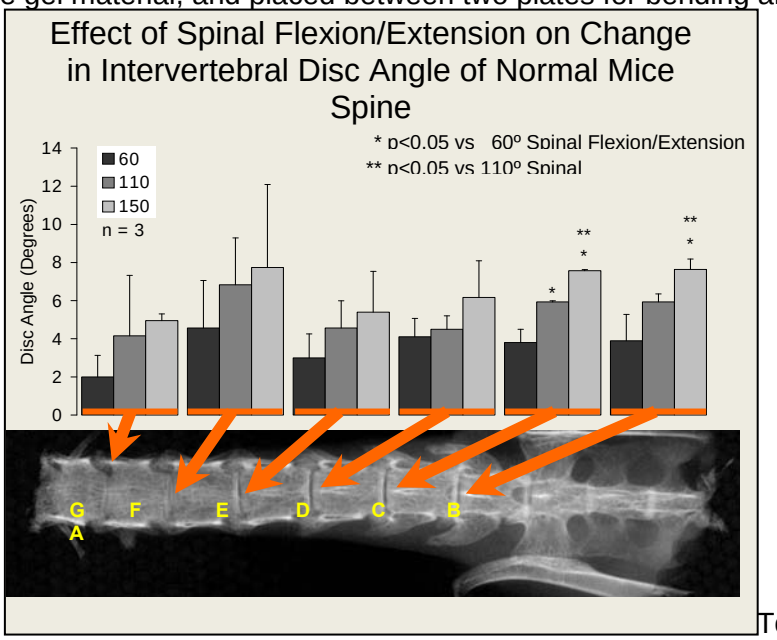

Figure 23: Results of analysis of the disc angle after bending at 60,110, and 150 degree angles. Each column of numbers represents the corresponding disc (arrow). The results suggest more variability in discs on the end of the animal, where the spine has been cut, versus internal or adjacent to the pelvis which remains on these tissues.

To determine what to expect for normal spine flexibility in these mice, we subjected a group which had received no treatment to this analysis. As can be seen in figure 23, the values obtained from subjecting the mice to 60°, 110°, and 150° angle varied significantly at the ends of the spine and most likely due to the isolation, and the fact that the spine had been cut. Discs within the center and lower spine showed significance between 60 and 110 degree shifting with little or no variability, and allowed us to focus on this region for analyzing our fusions (figure 24).

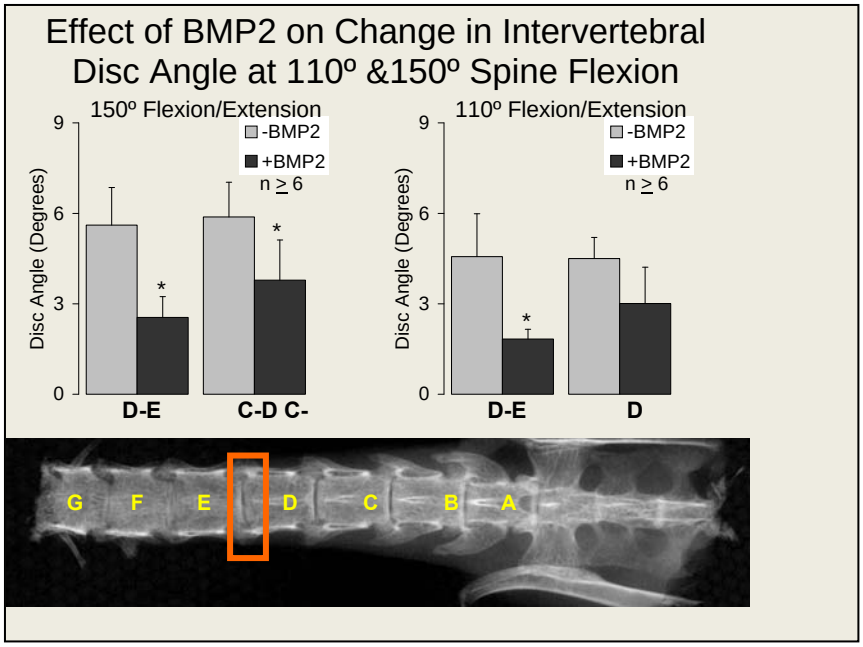

Figure 24: Results of analysis of the disc angle after bending at110, and 150 degree angles in tissues isolated from mice 6 weeks after induction with BMP2. The disc analyzed is listed as the disc between the two lettered vertebras. The disc which provided the most significance in limiting the disc angle is highlighted by the orange box. This sample is representative of the group of fused spines.

This manuscript should be in press shortly.

g. Once we have established methodology that leads to reproducible fusion we will further test this in a rat model of spine fusion using athymic rat's spine fusion using athymic rats. We will then compare and confirm that these results are similar to those obtained in immuno-competent mice. **(Months 40-48)**

These experiments are currently underway. We initiated experiments in the athymic rats, and bone

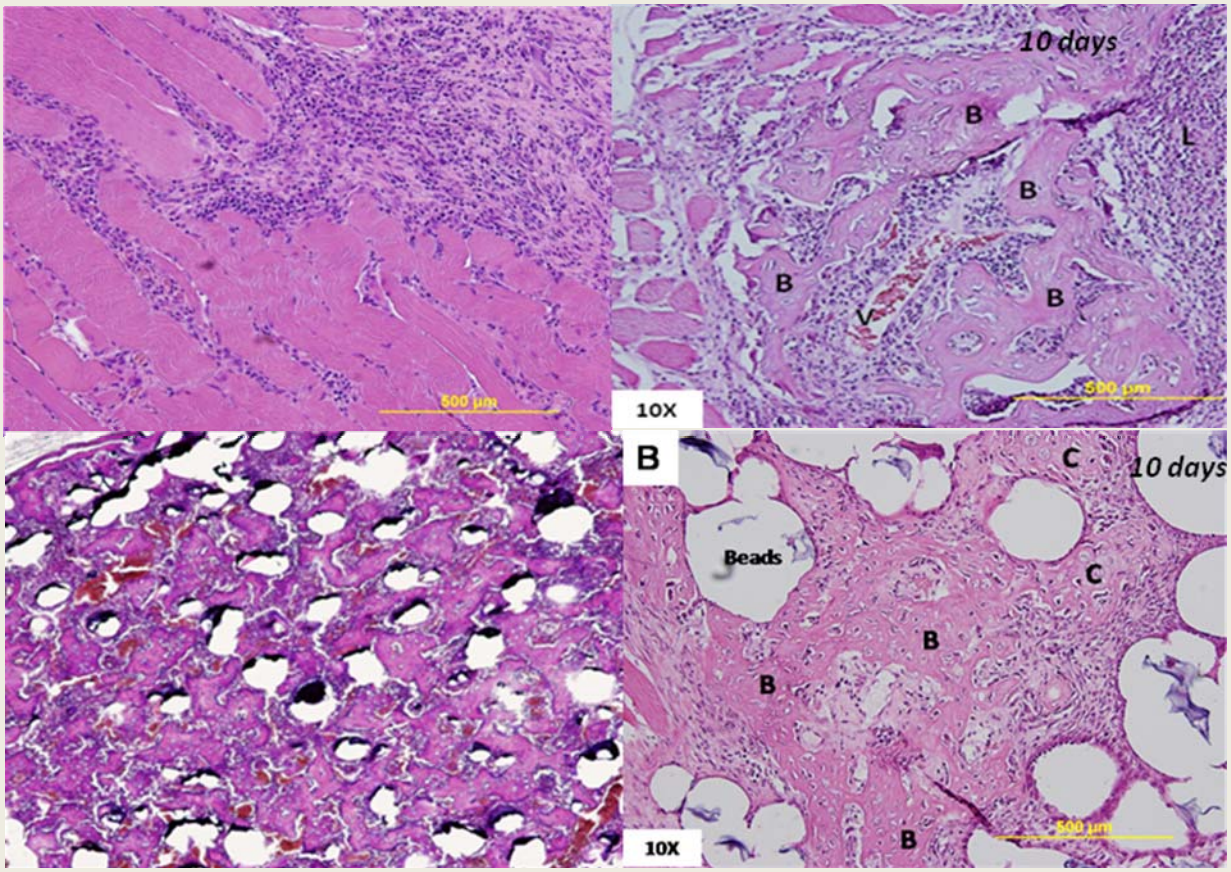

Figure 25: Photomicrograph of hematoxylin and eosin staining of tissue sections isolated 10 days after injection of either directly injected allogenic cells, microencapsulated allogenic cells, directly injected autologous cells, or microencapsulated autologous cells. B represents bone, C cartilage

formation was robust similar to our mouse models. However, when we initiated studies in normal Wistar rats, heterotopic ossification was completely abolished. Replacing the bone formation was a rapid immune response characteristic of a foreign body response. We decided that perhaps Wistar rat strains may vary much more than the counterpart mouse strains, so we next isolated skin fibroblasts from a littermate within our colony of Wistar rats. We also isolated bone marrow mesenchymal stem cells from this same animal. Both populations of primary cells were expanded and cryoperserved as cell stocks for future experiments. We validated equivalent BMP2 expression after transduction, as obtained from all other cells used in these experiments. We also re-validated the viability, BMP2 expression, and secretion, after micro-encapsulation. The cells were then either encapsulated or directly injected and resulting bone formation observed 2 and 3 weeks post-induction. Interestingly, the cells isolated from a littermate did not produce bone as determined by xray or histology, in the unencapsulated tissues, whereas the microspheres produced a significant amount of bone (figure 25). Analysis of the tissues receiving the unencapsulated littermate cells, showed a substantial foreign body response, with significant numbers of mature lymphocytes. We hypothesized from this result that the cells isolated from a littermate were functioning as allogenic cells, and inducing this reaction. To confirm this, we isolated skin fibroblasts from rats two weeks prior to induction of heterotopic bone. These primary skin fibroblasts were expanded and transduced with AdBMP2. We confirmed the transduction efficiency, expression of active BMP2 before and after encapsulation to the allogenic cells, and found they were comparable. Therefore we next tested the autologous cells in the rats, in comparison to the allogenic littermate cell line. Figure 25 shows photomicrographs of the hematoxylin and eosin stained tissues isolated 10 days after induction of bone, showing substantial bone in tissues receiving autologous cells regardless of the encapsulation, confirming our hypothesis. Again in these studies, allogenic cells could make as much bone as the autologous, if encapsulated in the hydrogel, suggesting that the gel was capable of masking cellular antigens that may launch a foreign body response. **Completion of this study demonstrates the final optimization process for development of this product. These findings confirm that a single qualified cell line can be readily transduced, encapsulated, and injected directly into the muscle tissue for heterotopic ossification and spine fusion. With the ability to use a single cell line, and limit detrimental inflammatory response is a landmark finding. Although we are currently completing the rat spine studies to show HO being generated in the rats can rapidly fuse the spine, similar to the mice, we have confirmed the ability to manufacture and implement this approach as a clinical reality.**

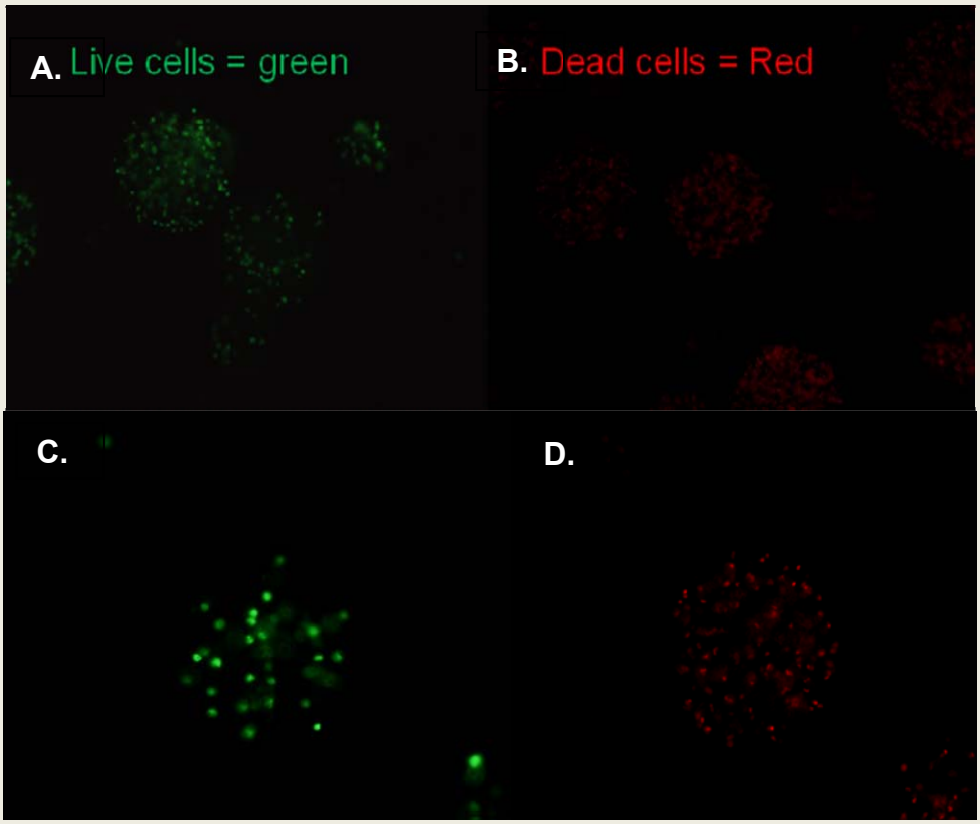

Figure 27: Analysis of AdBMP2-transduced cells (2500 vp/cell) within microspheres was assessed at day 7 using a LIVE/DEAD® Viability/Cytotoxicity Kit for mammalian cells (Invitrogen, Molecular Probes, Eugene, OR). Panel A and B show the cells within the microspheres after freezing, and panels C and D prior to freezing. Live cells are indicated by green and dead cells by red. Our preliminary quantification of the cells suggests that there are similar numbers of live and dead cells before and after freezing

h. To initiate toxicology studies, as potentially outlined in a pre-IND meeting with the FDA. **(Months 24-48)** **We have been focused on completing efficacy as described above, and now have obtained a final formulation that can readily be manufactured. To this end, we have focused on cryopreservation, of microbeads-AdBMP2 transduced cells, to complete the the formulation. In these studies we propose to freeze the encapsulated cells in a ready-to-go formulation that could be thawed just prior to the procedure, washed gently with PBS, and immediately loaded into a syringe.** If successful, batches of the materials could be generated and frozen as a bank for clinical implementation. We propose that the materials could be shipped to hospitals, or outpatient clinics, and then through image guided paraspinous injections. This would not require surgery, and would be able to be implemented through non-invasive injections.The patient could resume there normal activity, and fusion be confirmed through standard clinical means, at 2 and 4 weeks after injections. To confirm that the materials could survive cryopreservation we next transduced cells with adenovirus, and cryopreserved a portion of them, and then thawed, and plated to compare to the normal cells. Morphologically the cells appear normal after freezing; we next looked at cell viability after microencapsulation of the cells, both before and after freezing. As seen in figure 27, the cell viability appears to be similar between these populations, with dead cells (red-dsRED) being much lower, than the live (green – GFP) in both cases. We are currently measuring the level of BMP2 expression from frozen and non-frozen AdBMP2 transduced cells, encapsulated in microspheres, to determine the effects of freezing on transgene expression. However, we predict that it is highly unlikely to have changed, since the cell viability remains similar.

Our preliminary data suggests that freeze-thawing the encapsulated adenovirus transduced cells does not lead to cell death; so we next tested the ability for the cells to express the BMP2 transgene after freeze-thawing. Preliminary results suggest that there is no difference n the level of BMP2 expression after the cryopreservation of the microspheres (figure 28), suggesting that this is a viable way of storing the material after production. The material could then be shipped in these ready to go formulations, which would allow for easy implementation by the clinicians. This is a major advancement and we will complete this data for presentation to the FDA.

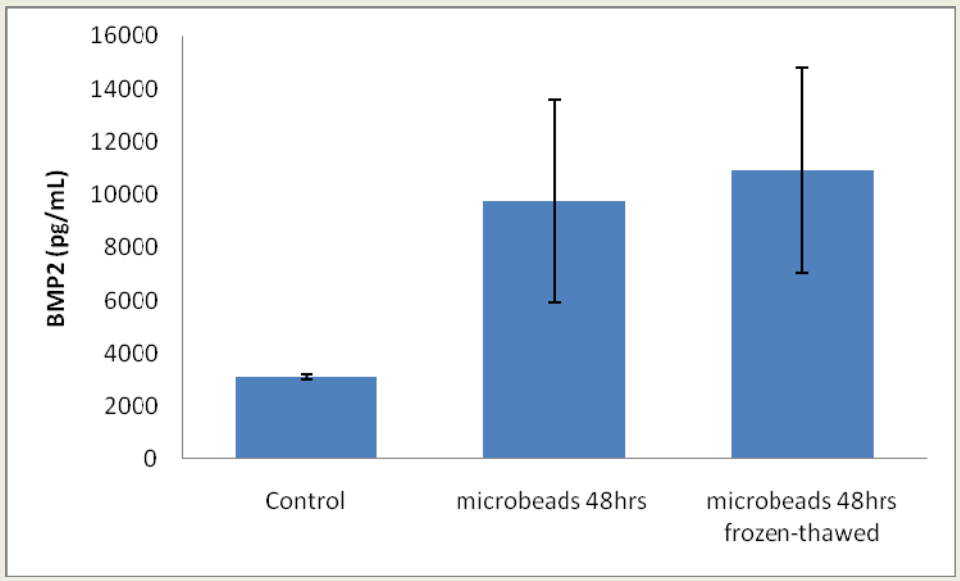

Figure 28: Quantification of BMP2 protein from AdBMP2 transduced cells, encapsulated into PEGDA hydrogel microspheres before and after freeze-thawing. The control is the background level of BMP2, without AdBMP2 transduction. The cells were either transduced and plated for 48 hours, or frozen fo 24 hours, and

Key Research Accomplishments

- We have developed a method for monitoring BMP2 expression in live animals through the use of dsRED. This optical imaging modality appears to be specific and significantly more sensitive than either lucerifase imaging or GFP detection. We have initiated studies to look at the regulated BMP2

carrying a dsRED gene and compare bone formation in the presence of long term versus short term BMP2 expression. This work has been accepted for publication in *Tissue Engineering*.

- We have developed a formulation of hydrogel that provides for sufficient BMP2 expression to induce *in vivo* bone formation. We have shown that these novel microbead structures efficiently secrete functional BMP2 and can produce heterotopic bone in the mouse hindlimb. The cells encapsulated in these structures survive a significantly longer time period than their directly injected counterparts, and they make significantly more bone than any of the other PEG-DA hydrogel structures tested. These are easily injected and appear to reside at the injected location. This work has been accepted for publication in *Tissue Engineering*.
- We have demonstrated that introduction of osteoclast degradation sites within this material provide selective degradation by osteoclasts similar to skeletal bone remodeling. We have synthesized the peptide sites and introduced them into the PEG-DA strands and succeeded in getting normal crosslinking of the material. We have then degraded the hydrogel completely in the presence of either a general protease (proteinase K) or a specific proteinase (cathespin K) but not with other selective proteinases. We have shown that both osteoblasts and osteoclasts can attach to the material, but only osteoclasts can lead to its degradation. We have initiated *in vivo* testing and found that the microbeads are degrading slowly, and appear to be replaced with mature bone. This work has been submitted for publication in *Biomaterials.*
- We have recently developed a method for confirming spine fusion through flexion and extension measurements. This is a critical component to characterizing the biomaterial, since on many occasions' microCT or x-ray analysis can appear as a true fusion, however, upon bending the heterotopic bone will break at the fusion site rather than constrain the spine, as a result of poor fusion, and remodeling with the normal skeletal bone. This work has allowed us to confirm that spine fusions as denoted by radiological or histological approaches are also capable of restraining motion in the spine, the clinical gold standard of spine fusion. This work has been accepted for publication in *J Orthopedic Res.*
- We have completed testing spine fusion in the mice using large groups, to ensure we have a valid sample size. The first groups used for this experimental design for direct injected cells and confirmed spine fusion within 4 weeks. This work has been submitted for publication *Spine J*
- We are currently now testing tentative spine fusions in both wild type mice and rats receiving the hydrogel encapsulated cells. We should complete this work in approximately 3 months.
- We have currently demonstrated the ability of the hydrogel encapsulation to prevent foreign body response which attenuates the bone formation. Thus we have demonstrated in wild type rats that an allogenic cell line, encapsulated with the PEGDA hydrogel, will provide robust bone formation observed in the mice, whereas without encapsulation, we observe no HO. We have shown that this is a result of the foreign cells, since autologous cells, restores the bone forming ability of the directly injected cells.
    - This is an extremely important finding for two reasons. First it demonstrates the ability to introduce foreign cells especially those transduced to express secreted factors with gene therapy vectors, without causing a foreign body response.
    - Secondly, it demonstrates the extremely challenges that scientists face in trying to implement stem cell strategies. If one cannot introduce cells other than autologous, stem cell strategies become extremely difficult. Thus approaches that mobilize or recruit stem and progenitors to the area of bone healing may be a more effective way of harnessing the potential of stem cells, than stem cell therapy.
- We are currently demonstrating the ability to cryopreserve the AdBMP2 transduced cells which have been encapsulated into the microspheres, and completing efficacy testing in rats with our final product.
- We are currently patenting this methodology

Reportable Outcomes:
Abstracts:
Oral presentation:
A model for neuronal regulation of heterotopic ossification. Authors: Sonnet C, Rodenberg EJ, Salisbury EA, Olmsted-Davis EA, Davis AR. Conference: 7th International Society of Musculoskeletal and Neuronal Interactions (ISMNI). Cologne, Germany, May 2010. Presenter - Corinne Sonnet.

Role of theperipheral nervous system in heterotopic ossification. Authors: Eric Rodenberg, Elizabeth Salisbury, Corinne Sonnet, Elizabeth Olmsted-Davis, and Alan R. Davis. Conference: AIMM/ASBMR John Haddad young investogators meeting. Snowmass Colorado, April 2010. Presenter – Elizabeth Olmsted-Davis

Ronke M. Olabisi, Chi-Wei Hsu, Alan R. Davis, Elizabeth A. Olmsted-Davis, Jennifer L. West. Cathepsin-K Sensitive Poly(ethylene) Glycol Hydrogels for Degradation in Response to Bone Formation. In Society for Biomaterials Annual Meeting and Exposition, San Antonio, TX, 22 - 25 April 2009.

Ronke M. Olabisi, ZaWaunyka Lazard, Mary Hall, Eva Sevick, Alan R. Davis, Elizabeth A. Olmsted- Davis, Jennifer L. West, Hydrogel microspheres increase cell survival and increase new bone volume in a gene therapy bone formation model. In Society for Biomaterials Annual Meeting and Exposition, Seattle, WA, 21 - 24 April 2010.

Poster presentation:
Z Lazard, R Olabisi, A.R. Davis, J. West, and E Olmsted-Davis. An injectable Method for Spinal Fusion. Texas Bone Program Annual Meeting, 2010. Houston TX.

E. Salisbury, Z. Lazard, E. Rodenberg, A.R. Davis, and E.A. Olmsted-Davis. Neuronal Regulation of Early Heterotopic Ossification. Texas Bone Program Annual Meeting, 2010. Houston TX.

Ronke M. Olabisi, Chi-Wei Hsu, Alan R. Davis, Elizabeth A. Olmsted-Davis, Jennifer L. West, Cathepsin-K and Osteoclast Sensitive Poly(ethylene) Glycol Hydrogels. In 56th Annual Meeting of the Orthopaedic Research Society, New Orleans, LA, 6 - 10 March 2010.

Ronke M. Olabisi, Chi-Wei Hsu, Alan R. Davis, Elizabeth A. Olmsted-Davis, Jennifer L. West, Cathepsin K Sensitive Poly(ethylene) Glycol Hydrogels for Degradation in Response to Bone Formation. In Gordon Research Conferences – Biomaterials: Biocompatibility / Tissue Engineering, Holderness, NH 19 - 24 July 2009.

Manuscripts:
We have four manuscripts in preparation; however, nothing has been accepted for publication yet.
Below is a description of the outlines for these manuscripts:

1. The first manuscript; “Assessing Mechanical Integrity of Spinal Fusion by in situ Endochondral Osteoinduction in the Murine Model”, describes the development of a representative biomechanical test for confirming spine fusion by a relevant clinical standard which is reduction of motion in the lumbar spine (*J. Ortho Res*., accepted, see appendix).
2. The second manuscript; “An Injectable Method for Spinal Fusion”, describes the cell based gene therapy system, which can reduce mobility, and fuse the spine through a single paraspinous injection. (In review *Molecular Therapy*, see appendix).
3. The third manuscript; “Cathepsin-K sensitive poly(ethylene Glycol) hydrogels for degradation in response to bone formation”, describes the *in vitro* studies with the PEG-DA hydrogel which can selectively be degraded with cathespin K. The manuscript presents all the biochemistry that went into designing the selectively degradable gel, demonstrating with purified cathespin K or general protease can degrade the material but other selective proteases cannot. Finally the manuscript presents the results of the studies to show selective degradation when incubated in the presence of osteoclasts, versus osteoblasts or other types of fibroblasts. (In review, *Biomaterials*, see appendix).
4. A fourth manuscript; “Hydrogel microsphere encapsulation of a cell-based gene therapy system increases cell survival of injected cells, transgene expression, and bone volume in a model of heterotopic ossification” demonstrates the benefits of using the PEG-DA hydrogel microbead structures for bone formation in mice. This manuscript is a comparison study between the microbeads and direct injection of the cells without hydrogel, in regard to cell viability, BMP2 synthesis and secretion, and bone formation. (*Tissue Engineering*, accepted, see appendix).
5. A fifth manuscript; “Microencapsulation of AdBMP2 transduced allogenic cells leads to robust bone formation in wild type rats”, is currently being assembled, and demonstrates the ability of the microencapsulation to mask antigens on the allogenic cells in outbred rats, leading to bone formation,

versus the unencapsulated allogenic cells which result in a large inflammatory response, but no bone formation. This work demonstrates also the ability to implement cell therapies where adenovirus is used, which would normally be removed. It allows for long term secretion of the transgene within the tissues. Finally the work also demonstrates the difficulties with cell therapies, in that even stem cell populations are unable to avoid the significant inflammatory response elicited from allogenic cells in outbred animals. Finally it demonstrates the differences between laboratory mouse strains, and working with other animal populations.

Conclusions:

We have demonstrated the ability of both the hydrogel encapsulated cells as well as the cells directly injected to induce heterotopic bone formation when implanted in the paraspinous musculature. This heterotopic bone formation can then rapidly fuse to the adjacent skeletal bone, even in the absence of injury or decortification. In both cases when cells are directly injected or hydrogel encapsulated the heterotopic bone can form a bridge between two or more vertebra to create spine fusion as demonstrated by histological, radiological and biomechanical analysis. We have optimized the hydrogel encapsulation and structures, to develop a method which rapidly generates small microbead structures, consisting of 1-100 AdBMP2 transduced cells. These encapsulation does not reduce transgene expression, or in this case secretion of the BMP2. It can freely diffuse into the media, similarly to the unencapsulated cells. Another benefit to the material is that there is absolutely no cell toxicity associated with the process. The cells tolerate the encapsulation, and have similar short term viability to the unencapsulated counterparts. Further, in vivo the hydrogel encapsulation actually protects the cells from targeted degradation, most likely due to the first generation adenovirus used in the transduction. Thus our data clearly shows that both cell lifespan and transgene expression are significantly expanded in vivo when cells are first encapsulated.

Interestingly, the microspheres not only lead to heterotopic ossification similar to the unencapsulated, but they appear to be capable of undergoing the same patterning, that is essential for long term viability of the HO and fusion. In our studies, we documented the patterning of the newly forming HO, to encompass the entire set of microbeads, but not invade any of the peripheral tissues, accept at points where it fused with the skeletal bone. Further, the interior amazingly functioned differently than the exterior which rapidly formed a thick layer of bone. The interior housed a tentative marrow cavity, with blood vessels, adipose, and nerves, suggesting that the normal skeletal bone architecture could be recapitulated even in the presence of the biomaterial. Finally we observed significant degradation and some removal-replacement of the material with bone, three weeks after delivery of delivery of the degradable sphere's encapsulating AdBMP2 transduced cell. This suggests that the material will slowly be removed without major disruption to the newly formed and fusing heterotopic bone. Thus, we have clearly demonstrated landmark steps in development of this therapy. HO can rapidly fuse into the vertebra without need for skeletal bone formation to create a stable fusion. Encapsulation of the cells in degradable hydrogel, allows for the cells to secrete BMP2 at designated locations. With bone only forming around the periphery of the beads, and eventual within. We are currently working on molding the microspheres into specific structures, implanting them and seeing if we can create specific shapes. With the ability to model specific structures, one could them provide an amazingly powerful tool for cranial facial reconstruction.

We have demonstrated the ability of the microspheres to protect the cells, and provide long term expression of the BMP2, even in when non-autologous cells were used. This provides significant advancement for manufacturing obstacles with other approaches in the literature. In our approach, the cells can be prequalified, and manufactured. Secondly, the transduction is transient, non integrating, so there is no worry that the insertion of the transgene will lead to disruption of a critical gene, or that instability of the genome, may lead to long term problems such as cancer, which have been reported for other types of integrating gene therapy approaches. Further, encapsulation of the cells, provides additional safety, that cells expressing BMP2 will not try to form any structures of the bone. In other words, our system is totally transient. It rapidly produces the fusion, allowing the skeletal bone, to take over maintaining the structure, while any potential adverse affects of the therapy are eliminated. Incorporation of the foreign cells chronically expressing BMP, would lead to a significant potential for adverse reactions in the skeletal bone and surrounding tissues. This family of factors is highly regulated, and involved in key patterning pathways that govern interactions between multiple tissues and structures. Leaving the gene permanently expressed in foreign stem cell integrating into the bone, even at low levels could lead to a significant adverse long term outcome including

chronic pain (Rosenberg et al, in preparation). Thus the ability to rapidly generate the fusion, and remove all the "foreign materials" so that the patient after healing is left only with their own cells, is a huge advantage.

Finally our work in the rat models, demonstrating that the allogenic primary cells, we have manufactured as a specific lot, and will use for completion of the efficacy testing, consistently produces bone formation at the targeted location, without causing any inflammatory reaction. This is the first time anyone has shown the ability to reproducible generate heterotopic ossification at a targeted location, in wild type outbred rats. From these data, we are nearing the end of phase 1 for this project, in that we now have a product that we can readily manufacture, and will reproducibly form HO, without adverse reaction. To further, these studies we are currently completing the efficacy data collection under GLP conditions, in wild type outbred rats. We have also working on confirming that the material will maintain its efficacy after cryopreservation of the material which will be critical to manufacturing and implementation of the therapy.

Completion of this project has and will continue to significantly advance the current state of gene therapy in this field by eliminating the search for an optimal osteoprogenitor cell, scaffolding, and allow for rapidly translation to the clinic. But even more importantly, it would offer a non-invasive alternative to current treatments for degenerative spine disorders. Posterolateral spine fusion, which normally results in 500-1000 cc of blood loss as well as a 5 to 7 day hospital stay and a recovery period of up to a year, could be performed on an outpatient basis with this minimally invasive procedure, without concern over undue morbidity. This technology would benefit a broad age range of patients, and greatly reduce treatment costs as well as loss work time. Our proposed method has the potential to improve the safety of current spine surgery techniques by offering a safe and efficacious outpatient alternative to surgery, which will eliminate patient down time, rehabilitation and associated risks with the current process. Finally it will provide an opportunity to patients who require spine fusion but are not candidates for major surgery.

References:

a. Hipp JA, Wharton ND. Quantitative motion analysis (QMA) of the spine. In: Yue JJ, Bertagnoli R, McAfee PC et al., eds. *Motion Preservation Surgery of the Spine*. 1st ed. New York: Elsevier Health, 2008

b. Zhao KD, Yang C, Zhao C et al. Assessment of noninvasive intervertebral motion measurements in the lumbar spine. *J.Biomechanics* 2005;38:1943-6.

c. Olmsted-Davis, E. A., Z. Gugala, et al. (2002). "Use of a chimeric adenovirus vector enhances BMP2 production and bone formation." Hum Gene Ther 13(11): 1337-47.

d. Olmsted, E. A., J. S. Blum, et al. (2001). "Adenovirus-mediated BMP2 expression in human bone marrow stromal cells." J Cell Biochem 82(1): 11-21.

e. Thies, R. S., M. Bauduy, et al. (1992). "Recombinant human bone morphogenetic protein-2 induces osteoblastic differentiation in W-20-17 stromal cells." Endocrinology 130(3): 1318-24.

f. Fouletier-Dilling, et al (2005). "A Novel Compound Enables High-Level Adenovirus Transduction in the Absence of an Adenovirus-Specific Receptor." Hum Gene Ther 16(11): 1287-1298.

g. Fouletier-Dilling, C. et al (2007). "Efficient and Rapid Osteoinduction in an Immune Competent Host." Hum Gene Ther 18(8):733-45.

Appendix:

1. Vessel Formation is Induced Prior to the Appearance of Cartilage in BMP2-Mediated Heterotopic Ossification; *Journal of Bone and Mineral Research*; Accepted.
2. An Injectable Method for Non-Invasive Spine Fusion;*The Spine Journal*; In review.
3. Hydrogel Microsphere Encapsulation of a Cell-Based Gene Therapy System Increases Cell Survival, Transgene Expression, and Bone Volume in a Model of Heterotopic Ossification; *Tissue Engineering*; Accepted.
4. Cathepsin-K Sensitive poly (ethylene Glycol) Hydrogels for Degradation in Response to Bone Formation: *Biomaterials*; In review.
5. Assessing Mechanical Integrity of Spinal Fusion by *in situ* Endochondral Osteoinduction in a Murine Modal; *J Orthopedic Surgery*; Accepted.

Revised Manuscript

Vessel formation is induced prior to the appearance of cartilage in BMP2-mediated heterotopic ossification

C. Fouletier Dilling[1], A.M. Wada[2], Z.W. Lazard[1], E.A. Salisbury[1], F.H. Gannon[3], T. J. Vadakkan[2], L. Gao[2], K. Hirschi[1,4], M.E. Dickinson[2], A.R. Davis[1,5], E.A. Olmsted-Davis[1,5]

[1]Center for Cell and Gene Therapy, Baylor College of Medicine, Houston, TX [2]Departments of Molecular Physiology and Biophysics, and Medicine, Baylor College of Medicine, Houston, TX [3]Department of Pathology, Baylor College of Medicine, Houston TX [4]Department of Pediatrics, Pediatrics-Nutrition, Baylor College of Medicine, Houston, TX [5]Department of Pediatrics, Hematology-Oncology, Baylor College of Medicine, Houston, TX

Funded in part by RO1EB005173-01, USMRMC 06135010 and USMRMC 06136005

Running title: Vessels form prior to cartilage

cdillingdk@yahoo.com, wada@bcm.tmc.edu, zwl@bcm.tmc.edu, salisbur@bcm.tmc.edu, fgannon@bcm.tmc.edu, vadakkan@bcm.tmc.edu, liangg@bcm.tmc.edu, mdickins@bcm.tmc.edu, khirschi@bcm.tmc.edu ardavis@bcm.tmc.edu, edavis@bcm.tmc.edu

Corresponding Author Alan R. Davis Center for Cell and Gene Therapy One Baylor Plaza Houston, TX 77030 Ph 713-798-1237 Fax 713-798-1230 ardavis@bcm.tmc.edu ar

Word count: Number of figures Abstract: 249
Black and White: 1 Manuscript: 6754 Color: 5

All authors have no conflicts of interest

Abstract

Heterotopic ossification (HO) or endochondral bone formation at non-skeletal sites, often results from traumatic injury, and can lead to devastating consequences. Alternatively the ability to harness this phenomenon would greatly enhance current orthopedic tools for treating segmental bone defects. Thus understanding the earliest events in this process would potentially allow us to design more targeted therapies to either block or enhance this process. Using a murine model of HO induced by delivery of adenovirus transduced cells expressing bone morphogenetic protein 2, BMP2, we show here that one of the earliest stages in this process is the establishment of new vessels prior to the appearance of cartilage. As early as 48 hours after induction of HO, we observed the appearance of brown adipocytes expressing VEGFs, simultaneous with endothelial progenitor replication. This was determined by using a murine model, which possesses the VEGF receptor 2 (flk-1) promoter containing an endothelial cell enhancer, driving the expression of nuclear-localized yellow fluorescent protein (YFP). Expression of this marker has previously been shown to correlate with the establishment of new vasculature (1) and the nuclear localization of YFP expression allowed us to quantify changes in endothelial cell numbers. We found a significant increase in Flk1-H2B::YFP cells in BMP2-treated animals as compared to controls. The increase in endothelial progenitors occurred three days prior to the appearance of early cartilage. The data collectively suggests that vascular remodeling and growth may be essential to modify the microenvironment and enable engraftment of the necessary progenitors to form endochondral bone.

Keywords: Bone morphogentic protein type2; heterotopic ossification; vessel formation

Introduction

Endochondral bone formation is thought to proceed through an ordered series of events, starting with the proliferation and “condensation” of presumptive mesenchymal cells to form avascular cartilage. Hence it is presumed that the lack of vasculature and associated cellular replication creates the hypoxic environment necessary for chondrogenic differentiation. However, recent data from our laboratory using a model of heterotopic ossification, suggests that vessels may play an essential role in the induction of chondrogenesis (2).

It has been well established that vessel formation plays a key role in late events during the process of bone formation. Vessels invade the perichondrium and hypertrophic zone and are required for the replacement of cartilage by bone (3). The angiogenic factor, vascular endothelial growth factor (VEGF) promotes vascular invasion via specific receptors, including Flk1 (VEGF-receptor 2) expressed in endothelial cells, in the perichondrium or surrounding tissue (4) (5). These events of cartilage matrix remodeling and vascular invasion are necessary for the migration and differentiation of osteoblasts and osteoclasts which remove mineralized cartilage matrix and replace it with bone. However, much less is known about the role of vessel formation prior to the appearance of the pre-cartilage tissue.

During normal wound repair, a series of cell signaling events are induced by the hypoxic state of the tissues, resulting in up-regulation of hypoxia inducible factor (HIF1) that in turn up-regulates a series of factors including several VEGFs (A, B, and D), leading to vessel formation. Hypoxia-induced angiogenesis has been proposed to be necessary for creating specialized vessels that facilitate progenitor homing and engraftment into damaged

tissues (6). Little is known as to whether such a process plays a key role in the repair of bone. Using a model of *de novo* bone formation to identify the earliest events in this process, we have demonstrated that myelo-mesenchymal stem cells are recruited to the tissues to form the early cartilage (7). One of the earliest events in this model is the appearance of brown adipocytes. These cells are capable of utilizing their uncoupled aerobic respiration to reduce localized oxygen tension and effectively pattern the newly forming cartilage condensations (8). This is consistent with *in vitro* data where bone marrow derived mesenchymal stem cells can undergo chondrogenesis in the presence of bone morphogenetic protein 2 (BMP2) and low oxygen (9). We also observed the appearance of vessels lining the edges of the perichondrial region, separated only by brown adipose, suggesting that perhaps the reduction in oxygen tension coordinately activates new vessel formation in the region (8). Thus, these progenitors may indeed be recruited to the site of new bone formation through the vasculature. In this study we focused on defining this tentative early vessel formation.

To determine this, we chose to employ a transgenic mouse model which expresses the fusion protein, human histone H2B with enhanced yellow fluorescent protein (EYFP) (H2B:YFP) in endothelial cells under the regulation of a Flk1 promoter/enhancer fragment (Flk1-H2B::YFP) (1). Recent improvements in genetically encoded fluorescent protein expression in animal models along with advances in optical imaging and image analysis software have enabled the analysis of many aspects of tissue development at a cellular level (10). Previous studies using this transgenic animal indicates that Flk1-H2B::YFP expression is restricted to endothelial cells of smaller and/or newly forming vessels (8), thus providing a mechanism for quantification of new vessels.

Here we demonstrate new vessel formation within the tissues prior to the appearance of the presumptive cartilage. Quantification of the number of endothelial cells shows that one of the first steps of bone formation is to induce additional endothelial cell proliferation. Histological analysis shows that increases in endothelial cell numbers are evident, just prior to the influx of chondrocytic progenitors. Immunohistochemical analysis of the tissues prior to the mesenchymal condensations, revealed a rapid and transient expression of VEGFA and D from the brown adipocytes. The data collectively, suggests that the brown adipocytes may play a key role in establishing patterning of the cartilage through regulation of oxygen tension within the tissues, through induction of both aerobic respiration, as well as early angiogenesis.

MATERIALS AND METHODS

Cell culture: A murine C57BL/6 derived cell line (MC3T3-E1) was obtained from American Type Culture Collection, propagated in αMEM supplemented with 10% fetal bovine serum (Hyclone, Logan, UT), 100 units/ml penicillin, 100 µg/ml streptomycin, and 0.25 µg/ml amphotericin B (Life Technologies Inc., Gaithersburg, MD). Briefly, the cells were grown in DMEM supplemented as described above and cultured at a subconfluent density in order to maintain the phenotype. All cell types were grown at 37 C and 5% CO_2 in humidified air.

Transduction of cells with adenovirus in the presence of GeneJammer®

***Adenoviruses*:** Replication defective first generation human type 5 adenovirus (Ad5) deleted in regions E1 and E3 was constructed to contain the cDNA for BMP2 in the E1 region of the viral genome (11). The virus particles (vp) to plaque forming unit (pfu) ratios

were: 55 and 200 for Ad5BMP2 and Ad5-empty respectively, and all viruses were shown to be negative for replication competent adenovirus.

The C57BL/6 cell line or MC3T3-E1 (1×10^6), were transduced with Ad5BMP2 or Adempty cassette control virus at a concentration of 5000 vp/cell with 1.2% GeneJammer® as previously described (12).

Heterotopic bone assay: The transduced cells were resuspended at a concentration of 5×10^6 cells/100 µl PBS, and then delivered through intramuscular injection into the hind limb quadriceps muscle of Flk1 mice. Animals were euthanized at daily intervals and hind limbs were harvested, embedded and placed at -80°C. All animal studies were performed in accordance with standards of the Baylor College of Medicine, Department of Comparative Medicine after review and approval of the protocol by the Institutional Animal Care and Use Committee (IACUC).

Histological analysis and staining analysis:

Soft tissues encompassing the site of new bone formation were isolated from the rear hind limb of the mice. Both the skin and skeletal bone were removed from the tissues prior to freezing. Serial sections (15 µm) were prepared that encompassed the entire tissues (approximately 50 sections per tissue specimen). We then performed Hematoxylin and Eosin staining on every 5^{th} slide which allowed us to locate the region containing either our delivery cells or the newly forming endochondral bone. Serial unstained slides were used for immunohistochemical staining (either single or double-antibody labeling). For double antibody labeling, samples were treated with both primary antibodies simultaneously

followed by washing and incubation with respective secondary antibodies, used at 1:500 dilution to which Alexa Fluor 488, 594, or 647 were conjugated. Primary antibodies were used as follows: SMA mouse monoclonal used at 1:200 dilution; Sigma Chem Co, St Louis, MO), CD31 (rat monoclonal used at 1:75 dilution; BD Pharmingen, San Diego, CA), Flk1 (goat polyclonal used at 1:100 dilution; R&D systems, Minneapolis, MN), Ki67 (rat monoclonal used at 1:100, Dako, Carpinteria, CA), VEGF-D (goat polyclonal used at 1:100 dilution, Santa Cruz Biotechnology, INC, Santa Cruz, CA). Stained tissue sections were examined by confocal microscopy (Zeiss Inc, Thornwood, NY, LSM 510 META) using a 20x/0.75NA objective lens.

Flk1 positive cell quantification in BMP -induced tissues: To quantify the increase in YFP positive cells in the BMP-induced tissues, frozen sections across these tissues were counterstain with DAPI and the YFP expression was compared to that obtained in the control tissues. First, a series of low magnification (5.4x and 12x) bright field images of a tissue section were taken and overlapped to reconstruct the tissue section using Adobe Photoshop CS3. The reconstructed montage image was used to measure the area of the tissue section using a manual contour tracing method (Zeiss Axiovision). The area of each of the frozen sections was calculated in a similar manner. Area measurements are used to determine the density of labeled cells as indicated below.

High resolution (10X/NA0.45, 1024x1024 pixels), dual channel images of tissue sections nuclear stained with DAPI were taken using a confocal microscope (Zeiss LSM 510 META). In each image, the number of nuclei in the DAPI and YFP channels was counted using a modified watershed segmentation algorithm (FARSIGHT, RPI) which makes use of both intensity and volume thresholds to distinguish two nuclei as separate. All

the nuclei counted using the software were DAPI positive. The fraction of DAPI stained nuclei marked by YFP were counted as YFP positive. The density of YFP positive cells in a tissue section was defined as the ratio of the number of YFP positive nuclei in the tissue section measured from the high magnification images to the area of the tissue section measured from the low magnification images. The density of the YFP positive nuclei was calculated for a number of control and BMP treated tissues at 2 and 4 days after injection. The ratios were then averaged over the various control and BMP2-treated tissues. The p-values were calculated using a Student's t-test.

Flk1-YFP positive cell association analysis:

To characterize the cell type(s) that express YFP in the adult muscle tissue, we performed immunoflourescent studies using endothelial cell marker CD31 and Flk1 antibodies; for vascular smooth muscle cells -smooth α actin (SMA). Association of cells expressing YFP with immuno-labeled cells was analyzed using (FARSIGHT, RPI, NY) and a custom program written in MATLAB (MathWorks, Natick, MA). After identification of each nucleus by DAPI staining, YFP positive and negative cells were then analyzed for association with fluorescent signals of each antibody. An intensity threshold was applied to the red channel in each image to identify a cell positive or negative for the immunofluorescent signal. Each identified nucleus and overlapping red channel were counted as CD31, Flk1, or SMA positive and then as either YFP negative and positive. Co-localization percentages are shown in the supplemental data section (Table S-1) and describe in detail the YFP positive cell types. The number of YFP+/Ki67+ nuclei in an area of the tissue was calculated by adding the YFP+/Ki67+ in each of the confocal images taken within the area. The area

fraction of YFP+/Ki67+ was defined as the total number of YFP+/Ki67+ in the images taken within the area divided by the number of images. The area fraction was measured for five different areas and the average area fraction was calculated for control and BMP treated tissues for every 5th slide sectioned throughout the entire hindlimb. The area fractions of YFP+/Ki67+ nuclei in the control and the BMP treated tissues on day 2 were 3.97 ± 2.96 and 6.11 ± 1.76 respectively. The area fractions for day 4 were 5.04 ± 0.72 and 6.41 ± 1.41 in the control and the BMP treated tissues. Based on the Student's t-test, the p value for the day 2 data was 0.21 and that for the day 4 data was 0.10. Taken together, the data supports the trend that YFP+/Ki67+ population increases on day 2 and day 4 after the BMP treatment.

Q-RT-PCR: Non-skeletal tissues (n=4 per group) surrounding the site of injection of the AdBMP2 or Adcontrol transduced cells were isolated at daily intervals for 7 days and prepared as total RNA using a Trizol reagent (Life Technologies, Carlsbad, CA) in accordance with the manufacturer's specifications. The two groups of RNAs were subjected to Q-RT-PCR analysis in parallel and the Ct values obtained normalized to both internal 18S ribosomal RNA used in multiplexing, and to each other to remove changes in gene expression common to both the BMP2 and control tissues by using the ® method of ΔΔCt along with Taqmanprimers and probes (Applied Biosystems, Carlsbad, CA) as previously described (8).

RESULTS

Upregulation of vessel markers prior to the onset of chondrogenesis:

We have previously described a model of rapid endochondral bone formation (13) in which mineralized bone is observed 7 days after the initial induction with BMP2. Observation of vessels lining the newly forming perichondrium suggests that vessels may undergo replication prior to chondrogenesis. To confirm this hypothesis, we examined tissues, at 24 hour intervals over the period leading up to chondrogenesis (day 5), for the presence or absence of endothelial cell replication. Figure 1 shows the co-expression of the endothelial cell specific factor, von Willibrand factor (VWF) (red) and Ki67 (green), a marker of cellular replication (14) in the vessels from tissues that received AdBMP2 transduced cells, starting 24 hours to 5 days (panels A-E, respectively). As can be seen in Figure 1, panel B, we did observe overlap of these two markers (yellow color), in tissues receiving the AdBMP2 transduced cellswhereas no replicating endothelial cells were observed in the control tissues (Panel F). We did not attempt to quantify the amount and apparent timing of replication using this method, because VWF is an extracellular matrix protein. Instead we employed the Flk1H2B::YFP model for quantifying endothelial progenitor replication over the course of early bone formation.

Flk1-H2B::YFP in vessels:

We next determined if there was a significant increase in the number of Flk1+ endothelial progenitors during bone induction, consistent with new vessel formation, prior to chondrogenesis. We chose to utilize the Flk1-H2B::YFP mouse model (1), in which new vessel formation could be readily quantified within the muscle tissues. Flk1 is a VEGF

receptor transiently expressed on endothelial cells, and is presumably thought to contribute to VEGF induced endothelial cell replication (15). Therefore quantification of the nuclear YFP expression within tissues from animalsreceiving either AdBMP2 or Adempty transduced cells allowed us to to quantify increases in the number of endothelial progenitors within the muscle prior to cartilage formation. We previously quantified the association of Flk1-H2B::YFP with other endothelial cells markers such as CD31, and found them to be 95% overlapping (supplemental data). Frozen sections were prepared by serial sectioning from Flk1-H2B::YFP adult hind limb soft tissue (n=4 per group) consisting of three groups, those receiving: (1) cells transduced with Ad5BMP2, (2) cells transduced with Ad5empty cassette control virus, and (3) normal mouse muscle. To ensure uniform quantification and adequate sampling, the entire region of soft tissues in the hind limb was sectioned and approximatelyever fifth section was for analyzed for YFP expression.

To quantify differences in the number of endothelial progenitors, the number of YFP+ cells per the total number of DAPI+ cells was determined using automated segmentation methods (see Materials and Methods). The total YFP+ cells was also quantified per total area of the tissue section to ensure there was no bias in the fields of view chosen for image analysis (see Materials and Methods). The total area of each tissue section was determined using a montage of images that were collected using wide-field microscopy (panels A and F) (figure 2). As can be seen in Figure 2, we found Flk1-H2B::YFP positive cells in both tissues receiving Adempty transduced cells (panels B-E) and AdBMP2 transduced cells (panels G-O). These panels are higher magnification confocal images of the region within the corresponding white box on the lower magnification high resolution wide-field montage of the entire tissues (panels A;

control and F; BMP2). The results of the quantification, (figure 3), shows the average number of Flk1H2B::YFP+ cells on day 2 and day 4. Analysis of the entire soft tissue within several mice showed a significant elevation in tissues receiving the AdBMP2 transduced cells ($p=0.017$, day 2 (Fig 3A) and $p=0.006$, day 4 (Fig 3B) as compared to the control, on both days 2 and 4. The peak was approximately 2 days after induction of bone formation with no statistically significant difference between these results and those obtained in tissue sections isolated 4 days after induction.

Endothelial progenitors undergo replication in tissues receiving AdBMP2 transduced cells: In the tissues receiving cells transduced with a control adenoviral vector, we observed randomly scattered YFP+ cells along the vessel structures, while in the tissues receiving AdBMP2 transduced cells we see clustering of the YFP+ cells (Figure 2). This prompted us to question whether the Flk1-H2B::YFP progenitors could be replicating, so we next quantified the number of Flk-H2B::YFP positive cells in these tissues. Representative images used for quantification of YFP positive cell proliferation activity are shown in Figure 4. Replicating endothelial progenitors were defined as nuclei positive for both Flk1-H2B::YFP (yellow) and the cell proliferation marker, Ki67 (red; figure 4). In both control and treated animals, we also observed proliferating cells, positive for Ki67, that did not overlap with Flk1-H2B::YFP. Quantification of cells positive for both Flk1-H2B::YFP and Ki67 (figure 4) indicates a large number of replicating endothelial progenitors in both control and BMP2 treated tissues at two days after induction. Therefore the percentage of dual positive cells was not significant at this early time point as compared to the control. However, by four days after induction with BMP2, we observed much fewer replicating Flk1-H2B::YFP cells in the control and significantly more in the experimental group (figure

4). This difference was found to be statistically signifcant.

Vascular Endothelial Growth Factor (VEGF) mRNA expression:

Endothelial progenitor replication appeared to start within 48 hours of induction with BMP2. This correlated with a significant elevation in the vascular endothelial growth factor, VEGF-D (also termed fos-induced growth factor, FIGF) and VEGFA, RNA expression (figure 5). Figure 5 show the changes in VEGF mRNA expression from day 1 after injection of AdBMP2-transduced cells until day 6 as determined by real time reverse transcription PCR (Q-RT-PCR). Both VEGF-A and VEGF-D mRNA expression was significantly increased on days 2 and 4 after induction of bone formation. VEFG-B and VEGF-C however, remained on the same level throughout the time course. Although the data cannot differentiate between expansion of cells expressing VEGF-A and -D elevated transcription within cells residing in the area, the results suggest that these potent endothelial growth factors are rapidly and transiently increased within the site of new bone formation prior to the onset of cartilage.

Role of brown adipose in vessel formation:

The data collectively suggests that vessel replication is occurring simultaneously with elevated expression of VEGFs within the tissues. Since one of the earliest events observed in our model, is the recruitment and expansion of brown adipocytes (8) we next chose to determine if these cells might be expressing the VEGFs.

Immunohistochemical analysis of Flk1-H2B::YFP tissues that received either

AdBMP2 or Adempty transduced cells, showed co-localization of VEGF-D (green; fig 6, panel c) and the brown adipocyte specific marker uncoupling protein 1 (UCP1; red; fig 6, panel d) (day 2). As can be seen in figure 6, panel e, the expression of UCP1 overlaps expression of VEGF-D, in cells which are adjacent to the Flk1-H2B::YFP+ endothelial progenitors, suggesting that the brown adipocytes may be contributing to the new vessel formation. We observed additional fluorescence within the surrounding muscle, which appears to be punctate, and not cell associated. This staining may represent secreted VEGF-D protein, in the tissues. To confirm the cell specific expression of VEGF-D in the brown adipocytes, we performed additional immunostaining, (Figure 6f). Positive expression of VEGF-D (brown staining) was observed only in the brown adipocytes, again suggesting that these cells may play a role in the regulation of new vessels.

Discussion

Similar physiological steps lead to bone formation during embryonic development and in adult organisms, for instance in fracture repair or heterotopic ossification. In both cases, bone formation begins with mesenchymal condensations and ends with maturation of the growth plate, recruitment of osteoblasts and the production of bone. Vascularization has been shown to play a critical role in this process, through the infiltration into cartilage to form vascularized bone (16). Here we present data that show that vessels play a much earlier role in patterning of the cartilage and bone. The results show the presence of new vessel formation prior to the onset of mesenchymal condensations and cartilage.

We have previously reported the presence of brown adipocytes within the tissues, two days after the initial induction. We have also shown that these cells regulate localized

oxygen tension through their unique metabolism (8). In this study we extend our knowledge of the functional role of brown adipocytes, to include their rapid and transient expression of the potent angiogenic factors VEGFA and D. Interestingly a similar rapid and transient expression of VEGFD has also been demonstrated in limb development and shown to be critical for patterning (17). We observed a biphasic expression pattern for VEGF-A and -D, suggesting multiple roles for this factor in bone formation. The second peak of expression correlates nicely with the transition of cartilage to bone formation which has been highly documented (16,18) However the first phase is less well studied, and in our model and appears to correlate with the establishment of new vessels just prior to the onset of chondrogenesis. Zelzer, *et al*, also reported a similar biphasic expression of VEGF-A during embryonic bone formation (19). In these studies, they showed two functional roles for VEGFA one prior to cartilage and one during the transition of cartilage to bone similar to our own observation in our model. The data collectively, suggests that the brown adipocytes may induce the synthesis of new vessels, as a component for patterning the newly forming cartilage. In the proposed model, the brown adipocytes induce new vessels, facilitating the recruitment of chondrogenic precursors, while at the same time lowering localized oxygen tension to allow for chondrogenic differentiation. In support of this mechanism, we show in this study, the presence of brown adipocytes, expressing VEGF-D only in areas adjacent to our newly expanding vessels as marked by Flk1H2B::YFP.

Using a model of rapid endochondral bone formation, we show the immediate expansion of vessels within the tissues in response to delivery of BMP2. Although BMP2/4 play a critical role in the patterning of cartilage and bone in the embryo (20), much evidence now links the bone morphogenetic proteins to a host of other earlier physiological functions

including vascularization of the early embryo (21) Thus it may not be surprising that the earliest stage of bone formation in our model is the induction of new vessel formation.

Upon BMP2 stimulation, the Flk-1-H2B::YFP endothelial progenitors expand, as the total number of positive cells per tissue area increases. The Flk1-H2B::YFP positive cells are clustered along individual vessels suggesting that these vessels are extending or remodeling in response to BMP2. At this point we can not determine whether this increase occurs via replication of tissue resident endothelial progenitors or the recruitment of progenitors to the site of new bone formation. Our data suggests that the expansion of these progenitors, at least in part, is due to the replication, since we observed an increase in the area of replicating endothelial cells within the tissues receiving AdBMP2 transduced cells on day 4 as compared to the control tissues. However, we can not rule out the possibility that at least some of these cells are recruited from either the circulation of surrounding tissues. Interestingly, their were significant clusters of replicating Flk1-H2B::YFP cells on day 2 in both tissue receiving the AdBMP2 and Adempty cassette transduced cells, suggesting that perhaps the initial inflammatory reponse may be somewhat masking the significance of the replication at this early time point. Alternatively, the increase in replication of the Flk1-H2B::YFP cell population at four days after induction of bone formation may represent the need for vascularization to recruit new chondro-osseous progenitors, since this coincides with the appearance of these cells within the tissues (22). However, recruitment from the surrounding tissue is equally likely, since recently, Kaplan *et al* (34) showed local stem and progenitor contribution to heterotopic bone formation in a murine model of stem cell transplantation, and this process may require new vessel formation for establishment of these cells.

Vascular endothelial growth factors (VEGFs) have been shown to be essential to expansion of both endothelial cells as well as vascular smooth muscle cells which assemble to form the vessel structure. Although VEGFA has been most commonly shown to be responsible for angiogenesis in most systems, recent studies in murine muscle, have found VEGF-D to be an extremely potent angiogenic factor (23). This family member is better known for its critical role in the expansion of lymphatic vasculature (23). In our model we see both factors highly expressed in the tissues receiving the BMP2 transduced cells, as compared to those receiving control cells. Again the rapid but transient elevation in VEGF expression suggests that these factors may be driving the endothelial cell replication. Knockout studies have confirmed that BMPs regulate vasculogenesis during embryonic development (24). Functional deletion of BMP-4 and the BMP I receptor in mice leads to impaired mesoderm precursors required for vascular development (25) (26). It has also been shown that addition of BMP neutralizing antibodies or noggin suppresses endothelial cell formation during development while addition of rhBMP4 promotes it (27).

We and others have recently shown the chondrocyte to be of myeloid original, which circulates to the site of new bone formation (28) (22). These cells must then recruit and pass from the vessels into the tissues, through a process known as extravasation (29) This process has been shown to require small vasculature, which has a reduced blood flow (29) Thus it is conceivable that brown adipocytes express the VEGFs to form new vessels, capable of permitting recruitment of chondrocytic progenitors to the correct location for endochondral bone formation. Since vascular invasion of the growth plate has been well documented to precede the recruitment of osteoblast progenitors to form the new bone (16,18,29,30), it would not be surprising to have an earlier phase of this process that

recruited the chondrocytic progenitors. We have previously shown that the brown adipocytes are capable of inducing hypoxia in the local environment which in the presence of BMP2 has been shown to induce chondrogenesis (8). Thus we propose that the brown adipocytes are capable of patterning the newly forming cartilage by inducing new vessel formation, while simultaneously removing oxygen through uncoupled aerobic respiration. Once the progenitors differentiate into chondrocytes, they then express a number of anti-angiogenic proteins, to prevent in growth of new vessels, thus momentarily attenuating this early wave of angiogenesis (31) (32) (33) (35). Thus the results presented in this study extend our knowledge about the critical nature vascularization plays not only in bone formation but in cartilage as well. The data collectively shows a novel process for patterning of new endochondral bone, in adult organisms. Further, this is one of the first studies that attempt to understand the biology of tissue engineering of cartilage. Surprisingly one of the critical components we have identified is contradictory to our current dogma, that cartilage does not require vessels. The study suggests that brown adipose may play a pivotal role in establishing new vessels, essential for recruitment of chondrogenic progenitors, and patterning of the tissues. These findings may ultimately play an important role in our efforts to replace damaged cartilage through tissue engineering.

Figure Legends:

Figure 1: Immunohistochemical analysis of endothelial cell replication in tissues isolated at daily intervals after induction of bone formation with cells expressing BMP2. (A-E) days 1, 2, 3 , 4, and 5 respectively, after injection of BMP2-producing cells, paraffin sections were prepared and stained with an antibody against Ki-67 followed by as secondary antibody conjugated to Alexa fluor 488 (green) mixed with an anti-Von Willibrand Factor (VWF) antibody followed by a secondary antibody conjugated to Alexa fluor 547 (red). **Panel F** shows a representative image, similar staining, taken from tissues isolated from mice injected with cells transduced with a control vector (Adempty).

Figure 2: Wide-field and confocal images of whole tissue sections and quantification of Flk1-H2B::YFP cells. (A,F) Representative montages of low magnification grayscale images (1 pixel = 0.003mm) used for calculating total area for tissue sections. A single representative tissue section is depicted after the entire hind limb muscles which encompassed the injection site were isolated 2 after receiving an intramuscular injection of cells transduced with either Ad empty control vector **(panel A)** or AdBMP2 **(panel B)** and sectioned at 15 uM thickness. Although every 5th section across the entire tissue was analyzed, we show only a single representative image of each type. The corresponding regions with positive YFP signal, shown by the boxed areas, were imaged by confocal microscopy (panels B-E, G-O) for counting the YFP positive cell numbers.

Figure 3: Increase in Flk-H2B::YFP positive cells in BMP2-induced tissue at Day 2 and 4. Quantification of Flk1-H2B::YFP cells within the tissues, two and four days afterinduction with AdBMP2 transduced or control cells. YFP nuclei were counted and reported as ratio of the total area of the tissue section determined using the wide-field montage. Flk-H2B::YFP positive cells were significantly elevated in the tissues receiving BMP2 as compared to the controls. The graph depicts the average number of Flk-H2B::YFP positive cells in 5 sections for Day 2 control, 7 sections for Day 2 BMP, 8 sections for Day 4 control, and 6 sections for Day 4 BMP. The number of images taken in each section ranged from 4 through 22.* denotes a significant difference as determined by the Student's t-test.

Figure 4: Quantification of YFP positive cell proliferation. Representative images of Flk1-H2B::YFP and the cell proliferation marker Ki-67. Co-localization of Flk1H2B::YFP (yellow) and Ki-67 (red), was detected in BMP2-treated and control tissues. Graphs show the total number of YFP+/Ki67+ in the images taken within the area divided by the number of images analyzed. The area fraction was measured for nine at day 2, five at day 4 BMP and eight at day 2, four at day 4 control different areas and the average area fraction was calculated for control and BMP treated tissues. The area fractions of YFP+/Ki67+ nuclei in the control and the BMP treated tissues on day 2 were 7.32 ± 3.26 and 10.20 ± 6.95 respectively. The area fractions for day 4 were 6.97 ± 2.32 and 11.26 ± 2.58 in the control and the BMP treated tissues. Based on the Student's t-test, the p value for the day 2 data was 0.29 and that for the day 4 data was 0.035. Taken together, the data showed that significant YFP+/Ki67+ population increases by day 4 after the BMP treatment, however, at day 2, there are no significant differences in dividing YFP cell population between control and BMP treated tissues.

Figure 5: Expression of VEGF-D during the early stages of endochondral bone formation. Results of real time quantitative RT-PCR analysis of *VEGF-A,-B,-C, and -D* mRNA levels in tissues surrounding the lesional site that received either the AdBMP2or Adempty cassette-transduced cells isolated at daily intervals for up to 7 days after initial injection. Four biological replicates were run in triplicate and the averages normalized against an internal standard (ribosomal RNA). The samples receiving AdBMP2 transduced cells were then compared to those obtained from the tissues receiving cells transduced with Adempty cassette virus. Therefore the graph depicts the fold changes in VEGF RNAs in the BMP2 samples over time as compared to the control tissues. Error bars depict ± one standard deviation unit. * denotes samples that had a statistically significant ($p < 0.05$) difference from all other samples by the ANOVA test.

Figure 6: Immunohistochemical staining for brown adipocytes expressing VEGFD (green color, c) in tissues isolated from the Flk1-H2B::YFP mice 4 days after receiving MC3T3 cells transduced with Ad5BMP2. Brown adipocytes were identified as cells expressing uncoupling protein 1 (UCP 1; **d,** red color) and the yellow color (**b**) represents the Flk-yfp+ endothelial cells within the muscle. The tissues were also stained with VEGFD antibodies (**c**) and counterstained with dapi (blue color, **a**) that stains the nucleus of cells. A merger of these stains (UCP-1, VEGF-D, and YFP) is shown in panel **e**. In panel **f** a paraffin section taken 4 days after injection of BMP2producing cells, was stained with an antibody against UCP1 and staining was visualized using 3,3'-Diaminobenzidine (DAB) as previously described (8). No staining was observed on a paraffin section taken 4 days after injection of cells transduced with the empty control vector Ad5HM4 (data not shown).

REFERENCES

1. Fraser ST, Hadjantonakis AK, Sahr KE, Willey S, Kelly OG, Jones EA, Dickinson ME, Baron MH 2005 Using a histone yellow fluorescent protein fusion for tagging and tracking endothelial cells in ES cells and mice. Genesis **42**(3)**:**162-71.
2. Shafer J, Davis AR, Gannon FH, Fouletier-Dilling CM, Lazard Z, Moran K, Gugala Z, Ozen M, Ittmann M, Heggeness MH, Olmsted-Davis E 2007 Oxygen tension directs chondrogenic differentiation of myelo-monocytic progenitors during endochondral bone formation. Tissue Eng **13**(8)**:**2011-9.
3. Colnot C, Lu C, Hu D, Helms JA 2004 Distinguishing the contributions of the perichondrium, cartilage, and vascular endothelium to skeletal development. Dev Biol **269**(1)**:**55-69.
4. Maes C, Stockmans I, Moermans K, Van Looveren R, Smets N, Carmeliet P, Bouillon R, Carmeliet G 2004 Soluble VEGF isoforms are essential for establishing epiphyseal vascularization and regulating chondrocyte development and survival. J Clin Invest **113**(2)**:**188-99.
5. Gerber HP, Vu TH, Ryan AM, Kowalski J, Werb Z, Ferrara N 1999 VEGF couples hypertrophic cartilage remodeling, ossification and angiogenesis during endochondral bone formation. Nat Med **5**(6)**:**623-8.
6. Li J, Zhang YP, Kirsner RS 2003 Angiogenesis in wound repair: angiogenic growth factors and the extracellular matrix. Microsc Res Tech **60**(1)**:**107-14.
7. Fouletier-Dilling CM, Gannon FH, Olmsted-Davis EA, Lazard Z, Heggeness MH, Shafer JA, Hipp JA, Davis AR 2007 Efficient and rapid osteoinduction in an immune-competent

host. Hum Gene Ther **18**(8)**:**733-45.
8. Olmsted-Davis E, Gannon FH, Ozen M, Ittmann MM, Gugala Z, Hipp JA, Moran KM, Fouletier-Dilling CM, Schumara-Martin S, Lindsey RW, Heggeness MH, Brenner MK, Davis AR 2007 Hypoxic adipocytes pattern early heterotopic bone formation. Am J Pathol **170**(2)**:**620-32.
9. Shen M, Yoshida E, Yan W, Kawamoto T, Suardita K, Koyano Y, Fujimoto K, Noshiro M, Kato Y 2002 Basic helix-loop-helix protein DEC1 promotes chondrocyte differentiation at the early and terminal stages. J Biol Chem **277**(51)**:**50112-20.
10. Hadjantonakis AK, Dickinson ME, Fraser SE, Papaioannou VE 2003 Technicolour transgenics: imaging tools for functional genomics in the mouse. Nat Rev Genet **4**(8)**:**613-25.
11. Olmsted EA, Blum JS, Rill D, Yotnda P, Gugala Z, Lindsey RW, Davis AR 2001 Adenovirus-mediated BMP2 expression in human bone marrow stromal cells. J Cell Biochem **82**(1)**:**11-21.
12. Fouletier-Dilling CM, Bosch P, Davis AR, Shafer JA, Stice SL, Gugala Z, Gannon FH, Olmsted-Davis EA 2005 Novel compound enables high-level adenovirus transduction in the absence of an adenovirus-specific receptor. Hum Gene Ther **16**(11)**:**1287-97.
13. Olmsted-Davis EA, Gugala Z, Gannon FH, Yotnda P, McAlhany RE, Lindsey RW, Davis AR 2002 Use of a chimeric adenovirus vector enhances BMP2 production and bone formation. Hum Gene Ther **13**(11)**:**1337-47.
14. Gerdes J, Schwab U, Lemke H, Stein H 1983 Production of a mouse monoclonal antibody reactive with a human nuclear antigen associated with cell proliferation. Int J Cancer **31**(1)**:**13-20.
15. Sato Y, Kanno S, Oda N, Abe M, Ito M, Shitara K, Shibuya M 2000 Properties of two VEGF receptors, Flt-1 and KDR, in signal transduction. Ann N Y Acad Sci **902:**201-5; discussion 205-7.
16. Reddi AH 1994 Bone and cartilage differentiation. Curr Opin Genet Dev **4**(5)**:**737-44.
17. Trelles RD, Leon JR, Kawakami Y, Simoes S, Belmonte JC 2002 Expression of the chick vascular endothelial growth factor D gene during limb development. Mech Dev **116**(1-2)**:**239-42.
18. Reddi AH 1992 Regulation of cartilage and bone differentiation by bone morphogenetic proteins. Curr Opin Cell Biol **4**(5)**:**850-5.
19. Zelzer E, McLean W, Ng YS, Fukai N, Reginato AM, Lovejoy S, D'Amore PA, Olsen BR 2002 Skeletal defects in VEGF(120/120) mice reveal multiple roles for VEGF in skeletogenesis. Development **129**(8)**:**1893-904.
20. Li X, Cao X 2006 BMP signaling and skeletogenesis. Ann N Y Acad Sci **1068:**2640.
21. Hogan BL 1996 Bone morphogenetic proteins in development. Curr Opin Genet Dev **6**(4)**:**432-8.
22. Shafer J DA, Gannon FH, Fouletier-Dilling CM, Lazard Z, Moran K, Gugala Z, Ozen M, Ittmann M, Heggeness MH, Olmsted-Davis E 2007 Oxygen tension directs chondrogenic differentiation of myelo-monocytic progenitors during endochondral bone formation. Tissue Eng **13**(8)**:**2011-9.
23. Rissanen TT, Markkanen JE, Gruchala M, Heikura T, Puranen A, Kettunen MI, Kholova I, Kauppinen RA, Achen MG, Stacker SA, Alitalo K, Yla-Herttuala S 2003 VEGF-D is the strongest angiogenic and lymphangiogenic effector among VEGFs delivered into skeletal muscle via adenoviruses. Circ Res **92**(10)**:**1098106.
24. Moser M, Binder O, Wu Y, Aitsebaomo J, Ren R, Bode C, Bautch VL, Conlon FL,

Patterson C 2003 BMPER, a novel endothelial cell precursor-derived protein, antagonizes bone morphogenetic protein signaling and endothelial cell differentiation. Mol Cell Biol **23**(16)**:**5664-79.
25. Mishina Y, Suzuki A, Gilbert DJ, Copeland NG, Jenkins NA, Ueno N, Behringer RR 1995 Genomic organization and chromosomal location of the mouse type I BMP-2/4 receptor. Biochem Biophys Res Commun **206**(1)**:**310-7.
26. Winnier G, Blessing M, Labosky PA, Hogan BL 1995 Bone morphogenetic protein-4 is required for mesoderm formation and patterning in the mouse. Genes Dev **9**(17)**:**2105-16.
27. Kelly MA, Hirschi KK 2009 Signaling Hierarchy Regulating Human Endothelial Cell Development. Arterioscler Thromb Vasc Biol.
28. Zhao Y, Glesne D, Huberman E 2003 A human peripheral blood monocyte-derived subset acts as pluripotent stem cells. Proc Natl Acad Sci U S A **100**(5)**:**2426-31.
29. Ruster B, Gottig S, Ludwig RJ, Bistrian R, Muller S, Seifried E, Gille J, Henschler R 2006 Mesenchymal stem cells display coordinated rolling and adhesion behavior on endothelial cells. Blood **108**(12)**:**3938-44.
30. Otsuru S, Tamai K, Yamazaki T, Yoshikawa H, Kaneda Y 2007 Bone marrow-derived osteoblast progenitor cells in circulating blood contribute to ectopic bone formation in mice. Biochem Biophys Res Commun **354**(2)**:**453-8.
31. Pufe T, Petersen WJ, Miosge N, Goldring MB, Mentlein R, Varoga DJ, Tillmann BN 2004 Endostatin/collagen XVIII--an inhibitor of angiogenesis--is expressed in cartilage and fibrocartilage. Matrix Biol **23**(5)**:**267-76.
32. Oshima Y, Sato K, Tashiro F, Miyazaki J, Nishida K, Hiraki Y, Tano Y, Shukunami C 2004 Anti-angiogenic action of the C-terminal domain of tenomodulin that shares homology with chondromodulin-I. J Cell Sci **117**(Pt 13)**:**2731-44.
33. Hayami T, Funaki H, Yaoeda K, Mitui K, Yamagiwa H, Tokunaga K, Hatano H, Kondo J, Hiraki Y, Yamamoto T, Duong le T, Endo N 2003 Expression of the cartilage derived anti-angiogenic factor chondromodulin-I decreases in the early stage of experimental osteoarthritis. J Rheumatol **30**(10)**:**2207-17.
34. Kaplan FS, Glaser DL, Shore EM, Pignolo RJ, Xu M, Zhang Y, Senitzer D, Forman SJ, Emerson SG 2007 Hematopoietic stem-cell contribution to ectopic skeletogenesis. J Bone Joint Surg Am **89**(2)**:**347-57.
35. Shukunami C, Iyama K, Inoue H, Hiraki Y 1999 Spatiotemporal pattern of the mouse chondromodulin-I gene expression and its regulatory role in vascular invasion into cartilage during endochondral bone formation. Int J Dev Biol **43**(1)**:**39-49.

Supplemental data:

To verify that the Flk-H2B::EYFP was restricted to endothelial cells, we first analyzed the normal adult muscle to examine that the Flk-1-H2B::EYFP expressed in the endothelial cells. YFP positive cells appeared to be association with the endothelial cells labeled by antibodies against CD31 and Flk1 (figure1). When endogenous Flk1 positive cells are immunolabled, smaller vessels showed co-localization of YFP and Flk1 positive cells,

however, not all the Flk1 positive vessels contained YFP positive cells. Since vascular smooth muscle actin (SMA) is also expressed by cell surrounding vascular endothelial cells, we examined whether the YFP expression is associated with the smooth muscle cells using SMA antibody for immuostaining, and we do see the YFP expression in smooth muscle positive vasculature (figure. 1). From our immunolocalization analysis, the endothelial marker VE-cadherin (data not shown) and CD31 marker also exhibit a similar localization pattern with YFP positive cells (figure. 1, table 1).

Using image analysis software, FARSIGHT (RPI, New York), we performed segmentation analysis on RGB images, where we associated immunostaining signals to the red channel, YFP to the green channel, and DAPI to the blue channel. First, DAPI stained nuclei in the blue channels were segmented using FARSIGHT. The total number of segmented nuclei was defined as the total number of cells. Similarly, YFP positive nuclei in the green channels were segmented and counted as YFP positive cells (figure. 1). The fraction of cells that were immumostaining positive was counted by taking the ratio of DAPI stained nuclei that were immumostaining positive (red channel) to the total number of DAPI stained nuclei. Then, the immuno-stained positive cells were classified as YFP positive cells and YFP negative cells. Data sets were quantified and described in the table 1. From this analysis, we demonstrated that adult muscle tissue express H2B::EYFP in the endothelial cells, however, they represents a subset of endothelial cells.

CD31 (8 pictures)	CD31+/DAPI+	YFP+ CD31+/YFP+	YFP+ CD31+/CD31+
Mean	84.56%	100.00%	20.74%
Stv	10.87%	†	16.95%
Confident Interval (95%)	7.10%	†	11.07%

Figure.1

Table.1

All nucleus → DAPI+ DAPI with CD31+ and YFP-→CD31+ DAPI with CD31-and YFP+ →YFP+

CD31 (8 pictures)	CD31+/DAPI+	YFP+ CD31+/YFP+	YFP+ CD31+/CD31+
Mean	84.56%	100.00%	20.74%
Stv	10.87%	†	16.95%
Confident Interval (95%)	7.10%	†	11.07%
VE-Cad (6 pictures)	**VE-Cad+/DAPI+**	**YFP+ VE-Cad +/YFP+**	**YFP+VE-Cad +/VE-Cad +**
Mean	87.67%	100.00%	8.61%
Stv	6.59%	†	3.67%
Confident Interval (95%)	4.31%	†	2.40%
FLK1 (6 pictures)	**FLK1+/DAPI+**	**YFP+ FLK1 +/YFP+**	**YFP+ FLK1 +/FLK1 +**
Mean	94.93%	100.00%	16.94%
Stv	5.22%	†	7.02%
Confident Interval (95%)	4.18%	†	5.61%
SMA (12 pictures)	**SMA +/DAPI+**	**YFP+ SMA +/YFP+**	**YFP+ SMA +/ SMA +**
Mean	62.64%	93.31%	23.53%
Stv	16.71%	10.04%	14.14%

CD31 (8 pictures)	CD31+/DAPI+	YFP+ CD31+/YFP+	YFP+ CD31+/CD31+
Mean	84.56%	100.00%	20.74%
Stv	10.87%	†	16.95%
Confident Interval (95%)	7.10%	†	11.07%
VE-Cad (6 pictures)	**VE-Cad+/DAPI+**	**YFP+ VE-Cad +/YFP+**	**YFP+VE-Cad +/VE-Cad +**
Mean	87.67%	100.00%	8.61%
Stv	6.59%	†	3.67%

DAPI with CD31+ and YFP+ →CD31+YFP+

Figure 1

Click here to download high resolution image

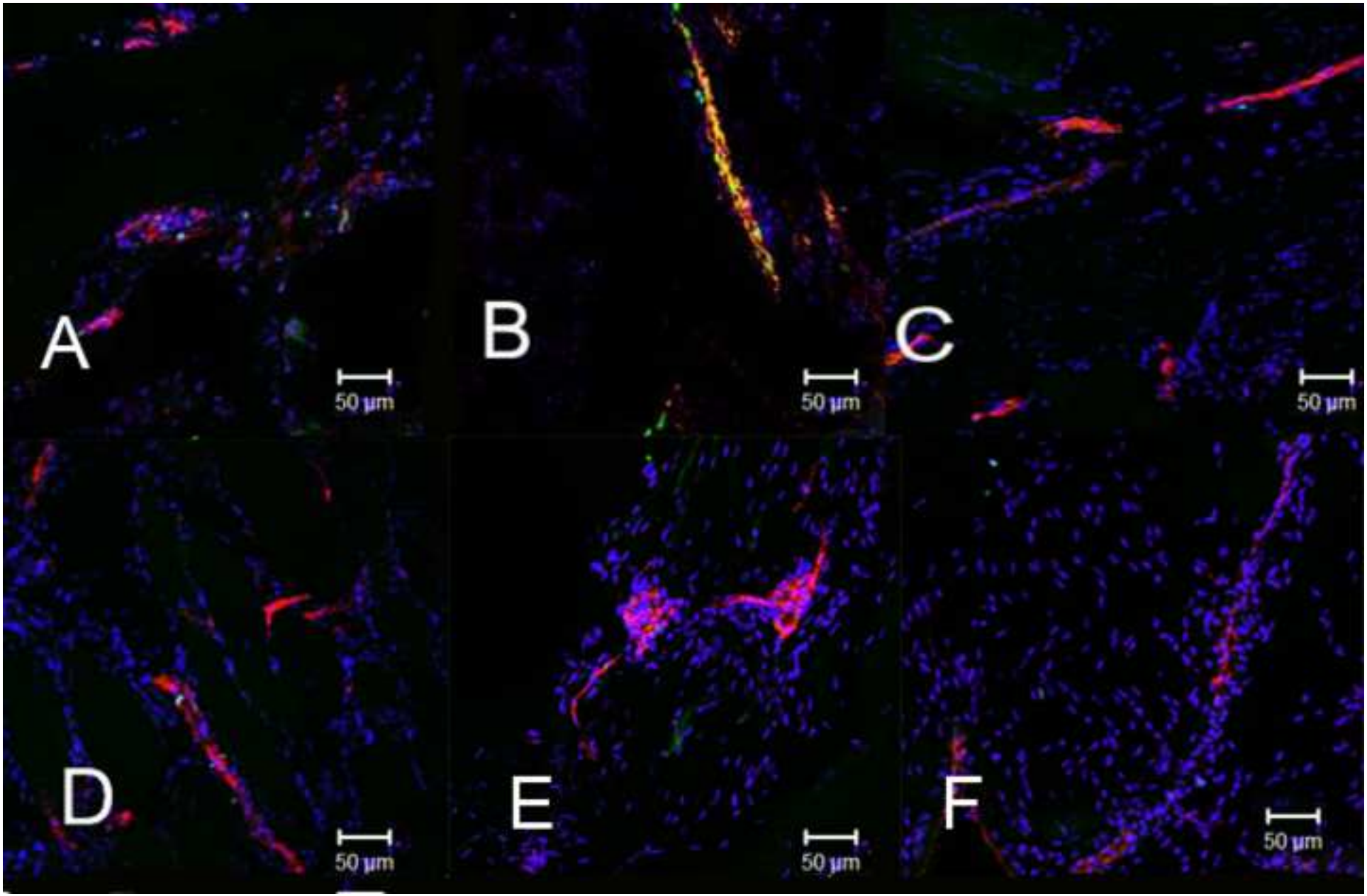

Figure 2

Click here to download high resolution image

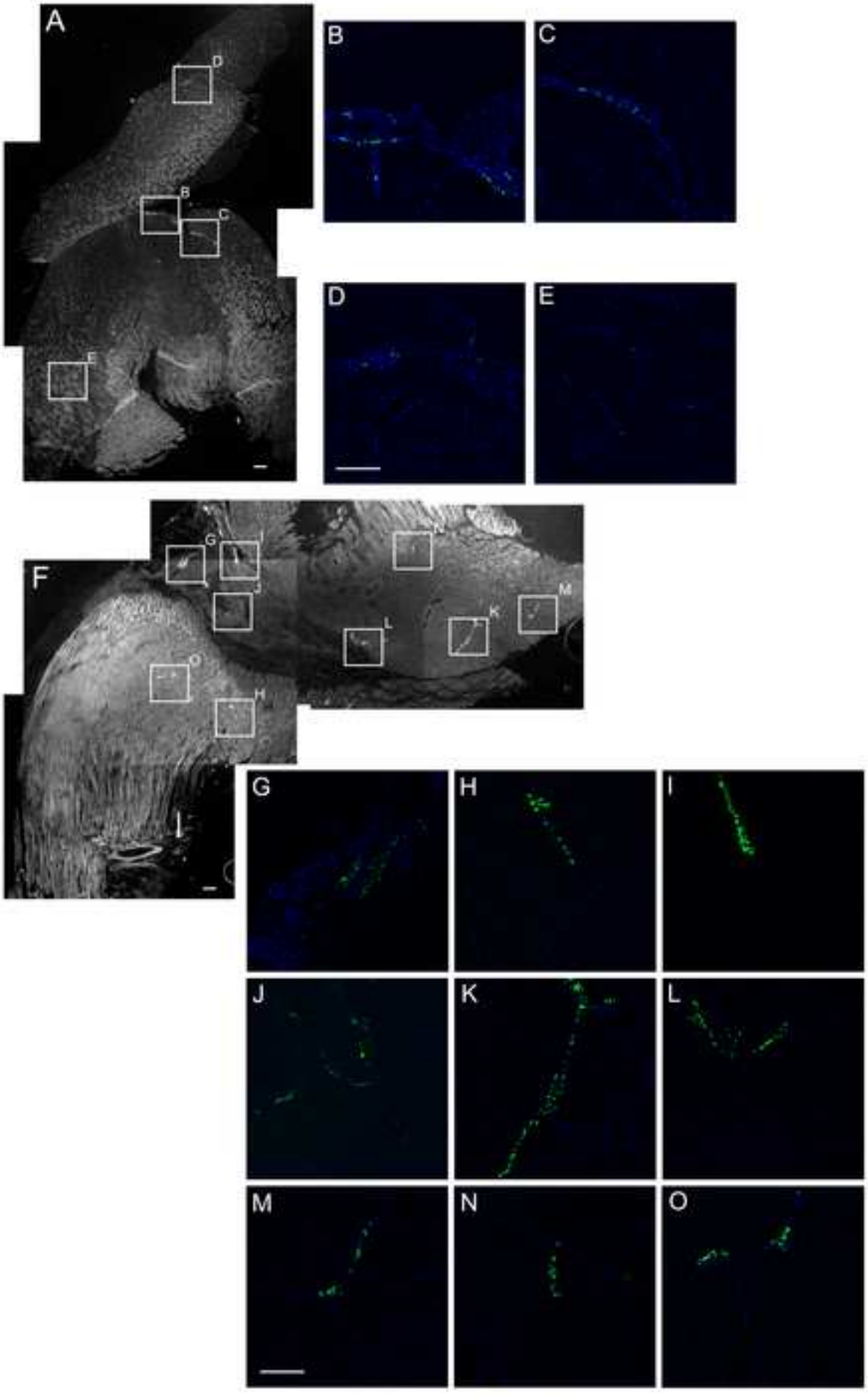

Figure 3

Click here to download high resolution image

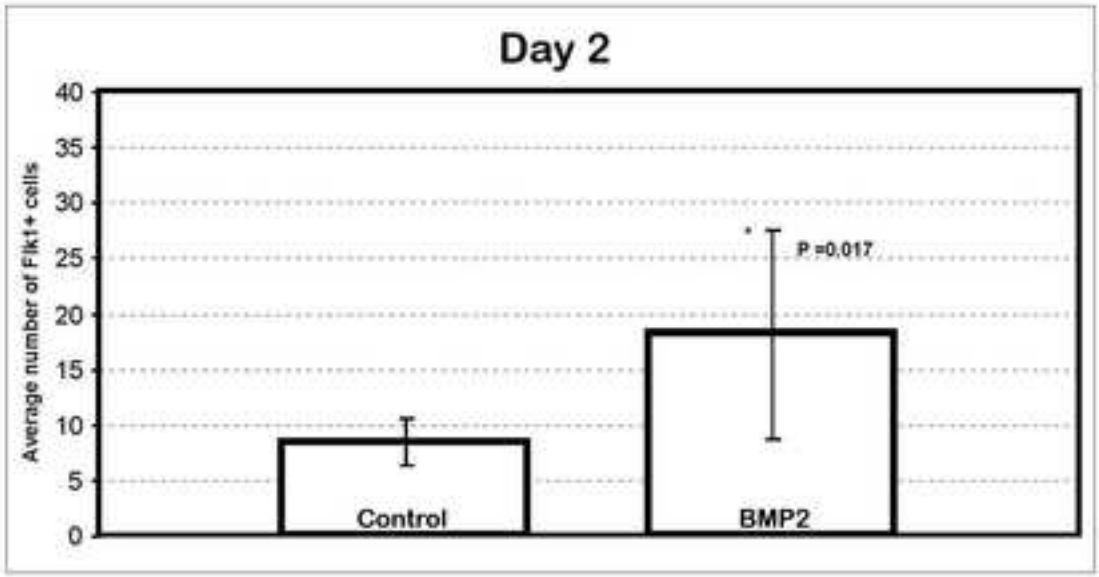

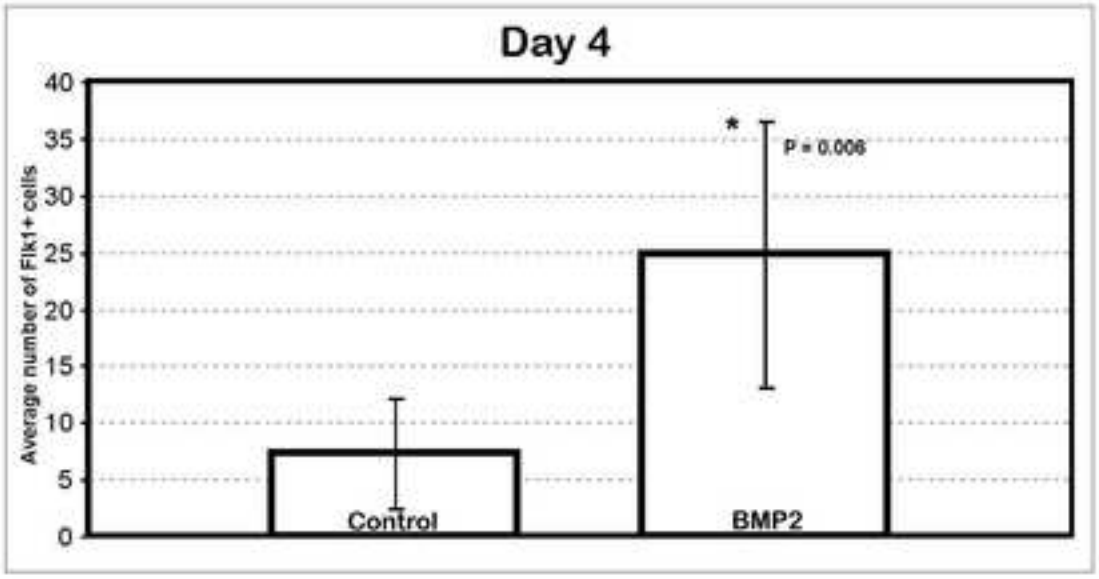

Figure 4

Click here to download high resolution image

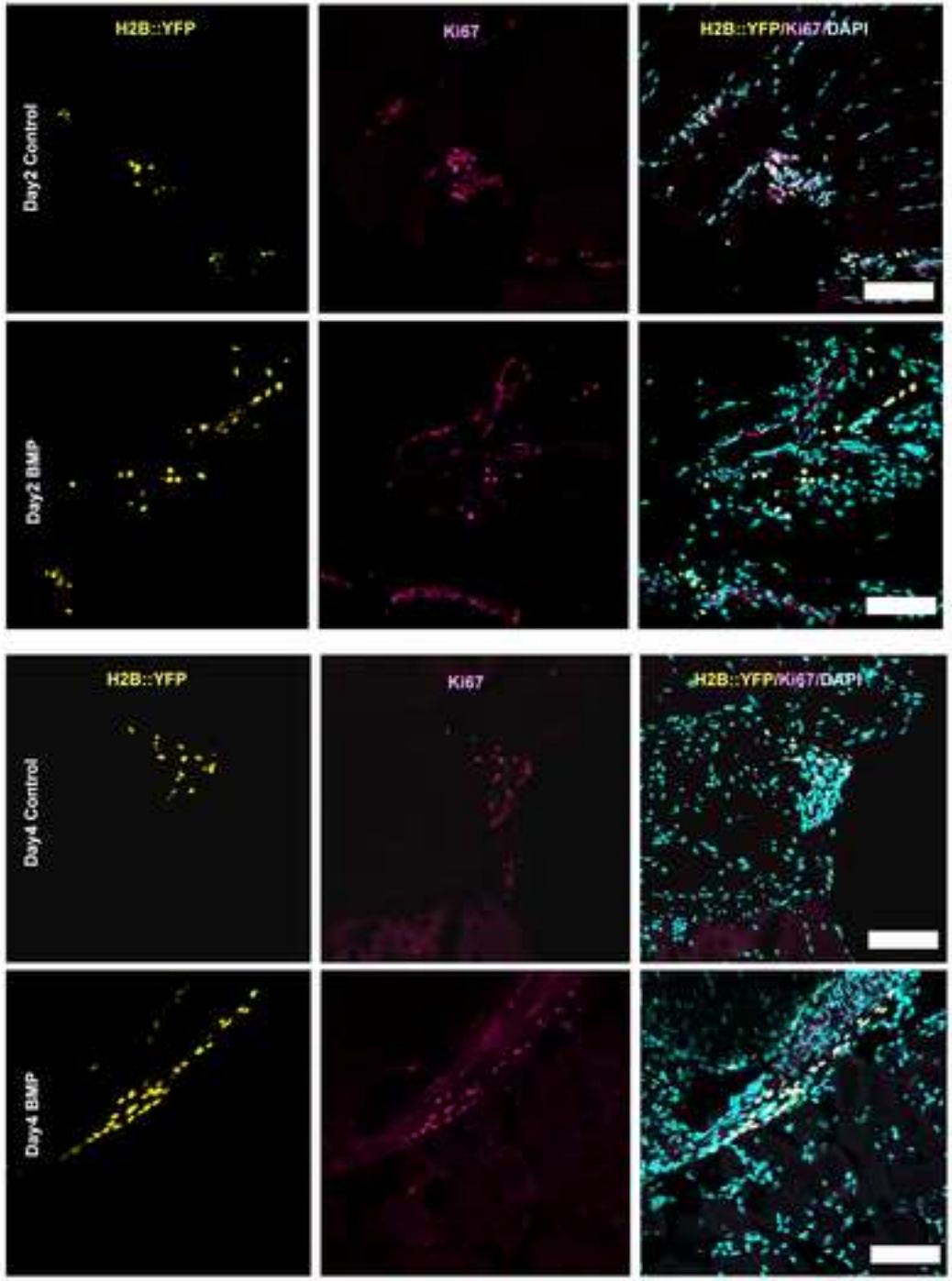

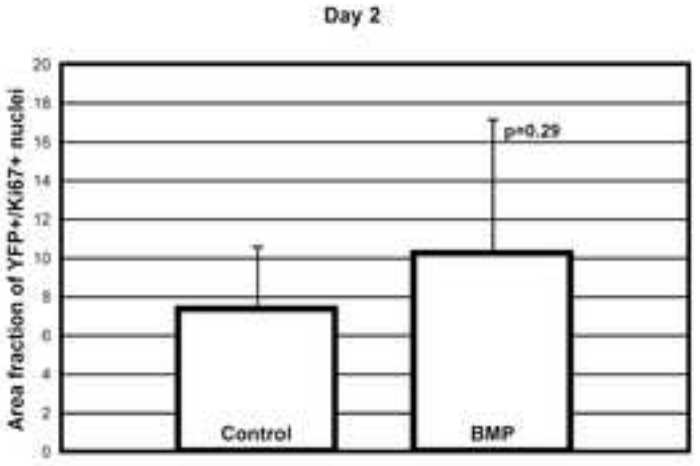

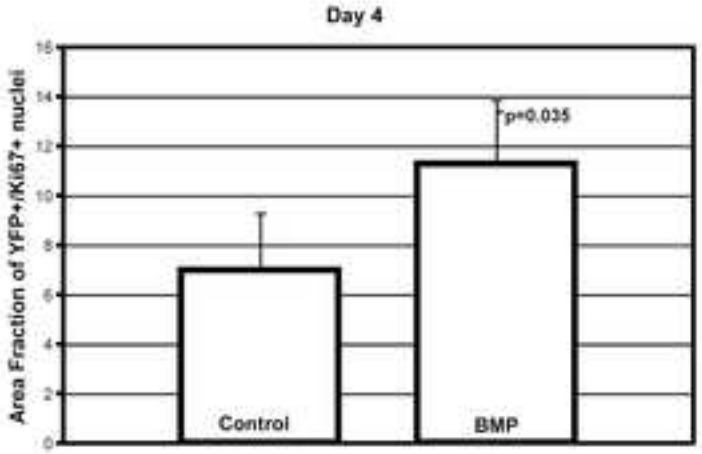

Figure 5

Click here to download high resolution image

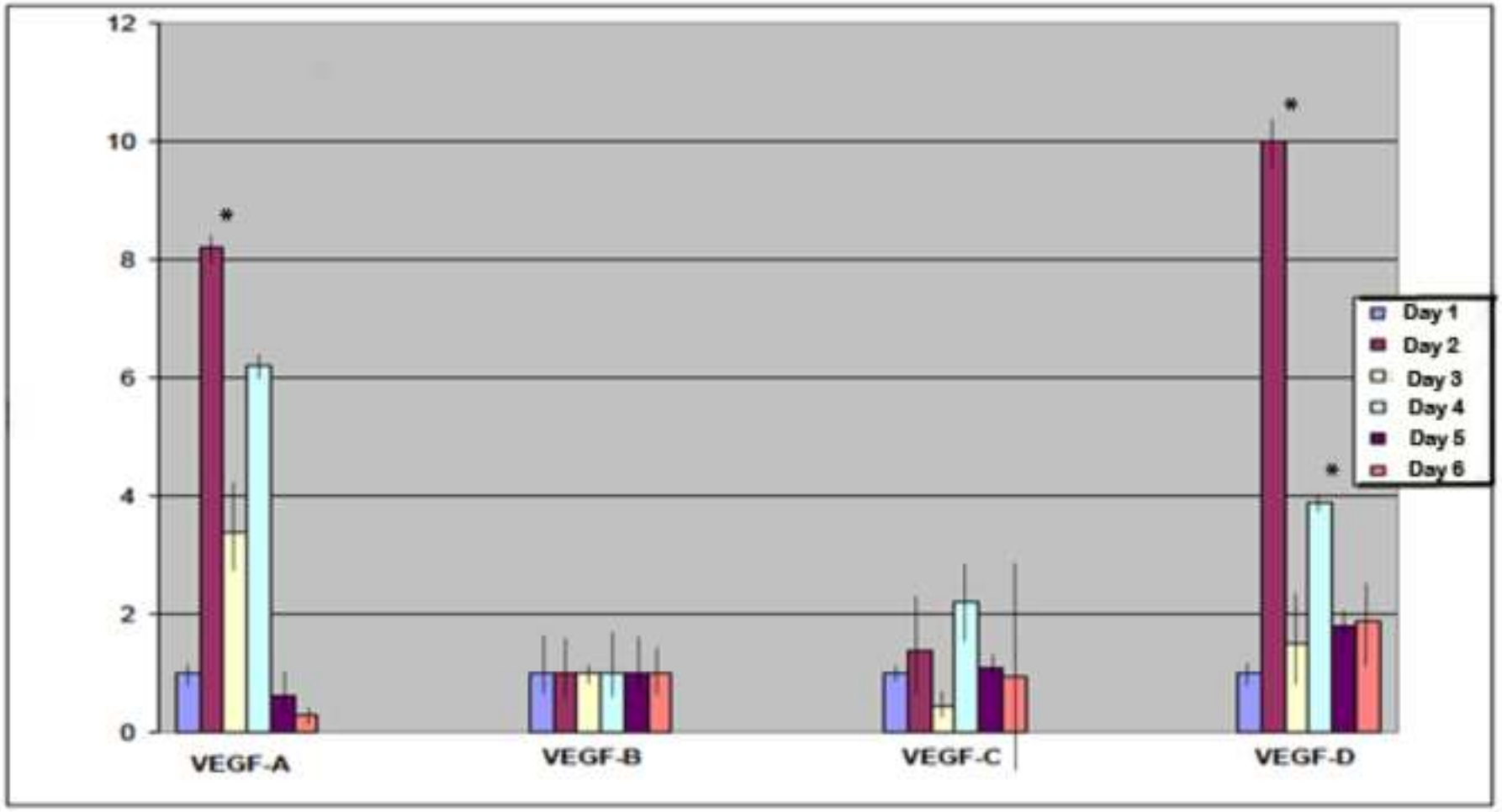

Figure 6

Click here to download high resolution image

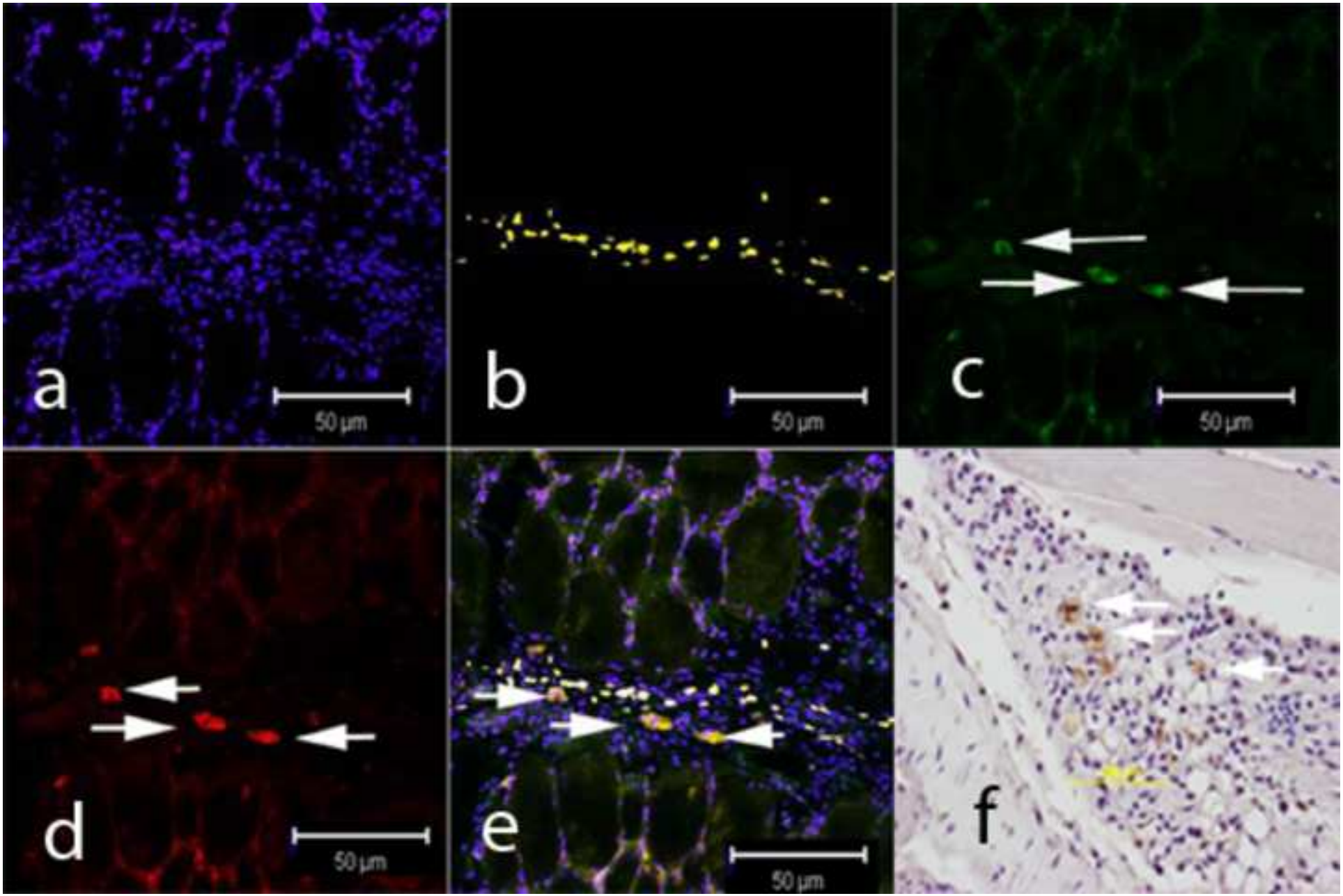

Non-Invasive Spine Fusion.

Ronke M Olabisi[1], Zawaunyka Lazard[2], Michael Heggeness[3], Kevin M Moran [3], John A Hipp[3], Ashvin Dewan[3], Alan R. Davis[2,3-4], Jennifer L. West[1] and Elizabeth A. Olmsted-Davis[2,3-4]

[1]Department of Bioengineering, Rice University, 6100 Main St. MS 144, Houston, TX 77005, USA

[2]Center for Cell and Gene Therapy, Baylor College of Medicine, Houston, TX 77030, USA;

[4]Department of Orthopaedic Surgery, Baylor College of Medicine, Houston, TX 77030, USA;

[5]Department of Pediatrics and Center for Cell and Gene Therapy, Baylor College of Medicine, One Baylor Plaza, Houston, TX 77030, USA;

Spine fusion has been achieved by a single injection of a cell-based gene therapy system, along the paraspinous musculature, which rapidly induces heterotopic ossification, and ultimately spinal arthrodesis. The system does not require carrier materials, additional hardware, or invasive surgery to decorticate the vertebral bone, but rather harnesses the body's capacity to rapidly produce heterotopic bone. By targeting the location of the heterotopic ossification, new bridging bone between the vertebras and fusion to adjacent skeletal bone was obtained as early as two weeks. Reduction in spine flexion-extension also occurred as early as two weeks after injection of the gene therapy system in 40% of the mice, with greater than 90% fusion by four weeks. These studies are the first to harness heterotopic ossification, and use it as a safe and efficacious injectable, system for the spinal arthrodesis.

Introduction:

Of the over 1 million bone grafts performed annually worldwide, 50% involve spinal fusions and 25% of these patients complain of donor site pain from the autograft harvest site for up to 2 years post-operatively(*1*). These complications have driven the search for and subsequent use of alternative treatments, such as the growing use of bone morphogenetic proteins (BMPs), which have long been demonstrated to induce bone formation (*2-4*)[2-5].

Recombinant human BMP2 (rhBMP-2) is FDA approved on collagen sponges for open long bone fractures and in metal cages for spinal fusion[2]. Without the sponge or the cage, the BMP2 cannot be localized and tends to diffuse from the desired site, reducing its efficacy and leading to adverse effects such as edema, ectopic bone formation and bone resorption in the graft area(*5*)[(3)]. Because BMPs are so rapidly diffused, large quantities of the protein are required, making the procedure very expensive (*3*). Furthermore, although the use of rhBMP-2 for spinal fusion may negate the need for an additional operation to harvest autograft bone, the method still necessitates an operation that introduces a permanent foreign object into the body(*4*). Furthermore, spinal fusion requires decortication of the transverse processes of the vertebrae targeted for fusion, stripping of all the paraspinous musculature from bone and a fairly long operative time(*1*) (*6*) [1, 10]. The decortication and stripping cause pain, and stripping the musculature compromises the stability afforded by these muscles and disrupt the blood supply to both bone and muscle, and promote scar formation. Finally even with addition of this morphogen, there is still a considerable failure rate in which the initial bone healing that was achieved was

inadequate to reduce motility of the spine (*5*) causing researchers to search for better methods of delivering higher doses of the BMP2 itself.

Recently Shore et al, (*7*) demonstrated that a mutation in the BMP2 receptor was responsible for the observed heterotopic ossification (HO) in the genetic disease fibrous dysplasia ossifican's progressiva (FOP). Soft tissues in individuals with this genetic disorder are replaced with heterotopic bone. The HO can rapidly form within a few days, and even replace skeletal bone if it becomes weight bearing. It readily fuses to the skeletal bone, and often leads to ankylosis of the joints. Harnessing this capacity in a targeted, controlled manner, would potentially allow for the regeneration of skeletal bones.

Gene therapy approaches hold much promise in achieving locally high levels of BMP2 for production of robust heterotopic ossification. However, many of the currently tested systems had difficulty in achieving efficient transduction of cells, and in turn expression of the BMP (*8*). In many cases, this problem was then enhanced by inclusion of a collagen sponge or other biomaterial that rapidly bind the BMP, again reducing its effectiveness[13]. Finally inclusion of the biomaterial and invasive decortication procedures cause undesired inflammation, which weakens bone healing (*5*)

Here we demonstrate the ability of cells expressing high levels of BMP2 to launch heterotopic ossification, at a targeted location, and ultimately fuse two or more vertebra within the lumbar spine. Fusion of both the heterotopic bone to the skeletal bone, and the resultant bridging of two vertebras were rapidly achieved, through simple injection. Within two weeks between 40-100% of the spines in two different murine models were considered fused by all criteria, radiological, histological, and biomechanical. In samples tested 4-6 weeks after induction, greater than 90% of the mice had achieved spine fusion in both models, and noticeable scoliosis was observed radiologically in the animal's spines suggesting that the fusion could restrain the spine, even during continued growth.

METHODS

Cell Culture

Human diploid fetal lung fibroblasts (MRC-5) and murine osteoblasts (MC3T3-E1) were obtained from the American Type Culture Collection (ATCC; Manassas, VA) and propagated in a humidified incubator at 37°C and 5% CO_2 in α-minimum essential medium (α-MEM; Sigma, St. Louis, MO) and Dulbecco's Modified Eagle's Medium (DMEM; Sigma, St. Louis, MO) supplemented with 10% fetal bovine serum (FBS; HyClone, Logan, UT), 1000 U/L penicillin, 100 mg/L streptomycin, and 0.25 µg/ml amphotericin B (Invitrogen Life Technologies, Gaithersburg, MD), as previously described (*9*)[12]. Murine stromal cells (W20-17; a gift from Genetics Institute, Cambridge, MA) were propagated and maintained as described by Thies *et al*(*10*).

Adenoviruses

Replication defective E1-E3 deleted first generation human type 5 adenovirus (Ad5) or a human type 5/35 adevnovirus (Ad5F35) in which the normal fiber protein has been substituted for the human adenovirus type 35 fiber (Ad5F35) were constructed to contain cDNAs for human BMP2 in the E1 region of the viruses(*11*). Two independent viruses were used based on their efficiency for transducing either human or mouse cells as described previously(*12*). For the viruses Ad5BMP2, Ad5F35BMP2, Ad5-empty cassette, and Ad5F35empty cassette the viral particle (VP)-to-plaque-forming unit (PFU) ratios were 55, 76, 200, and 111, respectively, and all viruses

were confirmed to be negative for replication-competent adenovirus. Ad5 viruses were used for the murine MC3T3-E1 cells and Ad5F35 viruses were used for the human MRC-5 cells (*12*).

Cell transduction

MC3T3-E1 cells (1×10^6) were transduced with Ad5BMP2 or Ad5-empty at a viral concentration of 5000 VP/cell with 1.2% GeneJammer®, as previously described(*12*). Briefly, GeneJammer® was added at 3% to α-MEM without supplements to and incubated for 10 min at room temperature. Ad5BMP2 or Ad5-empty was then added at the aforementioned concentrations and the mixture was further incubated for 10 min at room temperature. This virus solution was then diluted with supplemented α-MEM to achieve 1.2% GeneJammer® per volume. The resulting solution was next incubated 37°C for 4 hr with cells at an amount that just coated them, and then the mixture was diluted with supplemented medium at an amount appropriate for cell culture and incubated at 37°C overnight. MRC-5 cells were transduced as previously described with Ad5F35BMP2 or Ad5F35HM4 at a viral concentration of 2500 VP/cell(*11*). Briefly, virus was added to fresh supplemented DMEM and incubated with cells at 37°C overnight.

BMP-2 Quantification

BMP-2 expression was evaluated for MC3T3 and MRC-5 cells transduced with Ad5BMP2, Ad5-empty, Ad5F35BMP2 or Ad5F35HM4 using ELISA and alkaline phosphatase assays. Culture supernatant from transduced cells were collected 72 hours after adenovirus transduction and assayed with a BMP-2 Quantikine ELISA kit from R&D Systems (Minneapolis, MN) to measure BMP-2 expression. Transduced cells were cultured in 0.4 µm pore polycarbonate membrane transwell inserts (Corning Inc., Lowell, MA) and W20-17 cells were cultured in the wells of 6 well plates. After 72 hours W20-17 cells were assayed for alkaline phosphatase activity using a chemiluminescence procedure[18]. Three freeze-thaw cycles were performed in a 100-µM/cm^{2}concentration of 25mM Tris-HCl (pH 8.0) and 0.5% Triton X-100 in order to extract cellular alkaline phosphatase and this activity was then measured by adding a ready to use CSPD substrate with Sapphire-II enhancer (Tropix; Applied Biosystems, Foster City, CA) to the samples. After a 2 sec delay, the light output from each sample was integrated for 10 sec with a luminometer (TD-20/20; Turner BioSystems, Sunnyvale, CA). Alkaline phosphatase levels were recorded in relative luminescence units (RLU) and normalized to protein content with the bicinchoninic acid (BCA) assay, using bovine serum albumin to derive a standard curve. BMP2 protein levels and functional activity were found to be similar to previously published results per cell number and virus dose (*8*)

Spinal Fusion

Female NOD/SCID and C57BL/6 mice (8–12 weeks old; Charles River Laboratories; Wilmington, MA) and maintained in accordance to Baylor College of Medicine Institutional Animal Care and Use Committee (IACUC) protocols. Prior to paraspinous injections, the back of each mouse was prepared and a skin incision was made to reveal the paraspinous muscles. Although the injection could have been done without opening the skin, to insure appropriate placement of the material we opened the skin, prior to intramuscular injection. Transduced cells were removed with trypsin, resuspended at a concentration of 5×10^6 cells per 100 µl of PBS, and then delivered by intramuscular injection into the right paraspinous muscles along the length of the spine (Figure 1). After 2, 4 and 6 weeks, mice were sacrificed and the spines with attendant musculature were removed and fixed in formaldehyde solution (VWR; Sugar Land; TX).

MicroCT analysis

The intact spines were scanned at 14 µm resolution with a commercial micro-CT system (GE Locus SP, GE Heathcare, London, Ontario). Three-dimensional reconstructions of the spine and any mineralized tissue in the surrounding muscle were created at 29 µm resolution to visualize endochondral mineralized tissues. A volume of interest was defined for each specimen, and a threshold was chosen to exclude any non-mineralized tissue. The total volume of endochondral bone was then measured (eXplore MicroView, v. 2.0, GE Healthcare, London, Ontario) and spines of the animals were not taken into account for the measurements of mineralized tissue in the muscles of the animals.

Histological analysis

Fixed spines were decalcified in hydrochloric acid, processed and embedded into a single paraffin block, where serial sections were then cut at a thickness of 5-7 µm. The sections were stained with hematoxylin and eosin and observed under light microscopy. To further confirm the vertebral fusion, a subset of spines (n=9) were immersed in bleach for approximately one hour which removed all soft tissues. Midway through this process, nylon wire was threaded up the spinal canal in order to maintain the relative position of the vertebrae.

Biomechanical Testing

Prior to sectioning, formaldehyde fixed spines were encased in alginate in order to obtain flexion and extension radiographs. Spines were suspended in an in-house mold. Alginate powder was combined in an equal volume to water (30 ml of each) and mixed until smooth. The alginate was poured into the mold and allowed to solidify. Solidified molds were placed in an in-house spring-loaded clamp with rigid 100° arcs (Figure 4). Radiographs were taken of molds in flexion and extension orientations for each spine. These digitized radiographs were used to quantify intervertebral motion with Food and Drug Administration (FDA)-approved software (KIMAX QMA, Medical Metrics, Inc.) that has been validated to measure intervertebral motion with an accuracy of better than 0.5° of rotation and 0.5 mm of translation (*13-14*)[20, 21]. Intervertebral motion was measured at each level. Preliminary data (unpublished) demonstrated that the normal mouse spine undergoes an average of 5° of intervertebral motion using this test. Spines were considered fused when adjacent vertebrae did not exhibit rotation beyond 1.5°.

Statistical Analysis

Statistical analysis was performed as described previously(*9*)[12]. Briefly, all data were taken in triplicate and reported as mean and standard deviation. A Student t test with 95% confidence interval ($p < 0.05$) was done between the untreated control and each experimental condition.

RESULTS

To determine if our cell based gene therapy system induces spine fusion through intramuscular injection without invasive surgery or additional carriers, we established two different murine models for testing. We have previously characterized these models and found the heterotopic ossification to be similar (12). Here we have chosen to deliver the cell based gene therapy system to the paraspinous musculature in the region of the vertebral laminae, to determine if we can target the heterotopic bone formation to this location, to form bridging bone between two or more skeletal vertebra and ultimately fuse the spine. Figure 1 shows a schematic depiction of this approach, in which either adenovirus transduced cells expressing functional BMP2, or cells transduced with a similar adenovirus vector lacking BMP2 (Adempty cassette) are delivered to the paraspinous musculature of a mouse through a simple injection at points adjacent to the

levels of desired fusion. With this system, heterotopic ossification is generated rapidly, fused and remodeled into two or more of the adjacent vertebra, to reduce spine motion.

Radiological Analysis of Bone Formation:

Accordingly, heterotopic bone formation was allowed to progress for 2, 4 and 6 weeks, after initial injection, and then spines removed and analyzed for the presence of heterotopic bone, and spinal arthrodesis. Heterotopic bone formation occurred along the injection site, adjacent to the spine, with greater than 90% bridging and fusing to the skeletal bone, in all cases which received the AdBMP2 (Figure 2, three dimensional reconstructions E-L). Two dimensional radiographs (figure 2, panels A-D and M-P) show the cross sections through the tentative fusion. As can be seen in these studies, both the immune incompetent system, in which NOD/Scid mice receive human cells transduced with AdBMP2 (panels I-P), and immune competent mice, C57BL/6 (panels A-H), receiving AdBMP2 transduced allogenic murine cells, appear to both produce similar bone within 4 and 6 weeks, with a remodeled appearance of a contiguous cortical bone exterior. Although we did observe a number of the samples in the NOD/Scid animals with potential points of fusion, panel N shows a scenario in which the heterotopic bone, although extensive, has not yet fused into the vertebrae. It appears in panel J, that the heterotopic bone occurred slightly distal to the vertebral bodies. Interestingly, we did not see similar findings in wild type mouse models, as seen in panel B even at two weeks the substantial bone has fused to the adjacent vertebra. Admittedly the new bone does not appear to be as organized and remodeled as the later samples (4 and 6 weeks; panels C and D.

As can be seen in the cross-sectional radiographs, vertebral cortical bone appears to be integrated with the heterotopic bone (figure 2, panel B-D, O-P). The points of fusion appear to be in the laminae region of the vertebra, with the majority of cases encompassing the entire spinous and transverse processes, suggesting significant fusion. However as can be seen in figure 2, panel D, we did observe some variation. In this case although the location of the fusion is unchanged, only limited portions of the spinous and transverse process are actually integrated. In no case did we observe bone formation or bridging in the samples receiving the Adempty cassette transduced cells. The apparent fusion appeared to be rapid, within two weeks, and limited in size and scale, to region of muscle which received the cells. Further, at no time did we observe bone formation within the spinal canal.

Histological Analysis of the Tentative Spine Fusion:

To confirm that the apparent mineralized bone observed on the radiographs is true osteoid, and that it has integrated at these tentative points of fusion, we isolated the spine and adjacent tissues for histological analysis using techniques previously described (*15*). The spines were embedded in paraffin blocks, five micron sections cut, and every 5^{th} section was stained with hematoxylin and eosin to identify the tentative point of fusions. Representative photomicrographs (2X and 4X) of samples from either model, taken 2, 4 and 6 weeks after induction of heterotopic ossification are shown in figure 3. In all cases we observed structures of mature bone, such as osteoclasts, osteocytes and tentative bone marrow elements in the heterotopic bone, as well as cartilage, analgous to the growth plate structures in the normal long bone. However the heterotopic bone appeared to grow in a direction towards the skeletal bone, with the most mature bone being distal to the skeletal bone in the 2 week samples. As can be seen in figure 3, panel A-B, there is substantial new bone, adjacent and fused with the more mature vertebral bone,

along the transverse process, and laminae region of the vertebra. Although we did observe mature bone, with tentative marrow elements, at 2 weeks; this structure was always distal to the vertebra bone (data not shown), suggesting that the orginal heterotopic ossification started *de novo*, in the muscle and grew towards the vertebrae, encompass the bone. By four weeks, figure 3, panel C-D, the heterotopic bone, is much more mature, and we observed at the point of fusion, a very cellular reaction, that appears to be rapidly removing the mature cortex of the skeletal bone. It is unclear whether the large number of cells is recruited to this boundary, or expanding from the vertebral periosteum, but as noted in panel G, the mature cortical bone of the vertebra appears to be moth eaten, and undergoing removal, by the maturing heterotopic bone. However, by 6 weeks, this boundary is now completely remodeled figure 3; panel E-F with the two bones being contiguous as one integrated structure, with a well defined cortex, and trabecular interior, which houses the bone marrow. Interestingly, the only evidence remaining of the newly formed heterotopic ossification is the presence of substantial amounts of adipose tissue which is found within heterotopic regions, versus the mature marrow within the vertebra (panel F). As can be seen in figure 3, in all cases there appears to be fusion with the transverse process, within the laminae region of the vertebra, which was the target region for fusion. Depending on the depth of the section, we observed more or less of this region involved in the fusion site. In many cases the fusion actually encompassed both the spinous process through the laminae to the transverse process. In all tissues analyzed, the vertebral body did not appear to undergo growth, and there was no evidence of new bone formation within the spinal canal, similar to our observed radiological findings.

Biomechanical Analysis to Confirm Reduced Motion of the Spine:

The clinical goal of spine fusion is to reduce motion within the vertebral column; therefore, we developed a method for measuring flexion-extension of the spine. In this analysis spines were x-rayed before and after bending, and intervertebral motion was quantified using KIMAX QMA software (Medical Metrics, Inc.) that has been validated to measure intervertebral motion with an accuracy of better than 0.5° of rotation and 0.5 mm of translation (*13-14*). Results of this analysis are shown in Table 1. In no cases, did tissues receiving the Adempty cassette transduced cells, show a reduction in motion or spine stiffing. Whereas in NOD/Scid animals which received the human cells transduced with AdBMP2, approximately 40% of the spines in two weeks and 90% in the 4 and 6 weeks had reduced movement, consistent with fusion of at least one level. Interestingly, the C57BL/6 group receiving AdBMP2 transduced cells, at all time points, consistently showed a reduction in motion within the lumbar spine correlating with fusion (Table 1).

Table 1: Spinal fusion in injected animals

Group	N	Strain	Time	Spines with 2 or more vertebrae fused (%)
Adempty cassette transduced cells	9	NOD/Scid	6 weeks	0 %
AdBMP2 transduced cells	9	NOD/Scid	2 weeks	44 %
AdBMP2 transduced cells	9	NOD/Scid	4 weeks	90 %

AdBMP2 transduced cells	9	NOD/Scid	6 weeks	90 %
Adempty cassette transduced cells	8	C57BL/6	6 weeks	0%
AdBMP2 transduced cells	8	C57BL/6	2 weeks	100%
AdBMP2 transduced cells	4	C57BL/6	4 weeks	100%
AdBMP2 transduced cells	8	C57BL/6	6 weeks	100%

Functional Demonstration of Fusion:

To further confirm the spine fusion, the isolated spines used for the mechanical testing, were bleached to remove soft tissues, and analyzed on a gross level to see if the bone was contigous. As can be seen in figure 5, panel A, a representative 6 week spine shows, that in this fusion, 5 vertebrae of the lumbar spine are actually remodeled into a single structure. In all cases in which we observed biomechanical constraint of the spine, after induction of bone formation, we also observed integration of the vertebra with the heterotopic bone after removal of the soft tissues. However, in some of the early time points in the NOD/Scid animals (2 weeks), which did not appear to be constrained after induction of bone formation, we observed heterotopic bone which was not integrated with the vertebra but rather individual bones, confirming our biomechanical findings.

Further, we noticed from the radiomicrographs a distinct scoliosis in 6 week old growing mice, which received the Ad5BMP2 transduced cells injected into one side of the paraspinous musculature that parallels the spine, in both immune competent and incompetent models. As seen in figure 5, panel C, representative radiographs show a distinct curvature of the spine towards the area of new bone formation and tentative fusion. This was observed in a large number of animals with heterotopic bone and tentative fusion, but absent in animals which received the control cells (panel B).

DISCUSSION

Our system is the first approach reported in the literature to achieve rapid and clinically relevant spinal fusion in an animal model, through a single intramuscular injection. This system is quite versatile, in that any cell can be used as a delivery cell, as long as adequate transduction with adenovirus is achieved (*16*). Thus qualified cell lines used in current clinical trials, such as mesenchymal stem cells, can be readily adapted for use in this cell based gene therapy system, making it very feasible to introduce clinically.

The results suggest that heterotopic bone can be rapidly induced by delivering locally high levels of BMP2. This is not surprising since recombinant BMP2 is current used clinically, however the rapid one week time frame has not previously been reported (see ref. (*4*) for review). This may be a direct result of our ability to produce high levels of BMP2 for a prolonged period of time. Taking cues again for the human genetic disease FOP, in which heterotopic ossification can

readily occur within one week; this disease is caused by a mutation in a BMP receptor that leads to constitutive activity, but can still be further activated through addition of BMP (*7*). Thus physiological doses of BMP2 normally released after trauma, effectively become high doses, leading to rapid heterotopic ossification at the local injury site. During adenovirus transduction, multiple virus particles enter the cell with large amounts of vector DNA being effectively delivered to the nucleus. Because of its episomal nature, the vector DNA is present at high copy number driving high-level expression of BMP2. Thus, one of the things separating adenovirus from other gene therapy vectors is the high level of transgene expression that can be achieved after efficient transduction.(*17*) As long as the virus can efficiently infect the specific cell types (*12*) this system can be used to produce these high doses of BMP. Thus we have developed this as a cell based gene therapy system rather than a direct approach, to circumvent potential problems with inefficient uptake of the adenovirus, prohibiting production of the levels of BMP2 that are necessary for achieving rapid fusion(*8*). This is perhaps why our approach is so extremely effective at making rapid targeted bone. Further, by prior transduction of the cells, with the virus, no free adenovirus is delivered to the animal, minimizing adverse effects from of the virus on other tissues.

Our system does not require a specific stem cell population to achieve fusion. Reported time scales for spinal fusion using MSCs range between 6 weeks and 3 months; using gene therapy approaches, spinal fusion typically proceeds between 4 and 12 weeks (*2, 18*). Nevertheless, despite the reported successes using these approaches, the successes are tempered with difficulties, whether with MSC populations, poor control over transgene expression or low gene transduction efficiencies(*2, 18*) (*19*). The work presented here circumvents these issues. Bone formation is observed within 1 week of injection, spinal fusion within 2 weeks (in 50% of the animals; 90% at 4 weeks). The rapid onset of bone in addition to the rapid clearance of the transduced cells bodes well for the future therapeutic application of this system in humans.

This study is the first to demonstrate the ability of heterotopic ossification to form bridging bone, and fuse adjacent vertebra bone, without contribution from the skeletal bones. Both current clinical approaches using recombinant BMP2, and other gene therapy approaches(*1*), require exposure of the vertebra and decortication to induce bone growth and ultimately fusion of the skeletal bone to heterotopic bone. Often autologous bone graft is harvested to use in place of ectopic bone, which requires an additional extensive surgical procedure. Here through both histological analysis and biomechanical analysis we demonstrate the ability of the heterotopic bone to fuse into skeletal bone without expsoure and decortication.

All spines receiving the AdBMP2 transduced cells appeared to have extensive heterotopic bone formation upon radiological analysis. In no cases did we observe any ossification in the spinal canal, or anywhere in the animals receiving Adempty cassette transduced cells. The results suggest that the heterotopic bone formation is both targetable to a discrete location. Upon radiological analysis, of samples taken 2,4, and 6 weeks after initial injection of the AdBMP2 transduced cells, heterotopic bone was found between the transverse process adjacent to the paraspinous musculature receiving the cells, and laminae, eventually encompassing these structures, to fuse the spine. In many cases we observed significant fusion of the entire laminae, from the tip of the spinous process, through the entire transverse process. Alternatively, we also observed smaller regions of fusion which did not encompass the spinous process, but rather only the transverse process. Here we attempted to show representative cross sections in all cases; however, we cannot rule out that some of the samples had more significant involvement of the laminae region, and that we perhaps missed the representative cross section. However, since

the material can targeted the location of bone formation, perhaps the variation observed could also be a result of placement of the materials within the spinous musculature of the mice. Regions of soft tissue adjacent to corresponding distal structures of the same vertebra were not involved in any bone formation and appeared normal in these radiographs.

We looked at two different models which we have previously characterized(*12*), and found that we could achieve fusion in both systems as little as two weeks after initial intramuscular injection. Surprisingly, we observed 100% fusion in the immune competent wild type mice within two weeks of induction, whereas the system which used human cells transduced with AdBMP2 had only 40% success rate at two weeks. Upon analysis of the three dimensional reconstructions, it appeared that the bone was slightly distal to the vertebra in the NOD/Scid immune incompetent mice, whereas it was more closely associated with the vertebra in the wild type. Previous comparisons of these two systems show that they function almost identically in production of heterotopic bone(*12*).Therefore it seems unlikely that this difference is linked to the immunodeficiency. One potential possibility is that as we progressed, we improved our ability to place the cells proximal to the vertebra within the paraspinous musculature, suggesting that placement maybe critical to the eventual fusion.

Histological analysis of this model, suggests that the heterotopic bone grows into the skeletal bone with a somewhat organized growth plate, cortex, and tentative periosteum, similar to the vertebral bone. Initially less mature bone is observed at the junction of fusion, and depending on the model, this result in reduction of motion in approximately 40-90 percent of the animals tested. Interestingly, as the two bones fuse there appears to be a cellular reaction, which is destructive to the vertebral cortex. This process allows for the replacement of the cortical boundary with mature trabecular bone and bone marrow over time. It is not surprising from these results that in all cases the latter 4 and 6 week structures are well fused both histologically and biomechanically. Interesting to note, by 6 weeks, the old vertebra structure is gone, with the only remnants of the newer heterotopic bone being found in the marrow cavity. This observation suggests that adipose may form in the bone marrow cavity prior to the housing of true bone marrow, since in all less mature heterotopic bone, we observed extensive white fat, while in the vertebral bone marrow there was very little if any present. Whether this tissue plays a key role in establishment of the marrow is yet to be determined.

Ideally, upon successful fusion, the newly fused heterotopic bone should restrict mobility within the spine. Therefore the stiffness of the spines, in which we observed tentative fusions, were measured using a biomechanical assay which can measure the changes in angle of the spine under force. As expected, we observed fusion in sample that had integrated collagen fibers, whereas those which appear as two separate structures under polarized light were not capable of reducing flexion-extension in our biomechanical assay.

In spines which had a significant reduction in the mobility, we observed well integrated collagen fibers running contiguously through the bone suggesting that it was a remodeled single structure. In these animals we also observed scoliosis, due to the arthrodesis. Since the epiphyseal growth plates of rodents do not close until two years of age (the approximate life span of laboratory mice), their skeletons essentially do not stop growing(*20*). The fusion of the vertebrae in essence mechanically fixed the right side of the spine, causing imbalanced growth, resulting in scoliosis.

The ability to fuse the spine without surgical intervention would be a significant advancement in healthcare. The creation of a bony fusion by means of the percutaneous injection of a biologically

active material, without extensive surgical dissection and bony decortication, would have many clear clinical advantages. The system presented herein could potentially markedly decrease the pain, blood loss, and recovery time for patients undergoing these procedures, thus significantly reducing healthcare and associated costs. Further, this system could potentially improve success rates of this procedure, thus improving the quality of healthcare in this arena overall.

Figure Legends:

Figure 1: Schematic depiction of spine fusion using the cell based gene therapy system. AdBMP2 transduced cells injected into the muscle, rapidly recruit host cells to undergo all stages of endochondral ossification (*15, 21*). Within one week mineralized osteoid can be detected in photomicrographs, and radiographs.

Figure 2: Radiographs of C57BL/6 (panels A-H) and NOD/Scid (panels I-P) spines imaged after intramuscular injection into the paraspinous musculature of cells transduced with Adempty cassette control virus (panels A, E, I, and M) or AdBMP2 (panels B-D, F-H, J-L, and N-P). Control animal injected with Ad5HM4 were scanned 6 weeks after delivery of the transduced cells (panels A, E, I and M). Mice receiving the AdBMP2 transduced cells, were scanned two weeks (panels B, F, J, N); four weeks (panels C, G, K, O); and six weeks (D, H, L, P) after the initial induction of heterotopic ossification. Two dimensional x-rays (panels A-D; C57BL/6 and panels M-P; NOD/Scid) show a cross section through the highlighted (green lines) area in the three dimensional reconstructions (panels E-H; C57BL/6 and I-L; NOD/Scid) of tentative fusions between the heterotopic ossification and the vertebral bone.

Figure 3: Representative photomicrographs of tentative vertebral fusion with the heterotopic bone, taken 2 (panels A-B; 2X and 4X respectively), 4 (panels C-D; 2X and 4X respectively), and 6 (panels E-F; 2X and 4X respectively) weeks after initial injection of the AdBMP2 transduced cells. The slides were stained with hematoxylin and eosin for viewing. Panel E is a representative photomicrograph (10X) of a sample taken 4 weeks after the initial injection of AdBMP2 transduced cells. As can be seen in this sample, there are a significant number of cells associated with the boundary between the new heterotopic and old vertebral bone.

Figure 4: **Left:** Schematic of the in-house flexion device. After 2, 4 or 6 weeks, spines were harvested, placed in the device to induce flexion or extension at 110º and radiographed. **Right:** Representative images used to evaluate biomechanical function of spinal fusion. Top panel shows spine in extension, bottom in flexion. Such images were evaluated with KIMAX QMA software (Medical Metrics, Inc.) to determine whether adjacent vertebrae moved past a predetermined threshold.

Figure 5: Spine fusion was observed in bones isolated from the mouse after induction of targeted heterotopic ossification (panel A). Associated soft tissues were removed by bleaching, leaving only the bone. A wire was threaded through the spinal column, to preserve the orientation of the vertebra. Unfused vertebrae hang free; fused vertebrae remain joined and rigid. Ruler is in millimeters. Radiographs of mouse spines 6 weeks after induction of spine fusion Adempty cassette (panel B) or AdBMP2 (panel C) transduced cells. Panel C, shows obvious curvature of the spine suggesting a significant scoliosis, as compared to the normal mouse spine, shown in panel B.

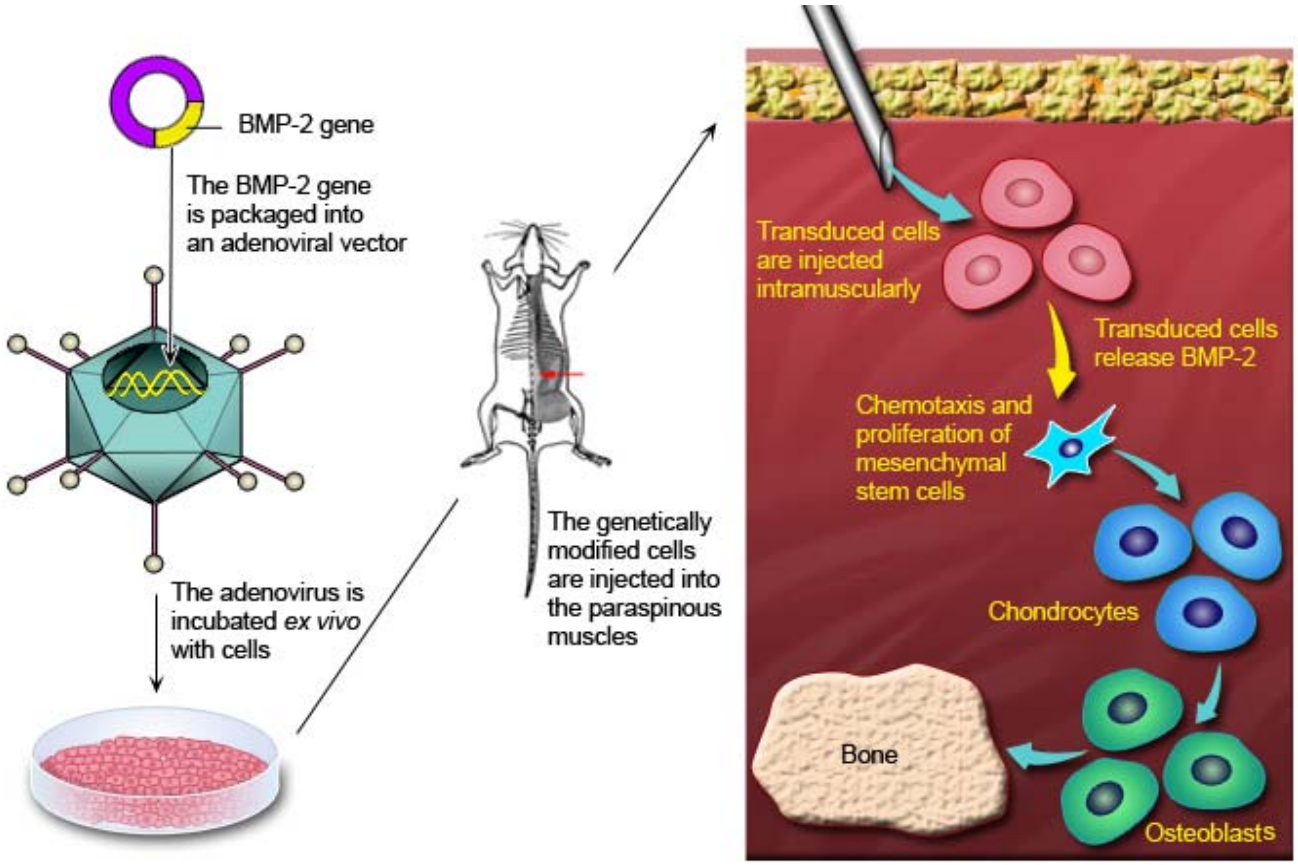
BMP-2 gene
The BMP-2 gene is packaged into an adenoviral vector
The adenovirus is incubated *ex vivo* with cells
The genetically modified cells are injected into the paraspinous muscles
Transduced cells are injected intramuscularly
Transduced cells release BMP-2
Chemotaxis and proliferation of mesenchymal stem cells
Chondrocytes
Bone
Osteoblasts

Figure 1

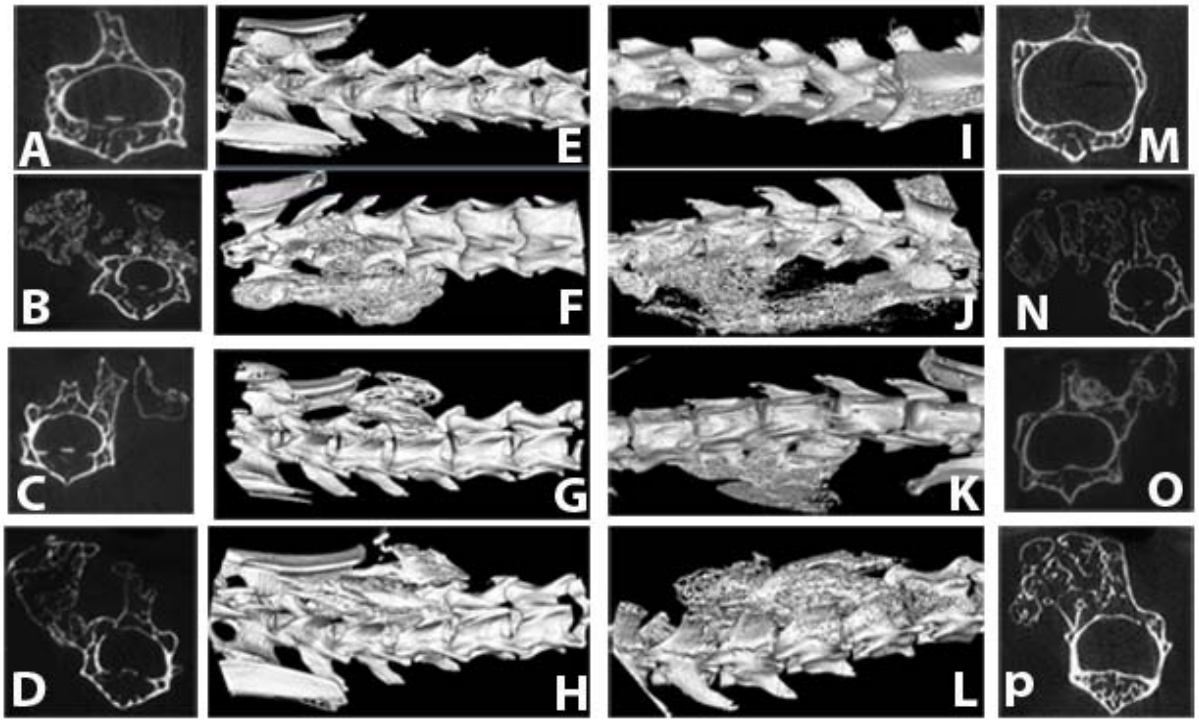

Figure 2

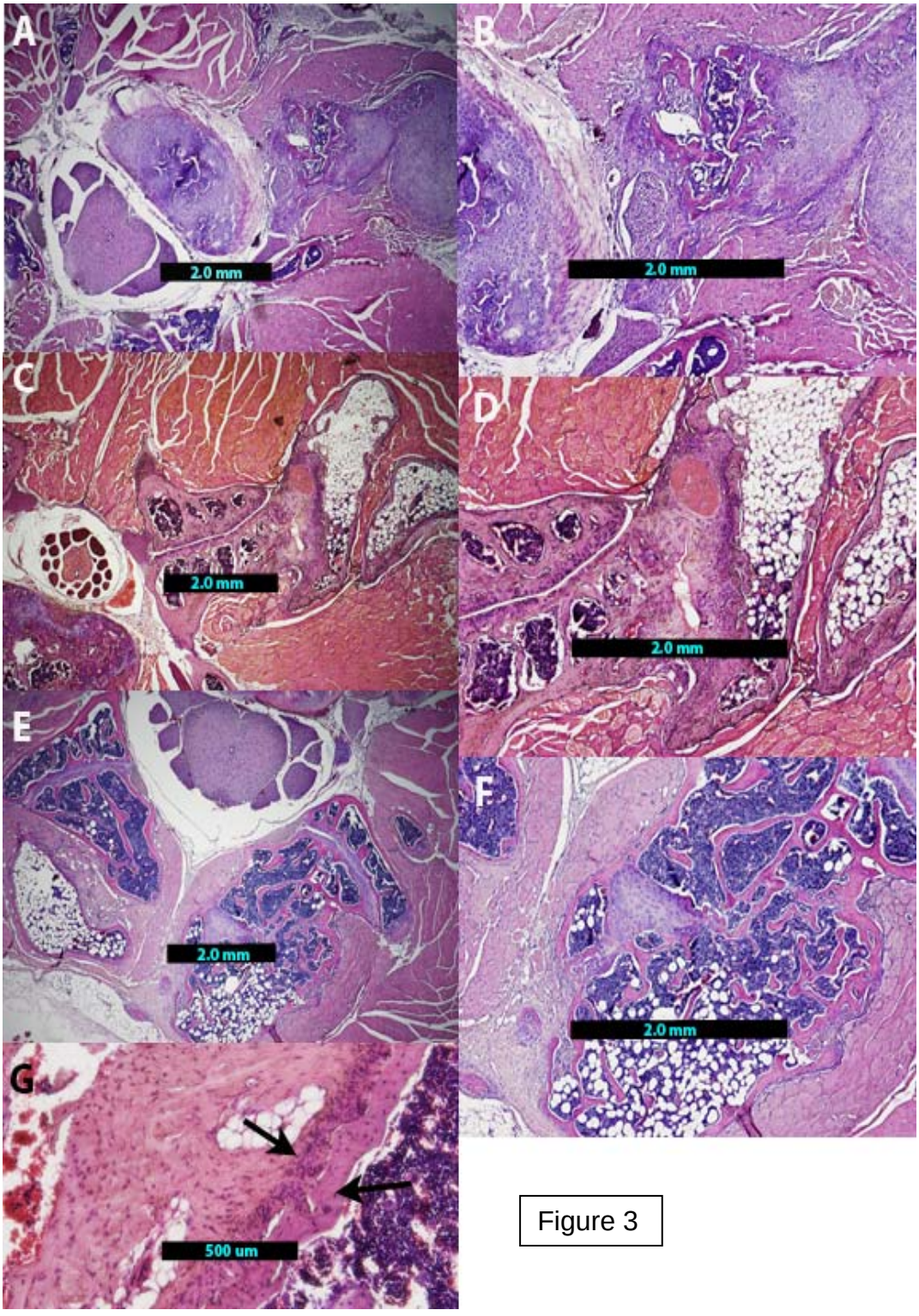

Figure 3

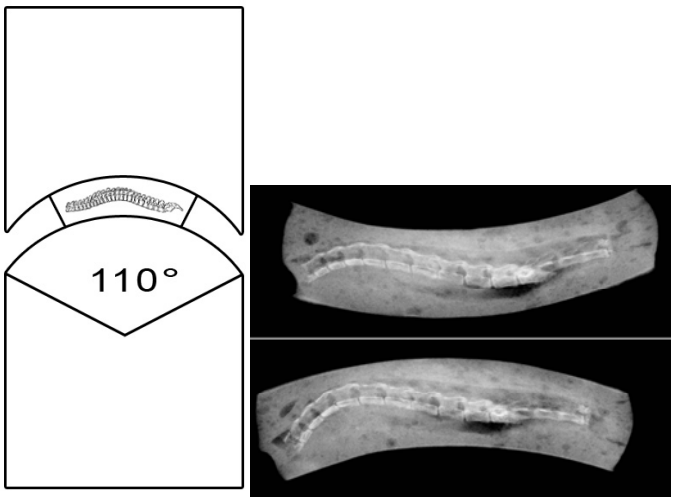

Figure 4 with table

A

B C

Figure 5

References

1. R. A. Deyo, A. Nachemson, S. K. Mirza, *N Engl J Med* **350**, 722 (Feb 12, 2004).
2. N. Kimelman *et al.*, *Tissue Eng* **13**, 1135 (Jun, 2007).
3. M. P. Lutolf *et al.*, *Nat Biotechnol* **21**, 513 (May, 2003).
4. F. Mussano, G. Ciccone, M. Ceccarelli, I. Baldi, F. Bassi, *Spine (Phila Pa 1976)* **32**, 824 (Apr 1, 2007).
5. K. R. Garrison *et al.*, *Health Technol Assess* **11**, 1 (Aug, 2007).
6. B. P. Hecht *et al.*, *Spine (Phila Pa 1976)* **24**, 629 (Apr 1, 1999).
7. E. M. Shore *et al.*, *Nat Genet* **38**, 525 (May, 2006).
8. E. A. Olmsted-Davis *et al.*, *Hum Gene Ther* **13**, 1337 (Jul 20, 2002).
9. C. M. Fouletier-Dilling *et al.*, *Hum Gene Ther* **18**, 733 (Aug, 2007).
10. R. S. Thies *et al.*, *Endocrinology* **130**, 1318 (Mar, 1992).
11. A. R. Davis, N. A. Wivel, J. L. Palladino, L. Tao, J. M. Wilson, *Mol Biotechnol* **18**, 63 (May, 2001).
12. C. M. Fouletier-Dilling *et al.*, *Hum Gene Ther* **16**, 1287 (Nov, 2005).
13. J. A. Hipp, C. A. Reitman, N. Wharton, *Spine (Phila Pa 1976)* **30**, 209 (Jan 15, 2005).
14. K. Zhao, C. Yang, C. Zhao, K. N. An, *J Biomech* **38**, 1943 (Sep, 2005).
15. E. Olmsted-Davis *et al.*, *Am J Pathol* **170**, 620 (Feb, 2007).
16. Z. Gugala, E. A. Olmsted-Davis, F. H. Gannon, R. W. Lindsey, A. R. Davis, *Gene Ther* **10**, 1289 (Aug, 2003).
17. K. L. Berkner, *Biotechniques* **6**, 616 (Jul-Aug, 1988).
18. O. N. Gottfried, A. T. Dailey, *Neurosurgery* **63**, 380 (Sep, 2008).
19. H. Aslan, D. Sheyn, D. Gazit, *Regen Med* **4**, 99 (Jan, 2009).
20. S. H. Windahl, G. Andersson, J. A. Gustafsson, *Trends Endocrinol Metab* **13**, 195 (Jul, 2002).
21. J. Shafer *et al.*, *Tissue Eng* **13**, 2011 (Aug, 2007).

Tissue Engineering

Tissue Engineering Manuscript Central: http://mc.manuscriptcentral.com/ten

Hydrogel microsphere encapsulation of a cell-based gene therapy system increases cell survival, transgene expression, and bone volume in a model of heterotopic ossification.

Journal:	*Tissue Engineering*
Manuscript ID:	Draft
Manuscript Type:	Original Article
Date Submitted by the Author:	
Complete List of Authors:	Olabisi, Ronke; Rice University, Bioengineering Lazard, ZaWaunyka; Baylor College of Medicine, Center for Cell and Gene Therapy Hall, Mary; The University of Texas Health Science Center, Center for Molecular Imaging Kwon, Sun Kuk; The University of Texas Health Science Center, Center for Molecular Imaging Sevick, Eva; The University of Texas Health Science Center, Center for Molecular Imaging Hipp, John; Baylor College of Medicine, Orthopaedic Surgery Davis, Alan; Baylor College of Medicine, Center for Cell and Gene Therapy Davis, Elizabeth; Baylor College of Medicine, Cell and Gene Therapy West, Jennifer; Rice University, Bioengineering
Keyword:	Bone < Tissue Engineering Applications, Cell Encapsulation < Enabling Technologies, Viral Gene Therapy < Enabling Technologies
Abstract:	Bone morphogenetic proteins are widely known for their osteoinductive activity; however, harnessing this capacity is still a high-priority research focus. Here we present a novel technology for the delivery of high levels of BMP-2, at a targeted location, for rapid endochondral bone formation. This system enhances our previously described cell-based gene therapy system by microencapsulating adenovirus-transduced cells in non-degradable poly(ethylene glycol) diacrylate (PEGDA) hydrogels prior to intramuscular delivery. In vitro studies to measure BMP-2 secretion, specific activity, and cell viability showed that AdBMP2-transduced cells in monolayer culture were similar to those derived from the same number of these transduced cells encapsulated into a microsphere structure, suggesting that the polymer did not adversely affect the gene therapy system. Furthermore, in vivo studies showed a significant increase in the length of transgene expression after microencapsulation when compared to the

	unencapsulated cells. In addition, when comparable numbers of transduced cells were intramuscularly injected into mice, the resultant heterotopic bone formation was approximately two-fold greater in volume relative to that from unencapsulated cells. The data suggests that microencapsulation prolongs BMP-2 expression and appears to spread the delivery of the protein over a greater area of tissue, resulting in a significant increase in the region of heterotopic ossification. Histological analysis of the resultant bone formation shows new bone forming directly around the encapsulated cells, compared to a very dense and significantly smaller region for the directly injected, unencapsulated cells. This suggests that the material can be used to form bone of a specific size and shape. Thus, incorporation of the PEGDA hydrogel microspheres significantly advances current gene therapy approaches for bone repair, particularly in scenarios of substantial traumatic injury.

Hydrogel microsphere encapsulation of a cell-based gene therapy system increases cell survival, transgene expression, and bone volume in a model of heterotopic ossification.

Ronke M. Olabisi Ph.D.[1], ZaWaunyka W. Lazard, B.S.[2], Christy L. Franco, B.S.[3], Mary A. Hall, Ph.D.[4], Sun Kuk Kwon, Ph.D.[5], Eva M. Sevick, Ph.D.[6], John A. Hipp, Ph.D.[7], Alan R. Davis, Ph.D.[8], Elizabeth A. Olmsted-Davis, Ph.D.[9] and Jennifer L. West, Ph.D.[10]

[1]Department of Bioengineering, Rice University, 6500 Main St. MS 142, Houston, TX 77030, USA; Office: (713) 348-3154, Fax: (360) 343-8819, ronke@rice.edu

[2]Center for Cell and Gene Therapy, Baylor College of Medicine, One Baylor Plaza MS BCM505, Houston, TX 77030, USA; Office: (713) 798-1238, Fax: (713) 798-1230, zwl@bcm.edu

[3]Department of Bioengineering, Rice University, 6500 Main St. MS 142, Houston, TX 77030, USA; Office: (713) 348-3153, Fax: (713) 348-5877, clfranco@rice.edu

[4]Center for Molecular Imaging, The University of Texas Health Science Center, 1825 Pressler Street Room SRB-330Q, Houston, TX 77030, USA; Office (713) 500-3565, Fax: (713) 500-0319, mary.hall@uth.tmc.edu

[5]Center for Molecular Imaging, The University of Texas Health Science Center, 1825 Pressler Street Room SRB-330Q, Houston, TX 77030, USA; Office (713) 500-3565, Fax: (713) 500-0319, sunkuk.kwon@@uth.tmc.edu

[6]Center for Molecular Imaging, The University of Texas Health Science Center, 1825 Pressler Street Room SRB-330Q, Houston, TX 77030, USA; Office (713) 500-3565, Fax: (713) 500-0319, eva.sevick@uth.tmc.edu

[7]Department of Orthopaedic Surgery, Baylor College of Medicine, One Baylor Plaza MS

SM2501, Houston, TX 77030, USA; Office: (713) 441-5702, Fax: (713) 986-5771, jhipp@bcm.edu

[8]Center for Cell and Gene Therapy, Baylor College of Medicine, One Baylor Plaza MS BCM505, Houston, TX 77030, USA; Office: (713) 798-1237, Fax: (713) 798-1230, ardavis@bcm.edu

[9]Center for Cell and Gene Therapy, Baylor College of Medicine, One Baylor Plaza MS BCM505, Houston, TX 77030, USA; Office: (713) 798-1253, Fax: (713) 798-1230, edavis@bcm.edu

[10]*Corresponding Author,* Department of Bioengineering, Rice University, 6500 Main St. MS 142, Houston, TX 77030, USA; Office: (713) 348-5955, Fax: (713) 348-5877, jwest@rice.edu

Introduction

Although bone possesses the capacity to repair, major insults often require surgical intervention and bone grafting(1-3). In the U.S., approximately 550,000 million fractures annually require bone grafting(4), as do millions of total joint arthroplasties, spinal arthrodeses, maxillofacial surgeries and implant fixations(5). In an effort to circumvent the obstacles associated with grafts, researchers have used osteoinductive growth factors, such as BMPs[6, 7]. BMP-2 possesses the ability to induce *de novo* bone formation at targeted locations and is FDA approved.

Nevertheless, many clinicians have found recombinant BMP-2 to have inconsistent efficacy, especially in complex clinical scenarios such as traumatic injury(8-11). These findings have led to a renewed emphasis to develop better methods of delivering BMP-2[12]. BMPs are rapidly cleared when administered in solution[7], necessitating a carrier, like collagen, that can retain and sequester BMPs[6, 7]. BMPs have natural affinity for collagen[4, 7, 12]. Unfortunately, collagen can elicit an immune response[7, 13], presents handling difficulties, does not maintain a stable form, and use of a collagen sponge reduces the bioavailability of BMP to such a degree that large amounts are necessary for a therapeutic response[6, 7, 13, 14]. Given these drawbacks, the search for alternative carrier materials that are biocompatible, biodegradable, osteoinductive and osteoconductive are of the utmost importance[7, 15].

Here we present use of poly(ethylene glycol) diacrylate (PEGDA) hydrogels to encapsulate cells that produce and secrete high levels of BMP-2. PEGDA hydrogels are widely used in tissue engineering applications because they are bioinert and mimic many physical properties of soft tissues[6, 16]. Because of the immunoprotection they can provide, hydrogels are also used for cell encapsulation[6, 16, 17]. PEGDA hydrogels have demonstrated immunoprotection of porcine islets

while retaining diffusional release insulin, returning diabetic mice to normoglycemia.(18, 19) Previous attempts to encapsulate our cell-based gene therapy system into a macroscopic hydrogel resulted in a significant decrease in BMP-2 release and resultant bone formation as compared to un-encapsulated cells(6). Microencapsulation retains high-level BMP-2 expression from AdBMP2-transduced cells. The encapsulation of this cell therapy system into microspheres actually provides enhanced BMP-2 expression in the aggregate *in vivo* when compared to direct injection of cells. Further, gene expression is spatially controlled by encapsulating the cells in PEGDA hydrogel microspheres, and restricts rapid immune clearance of these delivery cells. Thus, per cell number injected, more host tissue was actually involved in heterotopic ossification, suggesting that inclusion of the hydrogel enhanced the efficacy of our cell therapy system. The resultant osteogenesis showed a pattern of heterotopic bone formation surrounding the microspheres in an integrated structure, suggesting that inclusion of the biomaterial would enable spatial control of new bone formation when compared to directly injected cells.

Methods

Cell Culture

Human diploid fetal lung fibroblasts (MRC-5) were obtained from American Type Culture Collection (ATCC; Manassas, VA) and propagated in a humidified incubator at 37°C/5% CO_2 in Dulbecco's Modified Eagle's Medium (DMEM; Sigma, St. Louis, MO) supplemented with 10% fetal bovine serum (FBS; HyClone, Logan, UT), 1000 U/L penicillin, 100 mg/L streptomycin, and 0.25 µg/ml amphotericin B (Invitrogen Life Technologies, Gaithersburg, MD)[20]. Murine bone marrow stromal cells (W20-17; a gift from Genetics Institute, Cambridge, MA) were

propagated as previously described[21].

Adenoviruses and cell transduction

Replication-defective E1-E3 deleted first generation human type 5 adenoviruses (Ad5) were constructed to contain cDNAs for BMP-2 in the E1 region of the virus[18]. Replication-defective human adenovirus type 35 fiber (Ad5F35) were constructed to contain cDNAs for BMP-2 in the E1 region of the virus[22]. For the viruses Ad5BMP2, Ad5dsRED, and Ad5empty cassette, the viral particle (VP)-to-plaque-forming unit (PFU) ratios were 1:83, 1:2 and 1:111 respectively, and all viruses were confirmed to be negative for replication-competent adenovirus. MRC-5 cells were transduced as previously described with Ad5BMP2, Ad5dsRED or Ad5empty cassette at a viral concentration of 2500 VP/cell[18,23]. Briefly, virus was added to fresh supplemented DMEM and incubated with cells at 37°C overnight.

Synthesis of Poly(ethylene glycol) Diacrylate.

Poly(ethylene glycol) diacrylate (PEGDA) was prepared by combining 0.4 mmol/mL acryloyl chloride, 0.2 mmol/mL triethylamine and 0.1 mmol/mL dry PEG (6000 Da; Fluka, Milwaukee, WI) in anhydrous dichloromethane (DCM) under argon overnight. The resulting PEGDA was then precipitated with ether, filtered, lyophilized and stored under argon at -20°C. PEGDA was analyzed by proton NMR (Avance 400 MHz; Bruker, Billerica, MA; solvent, N,N-dimethylformamide-d7) and only materials with a degree of acrylation >85% were used.

Microencapsulation

Hydrogel precursor solutions were formed by combining 0.1 g/ml 10 kDa PEGDA (10% w/v) with 1.5% (v/v) triethanolamine/HEPES buffered saline (HBS, pH 7.4), 37 mM 1-vinyl-2-pyrrolidinone, 0.1 mM eosin Y, and transduced MRC-5 cells for a final concentration of 6×10^4

cells/µl. A hydrophobic photoinitiator solution (2,2-dimethoxy-2-phenyl acetophenone in 1-vinyl-2-pyrrolidinone, 300 mg/mL) was combined in mineral oil (embryo tested, sterile filtered; Sigma-Aldrich, St. Louis, MO; 3 µl/ml). The microspheres were formed after adding the hydrogel precursor solution into the mineral oil, emulsifying by vortex for 2 s while exposing to white light for an additional 20 s. Microspheres were isolated by two media washes. Cells and microspheres were quantified by measuring the amount of soluble formazan produced by cellular reduction of the tetrazolium compound [3-(4,5-dimethylthiazol-2-yl)-5-(3-carboxymethoxyphenyl)-2-(4-sulfophenyl)-2H-tetrazolium, inner salt; MTS]. Briefly, cells were counted with a Coulter Counter and a serial dilution was used as a standard curve. Microsphere and cell samples were plated in a 24-well plate with 1 ml of culture medium, and 200 µl of CellTiter 96® AQueous One Solution Reagent was added into each well. The plate was incubated for 1 hour at 37°C in a humidified, 5% CO_2 atmosphere and then the absorbance was recorded at 490 nm. To ensure proper comparisons between the microspheres and the monolayer cells we measured the loss of cells following the encapsulation procedure and loss in the injection needle. Approximately 80 % cell loss occurs during encapsulation and injection (Figure 1A), which is accounted for and equalized between groups prior to injection.

Preparation of cells for intramuscular injection

Cells transduced with Ad5BMP2, Ad5dsRED or Ad5empty cassette were removed with trypsin, and separated into two groups: direct injection and microencapsulation. Cells directly injected were suspended at a concentration of 5×10^6 cells per 100 µl of PBS and aspirated into a syringe with a 22 gauge needle. Microencapsulated cells were encapsulated at a concentration of 5×10^6

cells per 300 µl of microspheres, which were in turn suspended in 1 ml of PBS and aspirated into a syringe with an 18 gauge needle.

Viability assays

MRC-5 cells were transduced with Ad5F35BMP2, harvested and encapsulated in microspheres as described. One week after microencapsulation, microspheres were incubated with media and 2 µM calcein acetoxymethyl ester (calcein AM, Invitrogen, Inc.) for 20 min at 37°C in a humidified, 5% CO_2 incubator. Microspheres were imaged under a confocal microscope (ex/em ~495 nm/~515 nm).

BMP-2 Quantification

BMP-2 expression was evaluated for MRC-5 cells transduced with Ad5F35BMP2 or Ad5F35HM4 using ELISA and alkaline phosphatase (AP) assays. ELISA assays were performed with a BMP-2 Quantikine ELISA kit from R&D Systems (Minneapolis, MN) using culture supernatant collected 72 hours after adenovirus transduction. Transduced cells were microencapsulated or plated directly in 0.4 µm pore polycarbonate membrane Transwell inserts (Corning Inc., Lowell, MA) and W20-17 cells were cultured in the wells. After 72 hours, W20-17 cells were assayed for AP activity[22]. Cellular AP was extracted by conducting three freeze-thaw cycles on the W20-17 cells in a 100 µM/cm^2 concentration of 25 mM Tris-HCl (pH 8.0) and 0.5% Triton X-100. A chemiluminescent disodium 3-(4-methoxyspiroy distributes-4-yl) phenyl phosphate (CSPD) substrate with Sapphire-II enhancer (Tropix; Applied Biosystems, Foster City, CA) was added to the samples for enhanced AP sensitivity. The light output after a 2

sec delay was integrated from each sample for 10 sec with a luminometer (TD-20/20; Turner BioSystems, Sunnyvale, CA). AP levels were recorded in relative luminescence units (RLU). These AP levels were then normalized to protein content with the bicinchoninic acid (BCA) assay. Data are presented as percent AP induction relative to that of basal control cells not exposed to BMP-2. Statistical analysis was performed as described previously[20]. Briefly, all data were taken in triplicate and reported as mean and standard deviation. A Student t-test was done between the untreated control and each experimental condition.

Live animal optical fluorescence imaging.

Mice were imaged longitudinally for approximately one month post-injection of fibroblasts (± microencapsulation) transduced with Ad5dsRED (2500 vp/cell). Fluorescent imaging was performed at excitation and emission wavelengths of 568 nm and 610±30 nm, respectively. The excitation light was supplied by a 200 mW Argon/Krypton laser (Model No. 643R-AP-A01, Melles Griot Laser Group, Carlsbad, CA), and the emission light was collected after it passed through holographic (SuperNotch-Plus™ 568 nm, Kaiser Optical Systems Inc., Ann Arbor, MI) and bandpass (HQ610/60m, Chroma Technology Corp, Bellows Falls, VT) filters and was focused onto an electron-multiplying charge-coupled device (EMCCD) camera (Photon Max 512, Princeton Instruments, Trenton, NJ) using a Nikon camera lens (Nikkor 28 mm, Nikon Inc., Melville, NY). Exposure times were approximately 200 ms. Image analysis was performed using ImageJ. Fluorescence intensity (FI) was measured and recorded for a region of interest (ROI) for each site of the animal injected with cells. The ROI dimensions were constant for every site imaged and each ROI was chosen to include the optimal fluorescent signal for the

given site. A target to background ratio (TBR) of FI was calculated for each site by subtracting a background (B) ROI from the target (T) ROI, and then dividing the result by the background (B) ROI; TBR = (T-B)/B. The TBR value was plotted versus time (i.e., day post-injection of cells). Results represent the mean TBR of FI for unencapsulated and/or encapsulated Ad5dsRed or AdEmpty cassette transduced cells (n=4 per group). Statistical analyses were performed using the Student's t-Test, unpaired.

Heterotopic bone assay

Microencapsulated or unencapsulated cells were delivered by intramuscular injection into the hind limb quadriceps muscle of nonobese diabetic/severely compromised immunodeficient (NOD/SCID) female mice (8–12 weeks old; Charles River Laboratories; Wilmington, MA) (n = 6). Animals were euthanized two weeks after injection of the transduced cells. All animal studies performed were in accordance with an Institutional Animal Care and Use Committee (IACUC) approved protocol.

Histological analysis

Mouse hind limbs were harvested, fixed in formalin and decalcified. Hind limbs were then divided longitudinally and sectioned from the inner surface outward. Serial sections (5 µm) encompassing the entire hind limb reactive site were prepared. Every fifth slide was stained with hematoxylin and eosin. All sections were analyzed by light microscopy.

Microcomputed tomography

Micro-CT exams were obtained of the left and right legs at 15 µm resolution (eXplore Locus SP; GE Healthcare, London, ON, Canada). A hydroxyapatite phantom was scanned alongside each

specimen and was used to convert the scan data from arbitrary units to units of equivalent bone density. A 3D region-of-interest was defined for each specimen to isolate the new mineralized tissue from the normal skeletal structures (femur, tibia, and patella). The scans were thresholded to exclude any tissue with a density less than 100 mg/cc, and the tissue volume within the region of interest was calculated as a measure of the total amount of mineralized tissue. The tissue mineral content was measured as an estimate of the total mineral in the region and the tissue density was calculated to quantify the density of the mineralized tissue. The resulting data were analyzed by one-way ANOVA.

Results

Validation of the microsphere's containing AdBMP2-transduced cells.

High levels of BMP-2 can lead to rapid heterotopic ossification(8, 20, 24). We previously demonstrated rapid clearance of AdBMP2-transduced cells(20, 25), thus limiting both the levels and duration of BMP-2 that can be achieved locally. Thus, we encapsulated the transduced cells within PEGDA hydrogel microspheres. Cells were microencapsulated and then stained using a Live/Dead cytotoxicity assay where live cells enzymatically convert non-fluorescent calcein acetoxymethyl (calcein AM) into calcein (green), while ethidium homodimer (red) enters dead cells through damaged membranes. As seen in Figure 1, encapsulated cells showed high viability, 95±0.5%.

The level of BMP-2 in the culture supernatant was measured to determine if the protein could adequately diffuse from the microspheres. The release of proteins from hydrogels is related both to diffusion distances and the hydrogel mesh size(26). The hydrogels in the current study were

formed with 10% 10 kDa PEGDA, which has been estimated to have a mesh size of 280 Å(27). Proteins having radii smaller than the hydrogel mesh size enjoy relatively free diffusion through the polymer(28). Mature BMP-2 is a small protein (approximately 16 kDa) and it has been suggested that it dimerizes immediately after synthesis. The biologically active form of BMP-2 is a homodimer whose dimensions are 70 Å × 35 Å × 30 Å(29). Thus, BMP should readily diffuse through the microspheres. Equivalent numbers of cells were transduced with AdBMP2 or AdEmpty cassette (2500 vp/cell) and either placed in culture directly, or after microencapsulation. Culture supernatant was removed 72 hours later, and BMP-2 and its activity were quantified (Figure 2). BMP-2 was quantified by ELISA and found to be approximately 17,500 pg/ml and 15,000 pg/ml of culture supernatant for directly plated and microencapsulated cells, respectively. No BMP-2 was detected in either culture supernatant from AdEmpty cassette-transduced cells, or control cells. In macroscopic hydrogels, we observed a significant drop in the level of BMP-2(6) as compared to equivalent numbers of cells either directly plated or in microspheres. The data suggests that optimal BMP-2 production and secretion is achieved when cells are encapsulated into the smaller microsphere structures. Further, the data show that the PEGDA hydrogel material is not affecting the production, secretion or diffusion of BMP-2 within the microspheres (Figure 2A).

We next assayed BMP-2 activity in the culture supernatant to confirm that the protein that diffused through the PEGDA hydrogel possessed similar activity as BMP-2 in culture supernatant from cells directly plated. Culture supernatants were tested using the murine bone marrow stromal cell line, W20-17 cells, which have been shown to respond to functional BMP-2 by undergoing osteogenesis with a rapid increase in alkaline phosphatase (AP)(21). W20-17

cells were exposed to culture supernatants for 72 hours and then lysed for quantification of AP activity (Figure 2B). Both the culture supernatants from cells directly plated and encapsulated in microspheres led to significant elevation in alkaline phosphatase over control cells, suggesting the BMP-2 is functionally active. Further, supernatant from cells transduced with AdEmpty cassette did not elevate alkaline phosphatase (Figure 2B).

In vivo comparison of transgene expression with and without encapsulation in PEGDA hydrogel. Two days after the initial injection of cells, dsRED expression was readily detected whether cells were encapsulated or not and in no cases were cells or microspheres detected migrating from the injection site. Because solution spread is a function of injection volume(30, 31), dsRED expression in the tissues receiving the microspheres encompasses a larger volume than the encapsulated counterpart (Figure 3A). However, the magnitude of expression should not be affected by injection volume and dsRED expression was significantly elevated in microencapsulated cells compared to directly injected cells (Figure 3B), suggesting that the directly injected cells may already be starting to be cleared from the tissues. Reporter expression in animals receiving AdBMP2-transduced cells directly injected was substantially reduced after seven days and was indistinguishable from control (Figure 3B). This result was similar to our previous findings where the delivered cells are rapidly cleared(20). In contrast, the microencapsulated cells continued to be significantly elevated over background (Figure 3B). This was not due to autofluorescence of PEGDA indicated by the absence of signal at 590 ± 10 nm in microencapsulated control cells. This 590±10 nm dsRED fluorescent signal was significantly elevated over that of microencapsulated cells transduced with AdEmpty cassette for 15 days (Figure 3B). After 15 days, these levels dropped; however, signal was still detectable

(Figure 3A, arrows) in some animals, suggesting that the microencapsulated cells remained viable to express the dsRED transgene. Collectively, the data suggest that microencapsulation prolongs transgene expression within the tissues.

In vivo bone formation with and without microencapsulation in PEGDA hydrogels.

PEGDA microspheres encapsulating AdBMP2-transduced cells were next tested *in vivo* to determine whether prolonged BMP-2 expression could enhance heterotopic bone formation. Similar numbers of AdBMP2-transduced cells were injected, either directly or following microencapsulation, into the muscle in the mouse hind limb and the resulting heterotopic ossification was analyzed. MicroCT analysis of the resulting bone showed a significantly greater region or volume of heterotopic ossification in tissues receiving microspheres (Figure 4A, C) than those receiving directly injected cells (Figure 4B, D). Cross-sectional microCT analysis of the newly formed bone revealed a similar architecture between the groups. Heterotopic bone formed by both the microencapsulated cells and directly injected cells had a pattern of dense bone surrounding a hollow interior (Figures 4C and D); however the circumference of bone within the directly injected cells was significantly smaller.

Microencapsulated AdBMP2-transduced cells produced approximately twice the bone volume of un-encapsulated cells (Figure 5B). Despite the volumetric increase, the bone tissue mineral content was statistically similar between these groups, although trending towards an elevation in samples that received the microspheres (Figure 5A). This may result from the change in tissue mineral density of the new bone surrounding the microspheres (Figure 5C). It appears to be slightly less dense, leading to the overall similarity in mass between the two groups.

Interestingly, the less dense bone in the microsphere group may in part be related to the fact that the microspheres have spread out the BMP-2 release over a greater volume, and thus effectively diluted the concentration of BMP-2 in any given location.

From histological analysis, both groups had significant new bone formation within the muscle (Figure 6). In tissues that had received the direct injection of AdBMP2-transduced cells, there was a small compact piece of bone forming a ring-like structure encircling what appears to be blood and tentative stroma, and just exterior to this structure was significant adipose (Figure 6A). A similar structure was observed in tissues that had received microspheres (Figure 6B). Since the microspheres did not degrade, they appear histologically as gaps or holes within the matrix (Figure 6B). Thus, despite the presence of nondegradable microspheres, both structures were patterned to have a denser bone structure with a bone marrow-like cavity on the interior.

Discussion

Here we present a novel system for the sustained production and release of BMP-2 in a targeted manner. This approach expands on our previously reported cell-based gene therapy system, which successfully employs adenovirus transduction of fibroblasts to express high levels of BMP-2 at a targeted location(6, 20, 25). Because the transduced cells are rapidly cleared after injection, PEGDA was utilized as a carrier that would prolong the expression of BMP-2 within the tissues. We previously implanted AdBMP2-transduced cells that were macroencapsulated in larger hydrogels to demonstrate that encapsulated cells could continue to produce bone(6). In this study, we demonstrate that microencapsulated cells express and release high levels of BMP-2 and produce more bone volume than unencapsulated cells. Microencapsulation permits delivery via injection, avoiding surgery.

Hydrogels formed with PEGDA are widely used in tissue engineering applications because they are bioinert, FDA approved for oral, dermal and intravenous applications, and have tunable physical properties such as stiffness and permeability(6, 32, 33). Careful manipulation of these physical characteristics enable PEGDA hydrogels to better approximate a tissue of interest, to regulate nutrient/waste diffusion, or to prevent interaction with immune cells(6, 16). Current carriers in clinical use, such as collagen sponges, do not retain BMP-2 efficiently, require large amounts of recombinant BMP-2 for a therapeutic effect, and are often plagued with variability, such as differences in handling, material properties and in some cases triggering immunogenic responses[6, 7, 13, 14]. Furthermore, because collagen can bind BMP-2, our previous studies suggest that it reduced the efficacy of BMP-2 in general(34). Additionally, the inflammation associated with the collagen sponge can also reduce the ability to produce targeted bone formation.

Our approach avoids these issues because we use a biocompatible synthetic carrier, which minimizes immune response and does not bind BMP-2. In addition, our approach is independent of cell line, permitting the transduction of any type of cell(35), and with efficient transduction can deliver functional BMP-2 continually to the target site over several days. Furthermore, we are able to get high transduction efficiencies, requiring a modest quantity of cells and microspheres for a therapeutic effect. For instance, in our current system we injected just 300 µl of microspheres.

The millimeter-scale hydrogels employed in our previous study were a proof of concept and well exceeded the diffusion limit of oxygen(36). As a result, BMP-2 culture supernatant levels were significantly reduced in the beads compared to monolayer(6). The radii of the microspheres in

this study were roughly in the 50 - 150 µm range, providing excellent cell survival. Given the same volume of PEGDA carrier, when cells were: 1) encapsulated in a single hydrogel(6); 2) equally divided into four hydrogels(6) or 3) microencapsulated; the greatest amount of detectable BMP-2 in the culture supernatant came from the microspheres, which released identical levels as the monolayer.

Although cell viability between encapsulated and unencapsulated cells were comparable for the *in vitro* studies, this was not the case for the *in vivo* experiments. The data suggest that after injection, microencapsulated cells were viable for longer than unencapsulated cells, possibly due to immunoprotection. The duration of the dsRED fluorescence from microencapsulated cells demonstrates that microspheres are resistant to clearance. Furthermore, microencapsulation does not interfere with the expression of the BMP-2 transgene. Cells in both monolayer and microspheres were able to make identical levels of functional protein. Since bone formation occurred immediately surrounding the microspheres, the area of new bone formation could easily be defined by the volume of material delivered. This is not true for the directly injected cells that stay tightly clustered, and will reside in adipose regions that can easily be compressed to hold the additional volume. Thus exact spatial placement of the transduced cells, and resultant bone formation, is far less sensitive, and subject to other variables that may influence it, whereas, delivery of the microspheres, because of their structure, can fill large regions of the tissue, and produce bone of in a desired location and size. This is a critical parameter for implementation of the therapy to traumatic bone injury.

Interestingly, spreading out the region in which BMP-2 is expressed through microsphere delivery resulted in a significant increase in the volume of bone, and decrease in bone density.

We hypothesize that the decrease in density, is because the bone formation process overall was reduced, due to the lower concentration of BMP-2 over the greater volume. In comparison, the cells directly injected which sit as a cluster within the tissues would produce the same amount of BMP-2 but in a much smaller volume, and resultant bone formation shows a small dense compact bone. Surprisingly, marrow-like structures formed in both cases with similar patterning to the normal skeleton. This indicates that despite the hydrogel's capacity to dictate the shape of the newly forming bone, it does not interfere with the structural patterning that is part of the biology of bone formation. However, any interference of the hydrogel in the final bone density can be overcome by using hydrogels that are degradable.

Conclusions

We present a system for targeted bone formation, in which an ex vivo gene therapy system is encapsulated into PEGDA microspheres. This allows for prolonged expression of the BMP-2. Further, the microspheres are moldable and take up a specific volume that allows for bone to form immediately adjacent to their location in the tissues. Thus, the combination of BMP-2 cell-based gene therapy and PEGDA microencapsulation provides a novel method for forming bone of specific shape and size. Further, this system can provide a much longer window for expression of BMP within the target site. Our system is the first of its kind to induce bone formation and may impact gene therapy approaches to come.

Acknowledgements

Grant support: Defense Advanced Research Projects Agency W911NF-09-1-0040 and Department of Defense W81XWH-07-0281 and W81XWH-07-1-025. We thank Rita Nistal for performing the histology.

Author Disclosure Statement: No competing financial interests exist.

Figure Legends

Figure 1. Viability of AdBMP2-transduced cells (2500 vp/cell) within microspheres was assessed at day 7 using a LIVE/DEAD® Viability/Cytotoxicity Kit for mammalian cells (Invitrogen, Molecular Probes, Eugene, OR). **A.** Minimum intensity projection of a differential interference contrast (DIC) Z-stack. **B.** Maximum intensity projection of fluorescent Z-stack merge of red and green channels. The red channel was thresholded to eliminate diffuse virus staining. Dead cells appear red and live cells appear green. **C.** Overlay of panels A and B. Living cells accounted for 95.08% ± 0.47% of total cells encapsulated.

Figure 2. Comparison of BMP-2 expression, secretion and activity after PEGDA encapsulation. **A.** BMP-2 protein in culture supernatant taken from AdBMP2- or AdEmpty cassette-transduced cells (25000 vp/cell) (monolayer), or those encapsulated in PEGDA microspheres was quantified by sampling every other day for 9 days and evaluated using an ELISA. **B.** Alkaline phosphatase activity in W20-17 cells after addition of conditioned media from AdBMP2- or AdEmpty cassette-transduced cells (25000 vp/cell) (monolayer), or AdBMP2-transduced cells encapsulated in PEGDA microspheres. As a negative control, we also included culture supernatant from untransduced cells. Alkaline phosphatase activity is depicted as the average relative chemiluminescence units (RLU), where n=3. Error bars represent means ± SD for n=3. A Student t-Test was applied to demonstrate significance. AdBMP2-transduced monolayer and microsphere groups had significantly greater alkaline phosphatase activity and BMP-2 concentration levels ($p < 0.05$) when compared against other groups, but no differences when

compared to each other. In other words, microencapsulation had no effect on BMP-2 release and function.

Figure 3. Optical fluorescence imaging of mice injected with cells expressing dsRed. Top panels (A through C) are images of a representative mouse (n=4) injected with dsRed-expressing cells encapsulated in microspheres and bottom panels (D through F) are of a mouse injected with dsRed-expressing cells directly, without microspheres. The images were taken at day 4, 12 and 29 post-injection of cells. By day 29, the fluorescent signal is at background levels or undetectable for the mouse given dsRed-expressing cells without microspheres (F). Whereas, the signal remains detectable in the mouse given dsRed-expressing cells encapsulated in microspheres (C).

G. Mean Target-to-Background Ratio (TBR) of Fluorescence Intensity (FI) in mice given unencapsulated dsRed cells, microencapsulated dsRed cells or microencapsulated control cells. * $p \leq 0.05$ for microencapsulated dsRed cells versus microencapsulated control cells; † $p \leq 0.05$ for microencapsulated dsRed cells versus unencapsulated dsRed cells; ‡ $p \leq 0.05$ for unencapsulated dsRed cells versus microencapsulated control cells.

Figure 4. Micro computational analysis of the resultant heterotopic bone formation. Left images (**A, D**) are 3D surface renderings of the resultant heterotopic bone, while middle images (**B, E**) are cross-sectional slices through the new bone. Right images (C, F) show corresponding radiograms. Panels A - F show the resultant mineralization of the muscle tissues after injection

of AdBMP2-transduced cells (2500 vp/cell) encapsulated into PEGDA microspheres (**A - C**) or direct injection of unencapsulated AdBMP2-transduced cells (**D - F**). Both have a denser rim of bone, with a hollow interior structure, suggesting that the biomaterial did not alter bone patterning.

Figure 5. Quantification of the heterotopic ossification using microcomputational analysis. Cells were transduced with AdBMP2 and either directly injected or encapsulated into microspheres prior to injection, and the resultant heterotopic bone was analyzed two weeks later. Tissue parameters: **A.** bone tissue mineral content, **B.** bone volume of mineralized tissue, and **C.** bone tissue mineral density were calculated for the newly formed bone (n=6 per group). The means and standard deviations for each group were calculated and compared using a one-way analysis of variance. Results indicate that mineral content is statistically equivalent (p=0.2) between the groups, whereas the AdBMP2-transduced cells in microspheres had a significantly greater volume (p=0.038) than the AdBMP2-transduced cells directly injected. Alternatively, the bone tissue mineral density was significantly denser for the group receiving the cells directly as compared to those in microspheres (p=0.029). Panel **D.** shows a 3D volume rendering of new bone formed in cell only and microencapsulated cell groups, respectively.

Figure 6. Photomicrographs of heterotopic ossification. Hematoxylin and eosin stains of new bone formation by: **A.** directly injected and **B.** microsphere (μs) encapsulated cells. Both groups show small compact pieces of bone (arrowheads) forming ring-like structures, encircling what appears to be blood and tentative stroma in the inner region, with significant adipose (arrows) just exterior to the new bone. Scale bars are 500 μm.

1. Murugan, R., and Ramakrishna, S. Development of nanocomposites for bone grafting. Compos Sci Technol **65**, 2385, 2005.

2. Srouji, S., Blumenfeld, I., Rachmiel, A., and Livne, E. Bone defect repair in rat tibia by TGF- 1 and IGF-1 released from hydrogel scaffold. Cell Tissue Bank **5**, 223, 2004.

3. Yoneda, M., Terai, H., Imai, Y., Okada, T., Nozaki, K., Inoue, H., Miyamoto, S., and Takaoka, K. Repair of an intercalated long bone defect with a synthetic biodegradable bone-inducing implant. Biomaterials **26**, 5145, 2005.

4. Mussano, F., Ciccone, G., Ceccarelli, M., Baldi, I., and Bassi, F. Bone Morphogenetic Proteins and Bone Defects: A Systematic Review. Spine **32**, 824, 2007.

5. Mistry, A., and Mikos, A. Tissue engineering strategies for bone regeneration. Advances in Biochemical Engineering Biotechnology **94**, 1, 2005.

6. Bikram, M., Fouletier-Dilling, C., Hipp, J., Gannon, F., Davis, A., Olmsted-Davis, E., and West, J. Endochondral Bone Formation from Hydrogel Carriers Loaded with BMP2-transduced Cells. Ann Biomed Eng **35**, 796, 2007.

7. Lutolf, M., Weber, F., Schmoekel, H., Schense, J., Kohler, T., Müller, R., and Hubbell, J. Repair of bone defects using synthetic mimetics of collagenous extracellular matrices. Nat Biotechnol **21**, 513, 2003.

8. Bishop, G.B., and Einhorn, T.A. Current and future clinical applications of bone morphogenetic proteins in orthopaedic trauma surgery. Int Orthop **31**, 721, 2007.

9. Cahill, K.S., Chi, J.H., Day, A., and Claus, E.B. Prevalence, complications, and hospital charges associated with use of bone-morphogenetic proteins in spinal fusion procedures. JAMA **302**, 58, 2009.

10. Gautschi, O.P., Frey, S.P., and Zellweger, R. Bone morphogenetic proteins in clinical applications. ANZ J Surg **77**, 626, 2007.

11. Jung, R.E., Windisch, S.I., Eggenschwiler, A.M., Thoma, D.S., Weber, F.E., and Hammerle, C.H. A randomized-controlled clinical trial evaluating clinical and radiological outcomes after 3 and 5 years of dental implants placed in bone regenerated by means of GBR techniques with or without the addition of BMP-2. Clin Oral Implants Res **20**, 660, 2009.

12. Liu, Y., Hunziker, E., Vaal, C., and Groot, K. Biomimetic Coatings vs. Collagen Sponges as a Carrier for BMP-2: A Comparison of the Osteogenic Responses Triggered in vivo Using an Ectopic Rat Model. Key Eng Mater **254**, 619, 2004.

13. Schmoekel, H., Weber, F., Schense, J., Graetz, K., Schawalder, P., and Hubbell, J. Bone repair with a form of BMP-2 engineered for incorporation into fibrin cell ingrowth matrices. Biotechnol Bioeng **89**, 253, 2005.

14. Weber, F., Eyrich, G., Grätz, K., Maly, F., and Sailer, H. Slow and continuous application of human recombinant bone morphogenetic protein via biodegradable poly (lactide-co-glycolide) foamspheres. Int J Oral Maxillofac Surg **31**, 60, 2002.

15. Halstenberg, S., Panitch, A., Rizzi, S., Hall, H., and Hubbell, J. Biologically engineered protein-graft-poly (ethylene glycol) hydrogels: a cell adhesive and plasmin-degradable biosynthetic material for tissue repair. Biomacromol **3**, 710, 2002.

16. Peppas, N.A. Hydrogels. In: B. D. Ratner, A.S.H., F. J. Schoen and J. E. Lemons, ed. Biomaterials Science: An Introduction to Materials in Medicine. San Diego: Elsevier Academic Press, 2004, pp. 100-07.

17. Tsang, V., Chen, A., Cho, L., Jadin, K., Sah, R., DeLong, S., West, J., and Bhatia, S. Fabrication of 3D hepatic tissues by additive photopatterning of cellular hydrogels. Faseb J **21**, 790, 2007.

18. Cruise, G.M., Hegre, O.D., Lamberti, F.V., Hager, S.R., Hill, R., Scharp, D.S., and Hubbell, J.A. In vitro and in vivo performance of porcine islets encapsulated in interfacially photopolymerized poly (ethylene glycol) diacrylate membranes. Cell transplantation **8**, 293, 1999.

19. Slaughter, B.V., Khurshid, S.S., Fisher, O.Z., Khademhosseini, A., and Peppas, N.A. Hydrogels in Regenerative Medicine. Advanced Materials **21**, 3307, 2009.

20. Fouletier-Dilling, C., Gannon, F., Olmsted-Davis, E., Lazard, Z., Heggeness, M., Shafer, J., Hipp, J., and Davis, A. Efficient and Rapid Osteoinduction in an Immune-Competent Host. Hum Gene Ther **18**, 733, 2007.

21. Thies, R. Recombinant human bone morphogenetic protein-2 induces osteoblastic differentiation in W-20-17 stromal cells. Endocrinology **130**, 1318, 1992.

22. Olmsted, E., Blum, J., Rill, D., Yotnda, P., Gugala, Z., Lindsey, R., and Davis, A. Adenovirus-Mediated BMP2 Expression in Human Bone Marrow Stromal Cells. J Cell Biochem **82**, 11, 2001.

23. Davis, A., Wivel, N., Palladino, J., Tao, L., and Wilson, J. Construction of adenoviral vectors. Mol Biotechnol **18**, 63, 2001.

24. Kimelman, N., Pelled, G., Helm, G.A., Huard, J., Schwarz, E.M., and Gazit, D. Review: gene- and stem cell-based therapeutics for bone regeneration and repair. Tissue Eng **13**, 1135, 2007.

25. Fouletier-Dilling, C., Bosch, P., Davis, A., Shafer, J., Stice, S., Gugala, Z., Gannon, F., and Olmsted-Davis, E. Novel compound enables high-level adenovirus transduction in the absence of an adenovirus-specific receptor. Hum Gene Ther **16**, 1287, 2005.

26. van Dijk-Wolthuis, W.N.E., Hoogeboom, J.A.M., Van Steenbergen, M.J., Tsang, S.K.Y., and Hennink, W.E. Degradation and release behavior of dextran-based hydrogels. Macromolecules **30**, 4639, 1997.

27. Liao, H., Munoz-Pinto, D., Qu, X., Hou, Y., Grunlan, M.A., and Hahn, M.S. Influence of hydrogel mechanical properties and mesh size on vocal fold fibroblast extracellular matrix production and phenotype. Acta biomaterialia **4**, 1161, 2008.

28. Elbert, D.L., Pratt, A.B., Lutolf, M.P., Halstenberg, S., and Hubbell, J.A. Protein delivery from materials formed by self-selective conjugate addition reactions. J Controlled Release **76**, 11, 2001.

29. Scheufler, C., Sebald, W., and Hulsmeyer, M. Crystal structure of human bone morphogenetic protein-2 at 2.7 A resolution. J Mol Biol **287**, 103, 1999.

30. Myers, R.D. Injection of solutions into cerebral tissue: relation between volume and diffusion. Physiol Behav **1**, 171, 1966.

31. Tehovnik, E.J., and Sommer, M.A. Effective spread and timecourse of neural inactivation caused by lidocaine injection in monkey cerebral cortex. J Neurosci Methods **74**, 17, 1997.

32. Fu, J., Fiegel, J., Krauland, E., and Hanes, J. New polymeric carriers for controlled drug delivery following inhalation or injection. Biomaterials **23**, 4425, 2002.

33. Greenwald, R.B., Choe, Y.H., McGuire, J., and Conover, C.D. Effective drug delivery by PEGylated drug conjugates. Adv Drug Deliv Rev **55**, 217, 2003.

34. Gugala, Z., Davis, A., Fouletier-Dilling, C., Gannon, F., Lindsey, R., and Olmsted-Davis, E. Adenovirus BMP2-induced osteogenesis in combination with collagen carriers. Biomaterials **28**, 4469, 2007.

35. Gugala, Z., Olmsted-Davis, E., Gannon, F., Lindsey, R., and Davis, A. Osteoinduction by ex vivo adenovirus-mediated BMP2 delivery is independent of cell type. Gene Ther **10**, 1289, 2003.

36. Carmeliet, P., and Jain, R.K. Angiogenesis in cancer and other diseases. Nature **407**, 249, 2000.

Reprint Author: Jennifer L. West, Department of Bioengineering, Rice University, 6500 Main St. MS 142, Houston, TX 77030, USA

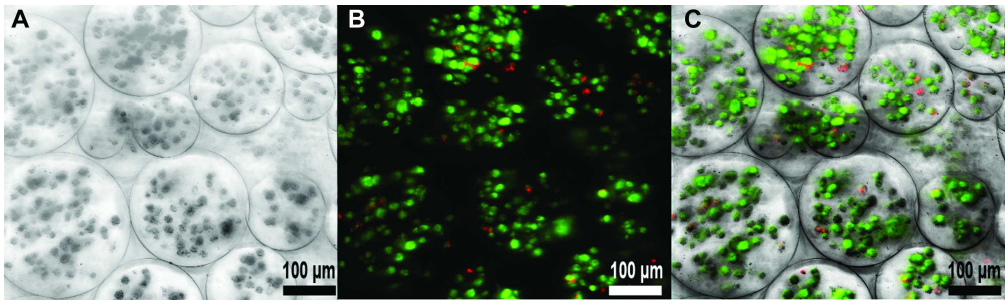

Viability of AdBMP2-transduced cells (2500 vp/cell) within microspheres was assessed at day 7 using a LIVE/DEAD® Viability/Cytotoxicity Kit for mammalian cells (Invitrogen, Molecular Probes, Eugene, OR). A. Minimum intensity projection of a differential interference contrast (DIC) Z-stack. B. Maximum intensity projection of fluorescent Z-stack merge of red and green channels. The red channel was thresholded to eliminate diffuse virus staining. Dead cells appear red and live cells appear green. C. Overlay of panels A and B. Living cells accounted for 95.08% ± 0.47% of total cells encapsulated.
254x75mm (300 x 300 DPI)

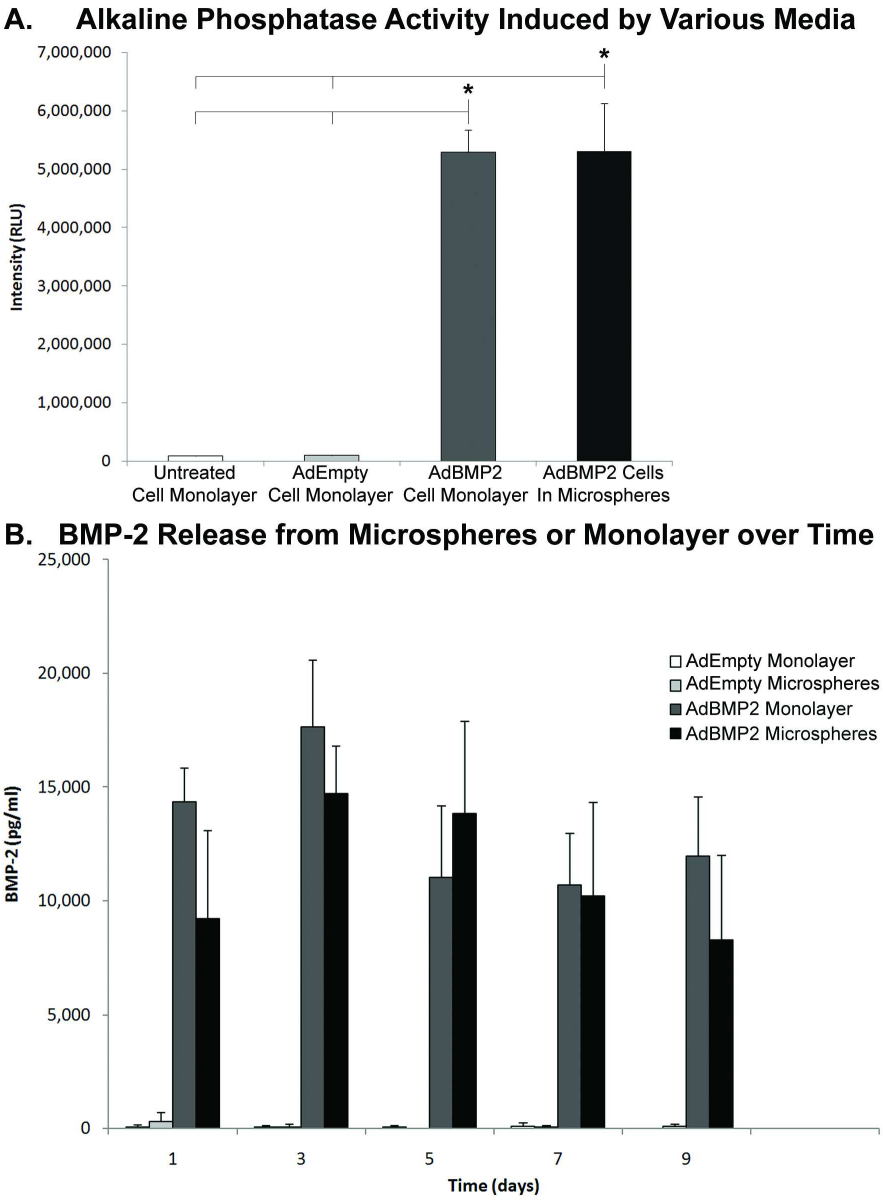

Comparison of BMP-2 expression, secretion and activity after PEGDA encapsulation. A. BMP-2 protein in culture supernatant taken from AdBMP2- or AdEmpty cassette-transduced cells (25000 vp/cell) (monolayer), or those encapsulated in PEGDA microspheres was quantified by sampling every other day for 9 days and evaluated using an ELISA. B. Alkaline phosphatase activity in W20-17 cells after addition of conditioned media from AdBMP2- or AdEmpty cassette-transduced cells (25000 vp/cell) (monolayer), or AdBMP2-transduced cells encapsulated in PEGDA microspheres. As a negative control, we also included culture supernatant from untransduced cells. Alkaline phosphatase activity is depicted as the average relative chemiluminescence units (RLU), where n=3. Error bars represent means ± SD for n=3. A Student t-Test was applied to demonstrate significance. AdBMP2-transduced monolayer and microsphere groups had significantly greater alkaline phosphatase activity and BMP-2 concentration levels ($p < 0.05$) when compared against other groups, but no differences when compared to each other. In other words, microencapsulation

had no effect on BMP-2 release and function.
152x203mm (300 x 300 DPI)

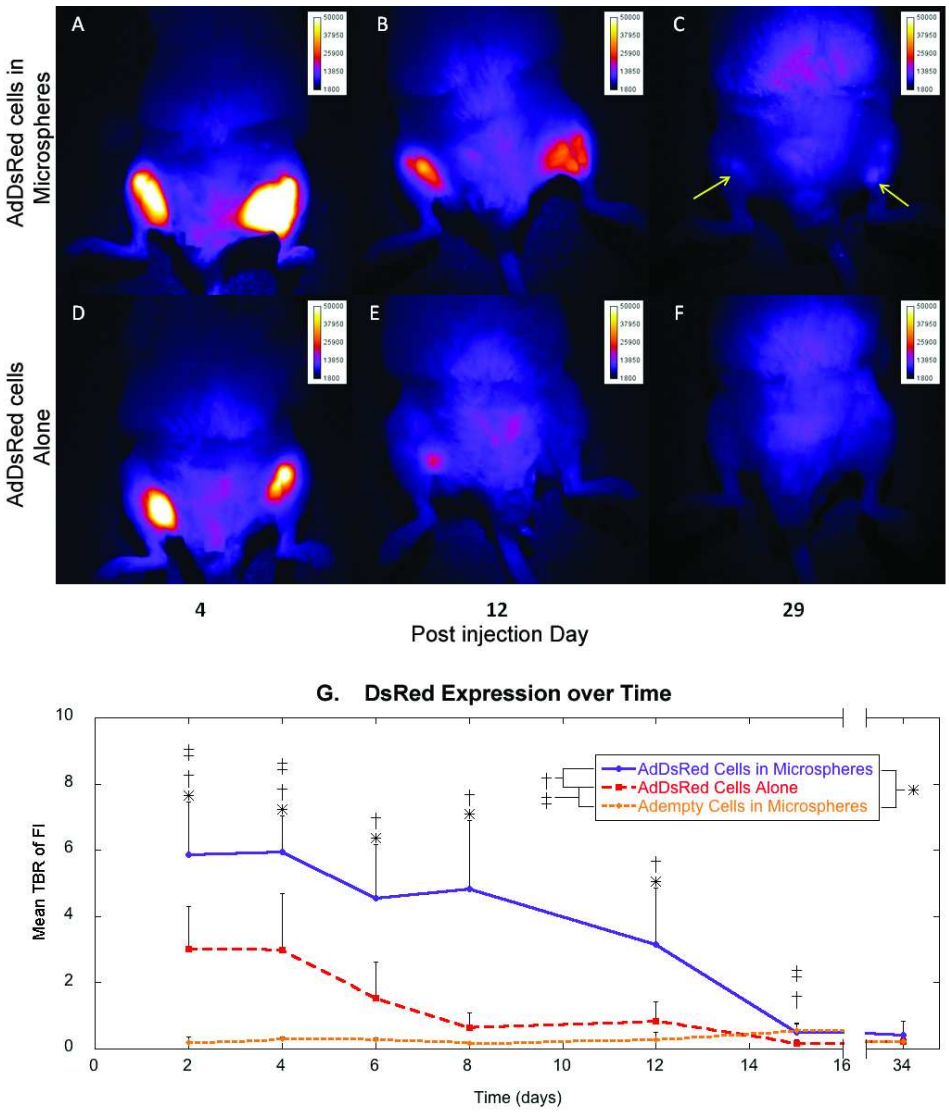

Optical fluorescence imaging of mice injected with cells expressing dsRed. Top panels (A through C) are images of a representative mouse (n=4) injected with dsRed-expressing cells encapsulated in microspheres and bottom panels (D through F) are of a mouse injected with dsRed-expressing cells directly, without microspheres. The images were taken at day 4, 12 and 29 post-injection of cells. By day 29, the fluorescent signal is at background levels or undetectable for the mouse given dsRed-expressing cells without microspheres (F). Whereas, the signal remains detectable in the mouse given dsRed-expressing cells encapsulated in microspheres (C).

G. Mean Target-to-Background Ratio (TBR) of Fluorescence Intensity (FI) in mice given unencapsulated dsRed cells, microencapsulated dsRed cells or microencapsulated control cells. * $p \leq 0.05$ for microencapsulated dsRed cells versus microencapsulated control cells; $p \leq 0.05$ for microencapsulated dsRed cells versus unencapsulated dsRed cells; ‡ $p \leq 0.05$ for unencapsulated dsRed cells versus microencapsulated control cells.

381x423mm (72 x 72 DPI)

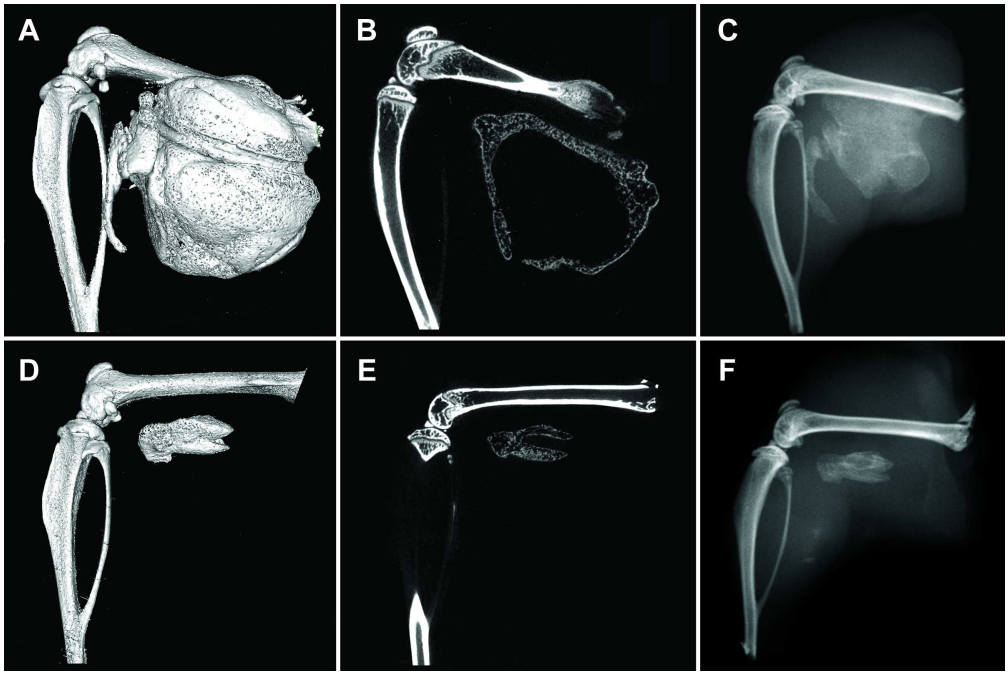

Micro computational analysis of the resultant heterotopic bone formation. Left images (A, D) are 3D surface renderings of the resultant heterotopic bone, while middle images (B, E) are cross-sectional slices through the new bone. Right images (C, F) show corresponding radiograms. Panels A - F show the resultant mineralization of the muscle tissues after injection of AdBMP2-transduced cells (2500 vp/cell) encapsulated into PEGDA microspheres (A - C) or direct injection of unencapsulated AdBMP2-transduced cells (D - F). Both have a denser rim of bone, with a hollow interior structure, suggesting that the biomaterial did not alter bone patterning.
846x564mm (72 x 72 DPI)

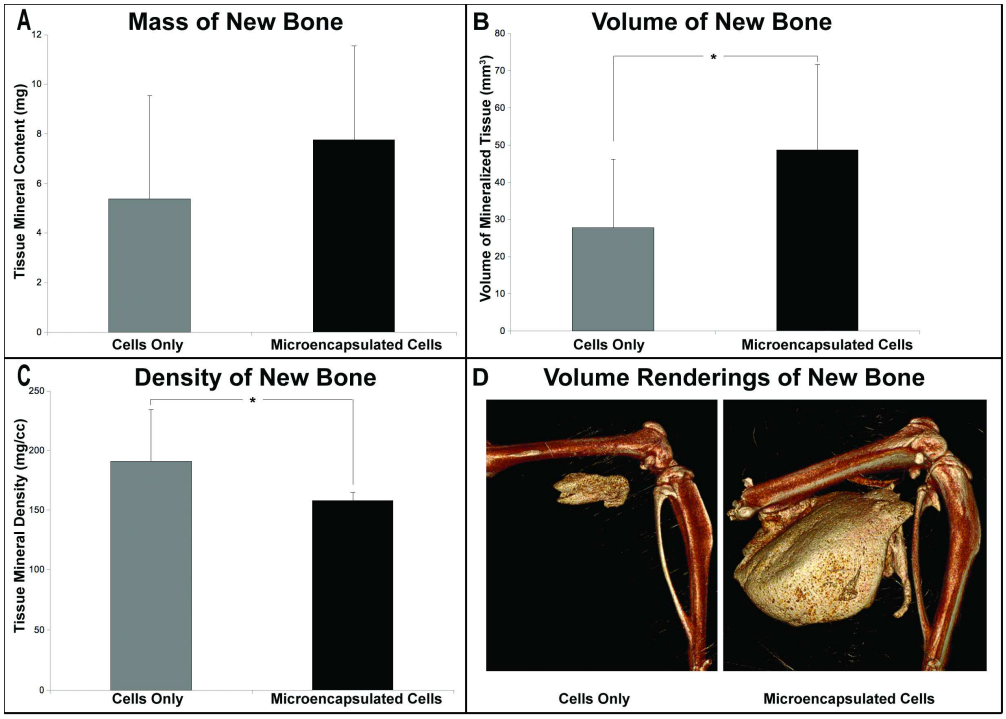

Quantification of the heterotopic ossification using microcomputational analysis. Cells were transduced with AdBMP2 and either directly injected or encapsulated into microspheres prior to injection, and the resultant heterotopic bone was analyzed two weeks later. Tissue parameters: A. bone tissue mineral content, B. bone volume of mineralized tissue, and C. bone tissue mineral density were calculated for the newly formed bone (n=6 per group). The means and standard deviations for each group were calculated and compared using a one-way analysis of variance. Results indicate that mineral content is statistically equivalent (p=0.2) between the groups, whereas the AdBMP2-transduced cells in microspheres had a significantly greater volume (p=0.038) than the AdBMP2-transduced cells directly injected. Alternatively, the bone tissue mineral density was significantly denser for the group receiving the cells directly as compared to those in microspheres (p=0.029). Panel D. shows a 3D volume rendering of new bone formed in cell only and microencapsulated cell groups, respectively.
868x619mm (72 x 72 DPI)

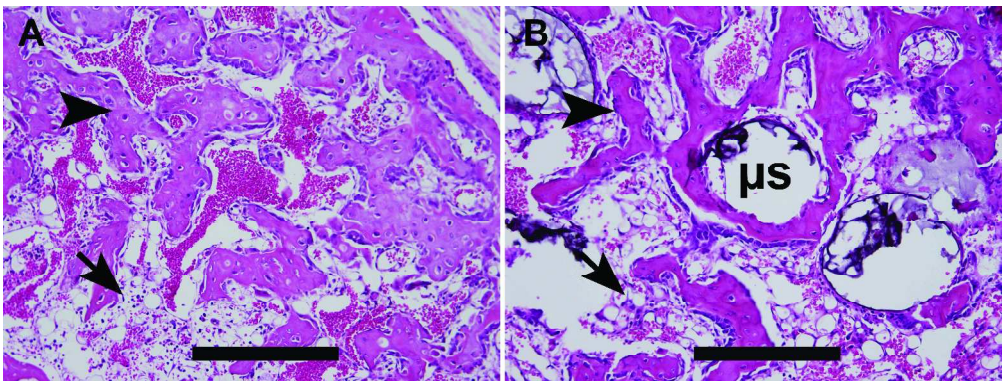

Photomicrographs of heterotopic ossification. Hematoxylin and eosin stains of new bone formation by: A. directly injected and B. microsphere (μs) encapsulated cells. Both groups show small compact pieces of bone (arrowheads) forming ring-like structures, encircling what appears to be blood and tentative stroma in the inner region, with significant adipose (arrows) just exterior to the new bone. Scale bars are 500 μm.
2892x1083mm (72 x 72 DPI)

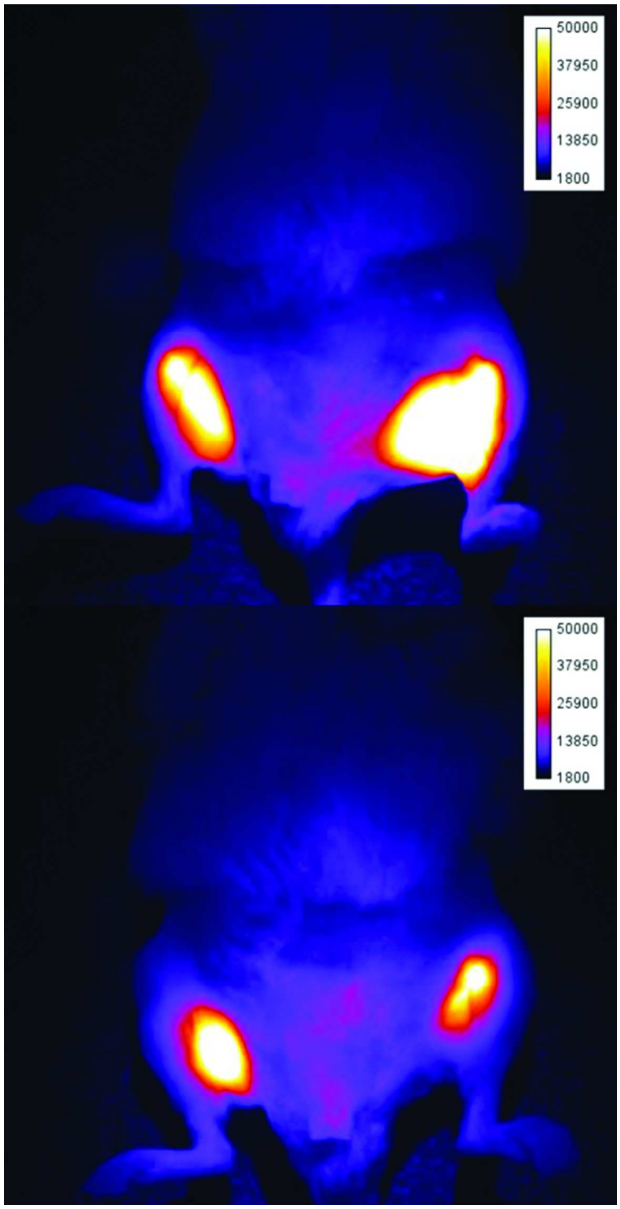

Image for consideration as cover art
197x385mm (300 x 300 DPI)

Cathepsin-K sensitive poly(ethylene Glycol) hydrogels for degradation in response to bone formation

Chih-Wei Hsu[a], Ronke M. Olabisi[a], Elizabeth A. Olmsted-Davis[b], Alan R. Davis[b], Jennifer L. West[a]

[a]*Department of Bioengineering, Rice University, 6100 Main St., MS 142, Houston, TX 77005, USA*

[b]*Center for Cell and Gene Therapy, Baylor College of Medicine, Houston, TX 77030, USA*

Abstract

In a previous study, we demonstrated that encapsulated cells transduced with rhBMP-2 in poly(ethylene glycol) diacrylate hydrogel gels can be osteoinductive and osteogenic as bone graft substitutes. A cathepsin k-sensitive PEG hydrogel was designed and tested to assist the system, which can be further integrated with surrounding tissue after implantation via bone resorption. A cathepsin K sensitive peptide GGGMGPSGPWGGK was synthesized and modified by acryloyl-PEG-succinimidyl carbonate to produce a crosslinkable GPSG hydrogel structure. Degradation profiles of the GPSG hydrogels were tested with cathepsin K and proteinase K as a positive control, which both released 80% of their tryptophan content compared to 40% release in nonspecific collagenases in a 24 hour time period. No degradation was observed when the hydrogels were incubated with plasmin or buffers. Differentiated MC3T3-E1 osteoblasts and RAW264.7 osteoclasts were seeded on GPSG hydrogels to test cell-induced degradation on the surface. Surface features and resorption pits were analyzed by differential interference contrast (DIC) and fluorescence images by confocal microscopy. In summary, we have developed a cathepsin k-sensitive GPSG hydrogel that can be degraded by cathepsin K in vitro and also be modified by RAW264.7 differentiated osteoclasts in cell culture studies.

Key words: Bioresorption, Bone graft, Hydrogel, Osteoclast, Scaffold.

1. Introduction

Bone grafting is a common procedure in orthopedic surgery, and both autografts and allografts have been commonly used in spinal fusion, revision total hip arthroplasty, maxillofacial reconstruction, and repair of segmental skeletal defects caused by tumor resection or trauma [1-4]. Although autografts are considered the gold standard for repairs of bone defects, its usage is limited by donor-site morbidity and availability, and the procedure also requires additional surgeries for graft harvesting often resulting in persistent postoperative pain and the risk of neurovascular damage at donor sites [5, 6]. Although no additional surgeries are performed on patients for allografts, these procedures hold risks of infection, immunorejection, disease transmission, and unfavorable mechanical properties [7-10]. Due to the high demand for bone grafts, several strategies have been developed to assist bone grafts or function as substitutes, such as demineralized bone matrix (DBM), ceramic, gene therapy, graft composite, or bone morphogenetic proteins (BMPs) [11-14]. In order to mimic the properties of autografts, an ideal bone-graft

substitute has to be osteoconductive, osteoinductive, and osteogenic. Furthermore, the bone grafts must be able to integrate with the host without triggering an immunoresponse [12].

Poly(ethylene glycol) diacrylate (PEGDA) hydrogel has been used as tissue engineering scaffolds in several applications [14-17]. PEGDA can be covalently crosslinked under UV or white light exposure with the aid of photoinitiators. A crosslinked PEGDA network is hydrophilic, low protein adsorption, and possesses tunable-mechanical properties. The capability to control its mesh size can also be used to regulate diffusion of gas, nutrients, and desired proteins throughout the structure [18]. A crosslinked PEGDA hydrogel structure can also be modified with tethered adhesive ligands or growth factors for cell attachment or stimulation [19]. Previous studies have also shown that PEGDA hydrogels can provide immuno-protection while encapsulated cells still functioned normally after xeno-transplantation [16, 20]. Although PEGDA is non-degradable, incorporating a short peptide sequence into the backbone of the polymer can modify the network structure to enable degradation by specific enzymes [21, 22]. Gobin et al. developed a collagnase-sensitive PEG scaffold by incorporating a peptide sequence LGPA to study the migration behavior of fibroblasts [21]. This scaffold has also been studied in the application of fabricating tissue engineered vascular grafts [15].

In a previous study, we demonstrated that encapsulation of adenovirus-transduced cells expressing recombinant human BMP-2 (rhBMP-2) within non-degradable PEGDA hydrogels can facilitate bone formation *in vivo* [14]. Human diploid fetal lung fibroblasts (MRC-5) were transduced with the adenovirus Ad5F35BMP2 and encapsulated within PEGDA hydrogels. Encapsulated cells transduced with rhBMP-2 in PEGDA hydrogels were implanted into the quadricep muscles of each of the two hind legs of female NOD/SCID mice. Endochondral bone was detected around implanted hydrogels after 3 weeks. This model demonstrated that the PEGDA scaffold provided osteoconduction, rhBMP-2 expressed by transduced cells provided osteoinduction, and the progenitor cells recruited by rhBMP-2 were osteogenic. However, because the implanted PEGDA hydrogels were non-degradable, the induced bone only formed shells around the hydrogel cores without penetrating or replacing the hydrogels. To better develop a bone graft substitute, the PEGDA hydrogel needed to be modified to enable integration within the surrounding tissue.

To better integrate the bone graft substitute with the host we chose to follow the process of bone remodeling. Bone remodeling is accomplished by the processes of bone formation and resorption [23]. Bone formation is accomplished following mineralization by matrix producing osteoblasts. Bone resorption is accomplished by osteoclasts. When the resorption cycle starts, ostoclasts will migrate and attach to resorption sites. Attached osteoclasts will then start to polarize and form new membrane domains. The apex membrane will form a functional secretory domain, the membranes around the attaching site will form a sealing ring, and the bottom of the membrane will form a ruffled border. Polarized osteoclasts secrete

hydrochloric acid to dissolve hydroxyapatite and proteases to degrade the type I collagen-rich organic matrix. The cell will then undergo apoptosis or revert back to a non-resorption stage [24].

The objective in this paper is to develop a PEG hydrogel system that will not only be an osteoconductive carrier for cells, but will also be gradually integrated with new endochondral bone via the process of bone remodeling. In this study, we developed a hydrogel system that can be gradually remodeled through bone resorption by osteoclasts. The degradable hydrogel is designed by introducing a short peptide fragment Gly-Pro-Ser-Gly (GPSG) of type I collagen (α-1) (160-163), which was found to be highly cleavable between serine and glycine by cathepsin K [25]. Cathepsin K is a protease predominantly expressed in osteoclasts during bone resorption [24, 26]. After incorporating this cathepsin K sensitive peptide into a PEG backbone, we tested the degradation profiles of the cathepsin K sensitive GPSG hydrogel *in vitro*. We also tested the hydrogel to determine whether it could be degraded by osteoclasts or osteoblasts.

2. Materials and Methods

2.1 Synthesis and characterization of acryloyl-PEG-succinimidyl carbonate (acrylol-PEG-SMC)

All reagents were obtained from Sigma unless otherwise noted. 50 mM of PEG (3,400 Da; Fluka, Milwaukee, WI) was reacted with 75 mM silver (I) oxide and 55 mM acryloyl chloride in anhydrous dichloromethane (anDCM). Thirty mM of potassium iodine was added as catalyst, and the mixture was reacted at 0-4 ^{O}C overnight. To purify the acryloyl-PEG-OH, silver (I) oxide was first removed by filtering the mixture through a Celite 521 pad (Spectrum Chemical Manufacturing Corp, Gardena, CA). For further purification, the filtrate was dried by using a Rotovap, re-dissolved in de-ionized water, and adjusted to pH 3 with 6N HCl. After heating to 35 ^{O}C and venting to air for 1 h, activated charcoal (Fisher Scientific, Pittsburgh, PA) was added to the mixture and stirred overnight to absorb iodine. The charcoal was then removed via filtration. Sodium chloride (25% W/V) was dissolved in the aqueous filtrate followed by DCM extraction. The organic phase was collected and extracted again with 2 M potassium bicarbonate to remove chloride ions. Acryloyl-PEG-OH was recovered by precipitation in cold ethyl ether, filtered, dried under vacuum overnight, and lyophilized until completely dry. To proceed with the succinimidyl carbonate conjugation, 25 mM acryloyl-PEG-OH was mixed with 75 mM pyridine and 100 mM N,N'-disuccinimidyl carbonate in anhydrous acetonitrile. After reacting under argon overnight, pyridine and acetonitrile were removed with a Rotovap. The mixture was then re-dissolved in anhydrous DCM and filtered to remove unreacted N,N'-disuccinimidyl carbonate. Acetate buffer (0.1 M, pH 4.5, 15% NaCl) was then used for phase extraction. The organic layer was collected and then dried by anhydrous $MgSO_4$. Acryloyl-PEG-SMC was recovered following precipitation in cold ethyl ether, filtered, and dried under vacuum overnight. The products were analyzed by ^{1}H-NMR (Advance 400, Bruker, Germany) and matrix-assisted laser desorption ionization time of flight mass spectrometry (MALDI-ToF; Bruker Daltonics, Billerica, MA) and stored at -80^{O}C under argon.

2.2 Synthesis and characterization of the cathepsin K sensitive PEG-GGGMGPSGPWGGK-PEG, PEG-RGDS, and fluorescently-labeled PEG-RGDS conjugates

The Cathepsin K-sensitive peptide sequence GGGMGPSGPWGGK was synthesized on an APEX 396 peptide synthesizer (Aapptec, Louisville, KY). A tryptophan residue was incorporated into the peptide sequence for the purpose of tracking *in vitro* degradation by monitoring UV absorbance at 280 nm. The peptide was then cleaved from the polystyrene resin (95 % trifluoroacetic acid, 2.5 % water, and 2.5 % triisopropylsilane), precipitated in ethyl ether, and purified by dialysis. Following purification, the molecular weight of the synthesized peptide was confirmed with MALDI-ToF. The crosslinkable cathepsin K sensitive acryloyl-PEG-GGGMGPSGPWGGK-PEG-acryloyl (GPSG) polymer was synthesized by reacting the peptide with acryloyl-PEG-SMC in a 2.1:1 (PEG:peptide) molar ratio in 50 mM sodium bicarbonate buffer (pH 8.5) at room temperature overnight. The product was dialyzed, lyophilized, and stored under argon at -20^{O}C until use. The cell adhesive peptide Arg-Gly-Asp-Ser (RGDS, American Peptide, Sunnyvale, CA) was also reacted with acryloyl-PEG-SMC in a 1.1:1 molar ratio to give acryloyl-PEG-RGDS. Conjugation products were analyzed by ^{1}H-NMR and gel permeation chromatography (GPC; Polymer Laboratories, Amherst, MA) with UV/Vis and evaporative light scattering detectors. Fluorescently Labeled acryloyl-PEG-RGDS was synthesized as previously described [27]. In brief, purified acryloyl-PEG-RGDS was mixed with Alexa Fluor 680 carboxylic acid (Invitrogen, Carlsbad, CA) in 50 mM sodium bicarbonate buffer in a 1:10 (acryloyl-PEG-RGDS:dye) molar ratio and allowed to react for 1 h at room temperature. The desired products were then purified by a Sephadex G-25 fine chromatography column (Amersham Bioscience, Uppsala, Sweden) followed by dialysis and then lyophilized. Recovered products were stored under argon at -20 ^{O}C until use.

2.3 In vitro degradation profiles of the GPSG hydrogel

The degradation profiles of GPSG hydrogel were measured by monitoring the release of tryptophan into solution after incubation with different enzymes. A pre-polymer solution was prepared by combining 0.1 g/ml crosslinkable GPSG polymer with 1.5 % (v/v) triethanolamine, 37 mM 1-vinyl-2-pyrrolidinone, and 1 % (v/v) of 10 mM eosin Y in tris buffered saline (TBS; pH 7.5, 10 mM $CaCl_2$, 0.1 % Tween 20, 0.2 mg/ml sodium azide). The precursor solution was sterilized by filtration using a 0.22 μm filter (Millpore Corporation Bedford, MA). For *in vitro* enzyme degradation test, 3 μL of pre-polymer solution was transferred to the bottom corner of each micro-cuvette (Brandtech, Essex, CT) and polymerized by exposing to visible light for 2 minutes. Following equilibrium swelling overnight in 250 μL TBS buffer, each hydrogel was incubated with 250 μL enzyme solution at 37^{O}C for 24 hours. Proteinase K (Invitrogen), plasmin, type I and type III collagenase (COL I and COL III; Worthington, Lakewood, NJ) were prepared in TBS buffer to the final concentration of 0.05 mg/ml. Procathepsin K (Enzo Life Science, Plymouth Meeting, PA) was first activated in 35 mM sodium acetate (pH 3.5) for 2 hours at room temperature. Activated cathepsin K was then

adjusted to 0.05 mg/ml in 50 mM sodium acetate buffer (NaOAc; pH 5.5, 2.5 mM EDTA, 1 mM DTT, 0.01 % Triton X-100, 0.2 mg/ml sodium azide). Hydrogels were also incubated in TBS and NaOAc buffer as negative controls. Degradation was evaluated by measuring the absorbance change at 280 nm of test solutions to monitor the release of tryptophan over time with a UV/Vis spectrophotometer (Carey 50, Varian, Palo Alto, CA).

2.4 Cell maintenance of MC3T3-E1 and RAW 264.7 cells

Murine pre-osteoblast cells MC3T3-E1 subclone 4 and macrophage cells RAW 264.7 (ATCC, Manassas, VA, USA) were recovered from liquid nitrogen and cultured in alpha-MEM medium (Gibco BRL, Canada) and DMEM (ATCC), respectively. Culture media were supplemented with 10 % fetal bovine serum (FBS; Atlanta Biologicals, Lawrenceville, GA), 100 U/ml penicillin, and 100 mg/ml streptomycin (Gibco BRL, Canada). Cells were incubated at $37^{O}C$ with 5 % CO_2. The medium was refreshed every 2–3 days and confluent cells were subcultured through trypsinization for MC3T3-E1 and scraping for RAW 264.7. All experiments were conducted using cells between passages 4-10. MC3T3-E1 cells were differentiated into osteoblasts via supplied 50 ug/ml ascorbic acid and 10 mM b-glycerophosphate to the growth medium. Differentiation medium was subsequently replaced every 2-3 days. To differentiate cells to multinuclear osteoclasts, RAW 264.7 were cultured at a density of 1.5×10^5 cells/cm^2 and allowed to adhere for 4 hours. Medium was then supplied with 30 ng/ml of receptor activator of nuclear factor kappa B ligand (RANKL; R&D Systems Inc., Minneapolis, MN) and replaced every 2 days. The cells were then cultured for 4 days before further use.

2.5 Serum gradient purification of differentiated multinuclear RAW264.7

Differentiated multinuclear RAW264.7 (dRAW264.7) were purified by a serum gradient [28]. After differentiation in culture medium supplied with 30 ng/ml RANKL for 4 days, dRAW264.7 cells were trypsinized and resuspended in 15 ml of Moscona's high carbonate (MHB; pH 7.2, 137 mM NaCl, 2.7 mM KCl, 0.4 mM NaH_2PO_4, 12 mM $NaHCO_3$, and 11 mM dextrose) solution. A serum gradient was prepared by placing a layer of 15 ml 70% FBS solution in MHB at the bottom of a 50 ml conical tube, and then slowly overlaying with a second layer of 15 ml 40% FBS solution. Fifteen ml of cell suspension was then slowly added to the top without disturbing the layers. The tube was then capped and held undisturbed at room temperature for 30 minutes to permit cells to separate based on size. The top 17 ml layer, middle 16 ml layer, and bottom 12 ml layer were collected separately. Cells in each layer were centrifuged down and seeded in tissue culture plates overnight. After attaching, cells were fixed and stained for the activity of tartrate-resistant acid phosphatase (TRAP).

2.6 Surface degradation studies of differentiated RAW 264.7 and MC3T3- E1 on GPSG hydrogels

Flat hydrogel sheets for surface degradation studies were formed by adding 10 mM acrylate-PEG-RGDS

and 1 mM Alexaflour 680 labeled acrylate-PEG-RGDS to the pre-polymer mixture and polymerizing between a mica sheet (Ted Pella, Inc., Redding, CA) and glass slide separated by a 1 mm Teflon spacer. The mica sheet resulted in hydrogels with atomically smooth surfaces. Both MC3T3-E1 and RAW 264.7 cells were differentiated for 4 days in differentiation media in tissue culture plates. Differentiated MC3T3-E1 (dMC3T3-E1) were subcultured and seeded on to the atomically smooth hydrogel surfaces at a density of 5 x 10^4 cells/cm^2. Differentiated multinuclear RAW264.7 osteoclasts collected at the bottom layer of serum gradient were also seeded on smooth hydrogel surfaces at the same density. Hydrogels seeded with both osteoblasts and osteoclasts were then cultured in differentiation medium for 48 hours before further analysis.

2.7 Confocal microscopy of pit formation on cathepsin K sensitive PEG hydrogel surface

After a 48 hour incubation on smooth hydrogel surfaces, cells were either detached from the hydrogel surface by 20 mM EDTA or fixed and stained with 4',6-diamidino-2-phenylindole (DAPI; Invitrogen) and rhodamine phalloidin (Invitrogen). Differential interference contrast (DIC) or fluorescence images were taken by LSM-5 LIVE microscope systems (Carl Zeiss Inc., German). Z-stack images were acquired with a 20X objective. The z distance between each step was 0.253 μm. Images were all processed with ImageJ 142 (NIH, Bethesda, MD). Three dimensional image reconstructions were processed using OsiriX Medical Imaging software (version 3.0.2; the OsiriX Foundation, Geneva, Switzerland).

3. Results

3.1 Characterization of synthesized materials.

^{1}H-NMR analysis demonstrated that acryloyl-PEG-SCM was successfully synthesized and conjugated to GGGMGPSGPWGGK and RGDS. After purification, the acryloyl-PEG-SCM showed the methylene protons of PEG as a triplet at 3.6–3.7 ppm, the succinimidyl carbonate protons at 2.6 ppm, as well as the acrylate protons at 5.9–6.4 ppm. After conjugation to GGGMGPSGPWGGK and RGDS, the peak for the succinimidyl carbonate protons disappeared, but peaks for the methylene protons of PEG and acrylate protons remained. The shift in molecular weight of conjugated products was also evaluated by GPC.

3.2 In vitro degradation of Cathepsin K-sensitive GPSG hydrogels

The hydrogels with the cathepsin K sensitive peptide GGGMGPSGPWGGK were designed to carry a cathepsin K sensitive cleavage site between serine and proline [25]. Proteinase K was used as a positive control. While the gel degrades, the peptide that was incorporated into the hydrogel structure will be cleaved by enzymes and gradually release into solution. The degradation profiles of GPSG hydrogels were measured by monitoring the concentration change of tryptophan in solution at UV absorbance of 280 nm. Crosslinkable GPSG hydrogels were polymerized in microcuvettes and incubated with enzyme solutions. After equilibilium swelling in TBS overnight, hydrogels were treated with different enzymes to evaluate the

degradation profiles (Figure 1). After incubation with different enzyme solutions for 24 hours, hydrogels in cathepsin K and proteinase K solutions has similar degradation profiles, both indicating a rapid tryptophan concentration increase within the first hour and reaching about 80% release of total tryptophan at 24 hours. No degradation was observed when hydrogels were incubated in TBS buffer, NaOAc buffer, and plasmin. Hydrogels incubated in nonspecific collagenase I and collagenase III solutions also released 40% of incorporated tryptophan after a 24 hour incubation.

3.3 Differentiation of RAW264.7

Raw 264.7 cells were differentiated in culture medium containing 30 ng/ml RANKL for 4 days. Differentiated cells were then trypsinized and separated by serum gradient based on gravity. Cells collected at the top, middle, and bottom fractions of the gradient solution were reseeded on tissue culture plate and stained for TRAP activity (Figure 2). Non-differentiated RAW264.7 cells were stained TRAP negative. Although all stained TRAP positive after differentiation, not all of the cells can fuse into multinuclear cells (Figure 2A). After separation by serum gradient, the top fraction of the gradient contained most of the mononuclear cells. The middle fraction of the gradient contained mixed groups of mononuclear and multinuclear cells. The majority of cells at the bottom fraction were multinuclear cells, which contained a very small portion of mononuclear cells (Figure 2B to D). The multinuclear cells collected at the bottom fraction were also stained TRAP positive, which indicted that they were active osteoclasts. The bottom fraction of TRAP+ dRAW 264.7 osteoclasts were then used for hydrogel degradation studies.

3.4 DIC images of cathepsin K sensitive hydrogel surfaces seeded with dMC3T3E1 and dRAW264.7

To evaluate if the GPSG hydrogels can be degraded by osteoblasts or osteoclasts, dMC3T3-E1 osteoblasts and dRAW264.7 osteoclasts were seeded on atomically smooth hydrogel surface polymerized against a mica sheet. After 48 hours, osteoblasts and osteoclasts were detached by 20mM EDTA, and the hydrogel surfaces were examined with DIC images under confocal microscopy (Figure 3). No features were detected on the surfaces seeded with dMC3T3-E1 osteoblasts (Figure 3A). On the surfaces seeded with dRAW264.7 osteoclasts, several features were observed after cells were detached (Figure 3B). The intensity profile of the DIC image (Figure 3D) suggests that the features on the hydrogels were depressions.

3.5 Three dimensional image reconstruction of dRAW264.7 cells on the surface of cathepsin K sensitive hydrogels

To further confirm the depressed imperfections observed on hydrogel surface were actual resorption pits generated by dRAW264.7, osteoclasts on GPSG hydrogels were fixed and stained with DAPI for nuclei and rhodamine phalloidin for F-actin. Hydrogels were then examined under confocal microscopy. dRAW264.7 cells stained with DAPI and rhodamine phalloidin showed multinuclear and polarized cells on the hydrogel

surface, and the GPSG hydrogel was polymerized with Alexafluor680 labeled acryloyl-PEG-RGDS (Figure 4A; Supplement A video). A sealing ring of F-actin and multiple nuclei were clearly observed (Figure 4B). On the hydrogel surface where the osteoclast was located, a decrease in the fluorescent signal was observed (Figure 4C). The z-stack images were then examined closely by three-dimensional reconstructions using a volume rendering method. Figure 4D is the side view, showing the osteoclast attached to the hydrogel. From the three-dimensional perspective of the image from the top (Figure 4E) and bottom (Figure 3F) of the hydrogel, the loss in fluorescent signal of the hydrogel reveals a hole in the hydrogel through which the cell can be seen. This signal loss is indicative of activity by the differentiated RAW264.7 osteoclasts, degrading the underlying hydrogel and creating a pit, resulting in the fluorescent intensity loss. No signal loss was observed on the gels seeded with dMC3T3-E1 cells.

4. Discussion

An ideal autologous bone graft substitute has to comprise the properties of an osteoconductive, osteoinductive, osteogenic, and bioresorbable material. We have previously demonstrated that encapsulated cells transduced with rhBMP-2 in poly(ethylene glycol) diacrylate hydrogel gels can be osteoinductive and osteogenic. But with non-degradable PEGDA hydrogel, newly induced bone could only form shells around hydrogel cores without further remodeling. Without removing the hydrogel, it highly restricts the application of this system. To better modify this system, we developed a PEG hydrogel system that can be remodeled specifically by the process of bone resorption, which will allow the hydrogel system to be able to support and protect transduced cells and also be gradually replaced via the process of bone remodeling.

In the current study, we have described a PEGDA hydrogel system which was designed to be specifically degraded by bone resorption. By synthesizing a cathepsin K sensitive peptide GGGMGPSGPWGGK that is derived from collagen type I, we have developed a PEGDA hydrogel containing GPSG that is highly sensitive to cathepsin K *in vitro*. We also tested the GPSG hydrogel with non-specific collagenases type I and III, which showed minor degradation effects when compared to cathepsin K. At the same enzyme concentration, cathepsin K demonstrates much higher cleavage ability than non-specific collagenases within 24 hours incubation periods. No degradation was observed when incubated GPSG hydrogels with plasmin.

Additionally, we tested the sensitivity of GPSG hydrogel seeded with osteoblasts and osteoclasts. While the GPSG hydrogel has been shown to be highly sensitive to cathepsin K compared to non-specific collagenases, we want to further test if cell attachment and migration of osteoblasts and osteoclasts will cause any degradation of the GPSG hydrogel. Ideally, we expected to observe resorption pits on the hydrogel surface after seeding with osteoclasts, with only minor degradation on surfaces seeded with

osteoblasts that is caused by collagenases. We have demonstrated that our GPSG hydrogel can be degraded by osteoclasts but not osteoblasts. When examined under DIC after cells removal, surface resorption pits were only observed on the GPSG hydrogel surfaces seeded with dRAW264.7 osteoclasts, but not with dMC3T3 osteoblasts after 48 hours of incubation. Surface resorption pits were further examined by fluorescence confocol microscopy while activated osteoclasts were still attached on the hydrogel surface, which confirmed the pits were generated by resorption of osteoclasts.

With this designed property, progenitor cells recruited by rhBMP-2 proteins will start the process of bone formation around the hydrogel. Once the shell of endochondral bone forms around the GPSG hydrogels, bone resorption will start to remodel the endochondral bone shell, along with the GPSG hydrogel core by cathepsin K. Osteoblasts will then move to the void left behind by the degraded hydrogel and replace it with bone. Controlled degradation via osteoclasts will not only allow the hydrogel to be gradually integrated with the surrounding tissue, it will also prolong the survival of the encapsulated cells and rhBMP-2 production. In the mean time, with the GPSG hydrogel being gradually removed during the process of bone remodeling, it will prevent the early rupture of the hydrogel and prevent the release of transduced cells from inducing an immunoresponse.

5. Conclusions

In summary, we have successfully modified the PEG hydrogel to be bioresorbable through the process of bone resorption. We developed a PEG hydrogel system incorporated with a cathepsin K sensitive peptide sequence GPSG, which can be gradually degraded by cathepsin K secreted by osteoclasts during the process of bone resorption. In the future, this system can be further investigated *in vivo* to match the speed of bone formation and hydrogel degradation for bone graft applications.

Acknowledgments

This research was supported by Department of Defense (W81XWH-04-1-0068).

References

1. Price CT, Connolly JF, Carantzas AC, Ilyas I. Comparison of bone grafts for posterior spinal fusion in adolescent idiopathic scoliosis. Spine (Phila Pa 1976) 2003 Apr 15;28(8):793-798.
2. Goldberg VM. Selection of bone grafts for revision total hip arthroplasty. Clin Orthop Relat Res 2000 Dec(381):68-76.
3. Nishida J, Shimamura T. Methods of reconstruction for bone defect after tumor excision: a review of alternatives. Med Sci Monit 2008 Aug;14(8):RA107-113.
4. Malizos KN, Zalavras CG, Soucacos PN, Beris AE, Urbaniak JR. Free vascularized fibular grafts for reconstruction of skeletal defects. J Am Acad Orthop Surg 2004 Sep-Oct;12(5):360-369.

5. Kim DH, Rhim R, Li L, Martha J, Swaim B, Banco RJ, et al. Prospective study of iliac crest bone graft harvest site pain and morbidity. Spine J 2009 Jun 17.
6. Ebraheim NA, Elgafy H, Xu R. Bone-graft harvesting from iliac and fibular donor sites: techniques and complications. J Am Acad Orthop Surg 2001 May-Jun;9(3):210-218.
7. Khan SN, Cammisa FP, Jr., Sandhu HS, Diwan AD, Girardi FP, Lane JM. The biology of bone grafting. J Am Acad Orthop Surg 2005 Jan-Feb;13(1):77-86.
8. Sutherland AG, Raafat A, Yates P, Hutchison JD. Infection associated with the use of allograft bone from the north east Scotland Bone Bank. J Hosp Infect 1997 Mar;35(3):215-222.
9. Tomford WW. Transmission of disease through transplantation of musculoskeletal allografts. J Bone Joint Surg Am 1995 Nov;77(11):1742-1754.
10. Wheeler DL, Enneking WF. Allograft bone decreases in strength in vivo over time. Clin Orthop Relat Res 2005 Jun(435):36-42.
11. Keating JF, McQueen MM. Substitutes for autologous bone graft in orthopaedic trauma. J Bone Joint Surg Br 2001 Jan;83(1):3-8.
12. Cornell CN. Osteobiologics. Bull Hosp Jt Dis 2004;62(1-2):13-17.
13. Mulconrey DS, Bridwell KH, Flynn J, Cronen GA, Rose PS. Bone morphogenetic protein (RhBMP-2) as a substitute for iliac crest bone graft in multilevel adult spinal deformity surgery: minimum two-year evaluation of fusion. Spine 2008 Sep 15;33(20):2153-2159.
14. Bikram M, Fouletier-Dilling C, Hipp JA, Gannon F, Davis AR, Olmsted-Davis EA, et al. Endochondral bone formation from hydrogel carriers loaded with BMP2-transduced cells. Ann Biomed Eng 2007 May;35(5):796-807.
15. Hahn MS, McHale MK, Wang E, Schmedlen RH, West JL. Physiologic pulsatile flow bioreactor conditioning of poly(ethylene glycol)-based tissue engineered vascular grafts. Ann Biomed Eng 2007 Feb;35(2):190-200.
16. Hill RS, Cruise GM, Hager SR, Lamberti FV, Yu X, Garufis CL, et al. Immunoisolation of adult porcine islets for the treatment of diabetes mellitus. The use of photopolymerizable polyethylene glycol in the conformal coating of mass-isolated porcine islets. Ann N Y Acad Sci 1997 Dec 31;831:332-343.
17. Buxton AN, Zhu J, Marchant R, West JL, Yoo JU, Johnstone B. Design and characterization of poly(ethylene glycol) photopolymerizable semi-interpenetrating networks for chondrogenesis of human mesenchymal stem cells. Tissue Eng 2007 Oct;13(10):2549-2560.
18. Cruise GM, Scharp DS, Hubbell JA. Characterization of permeability and network structure of interfacially photopolymerized poly(ethylene glycol) diacrylate hydrogels. Biomaterials 1998 Jul;19(14):1287-1294.
19. Mann BK, Schmedlen RH, West JL. Tethered-TGF-beta increases extracellular matrix production of vascular smooth muscle cells. Biomaterials 2001 Mar;22(5):439-444.
20. Sawhney AS, Pathak CP, Hubbell JA. Modification of islet of langerhans surfaces with

immunoprotective poly(ethylene glycol) coatings via interfacial photopolymerization. Biotechnol Bioeng 1994 Jul;44(3):383-386.

21. Gobin AS, West JL. Cell migration through defined, synthetic ECM analogs. FASEB J 2002 May;16(7):751-753.

22. Lee SH, Miller JS, Moon JJ, West JL. Proteolytically degradable hydrogels with a fluorogenic substrate for studies of cellular proteolytic activity and migration. Biotechnol Prog 2005 Nov-Dec;21(6):1736-1741.

23. Hill PA. Bone remodelling. Br J Orthod 1998 May;25(2):101-107.

24. Vaananen HK, Zhao H, Mulari M, Halleen JM. The cell biology of osteoclast function. J Cell Sci 2000 Feb;113 (Pt 3):377-381.

25. Nosaka AY, Kanaori K, Teno N, Togame H, Inaoka T, Takai M, et al. Conformational studies on the specific cleavage site of Type I collagen (alpha-1) fragment (157-192) by cathepsins K and L by proton NMR spectroscopy. Bioorg Med Chem 1999 Feb;7(2):375-379.

26. Lecaille F, Bromme D, Lalmanach G. Biochemical properties and regulation of cathepsin K activity. Biochimie 2008 Feb;90(2):208-226.

27. Hahn MS, Taite LJ, Moon JJ, Rowland MC, Ruffino KA, West JL. Photolithographic patterning of polyethylene glycol hydrogels. Biomaterials 2006 Apr;27(12):2519-2524.

28. Collin-Osdoby P, Yu X, Zheng H, Osdoby P. RANKL-mediated osteoclast formation from murine RAW 264.7 cells. Methods Mol Med 2003;80:153-166.

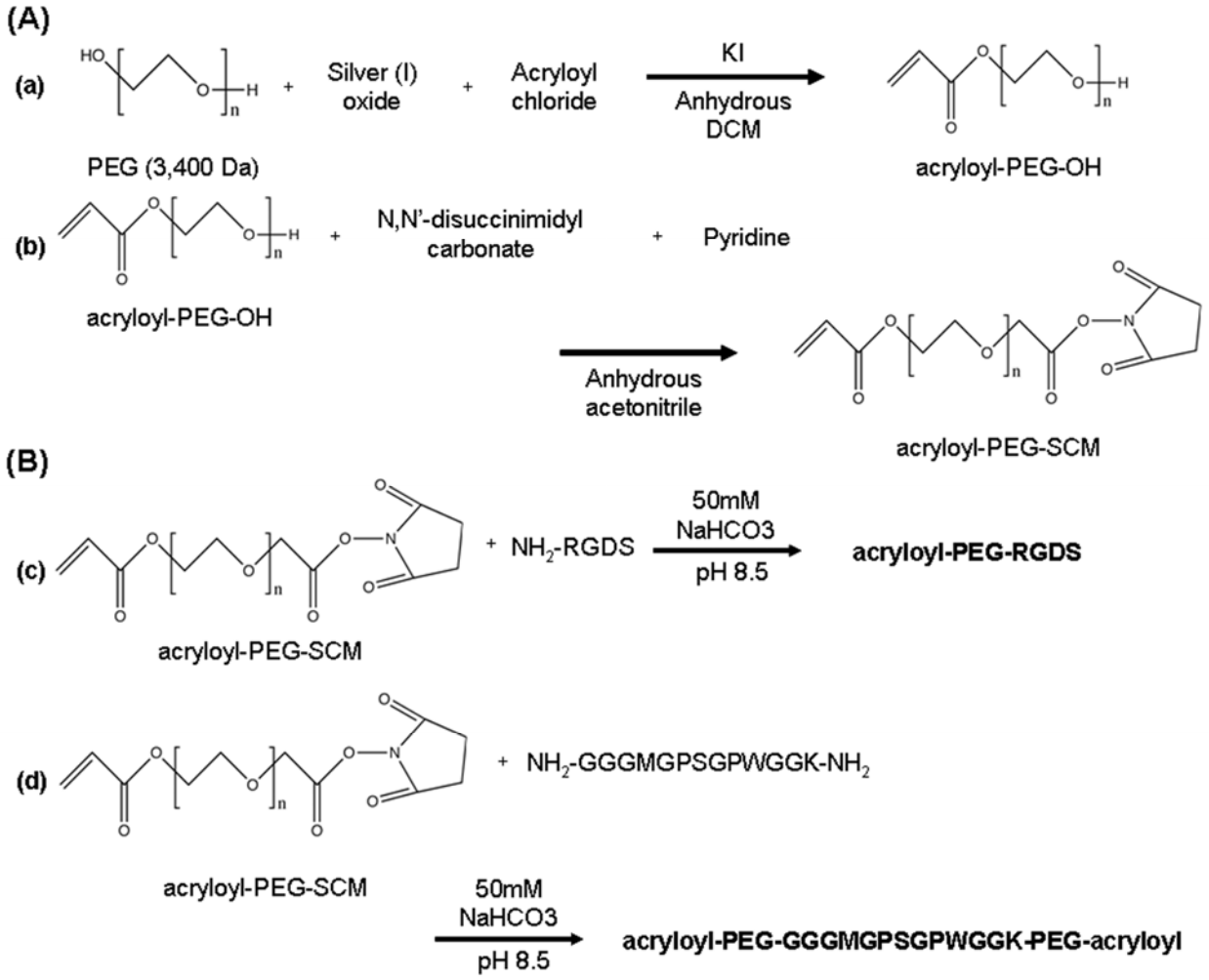

Scheme 1. (A) Synthesis of acryloyl-PEG-succinimidyl carbonate (acryloyl-PEG-SCM) and (B) modification of PEG derivatives. 3,400 Da PEG was first proceeded with (a) monoacrylation to produce acryloyl-PEG-OH. Monoacrylated PEG was then reacted with N,N'-disuccinimidyl carbonate to produce acryloyl-PEG-SCM (b). Acryloyl-PEG-SCM was then reacted with adhesive ligand RGDS to form acryloyl-PEG-RGDS (c) or reacted with cathepsin K-sensitive peptide GGGMGPSGPWGGK to form crosslinkable cathepsin K sensitive GPSG polymer (d).

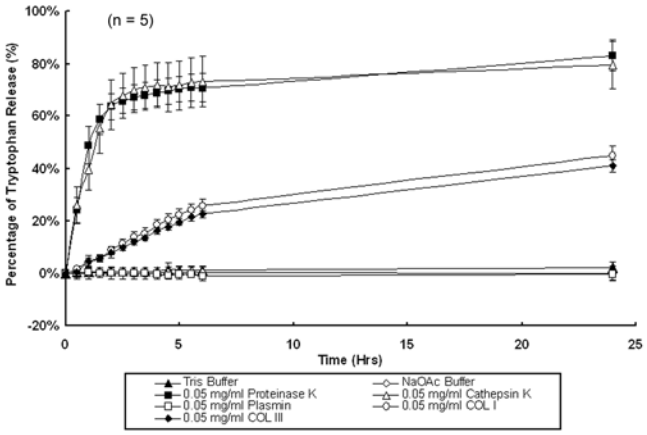

Figure 1. Degradation profiles of cathepsin K-sensitive GPSG hydrogels. Hydrogel droplets (3 μl) were polymerized in each micro-cuvette and swelled overnight with 250 μl of TBS buffer. Each hydrogel was incubated in buffer or enzyme solution at 0.05 mg/ml at 37^{O}C. UV absorbance at 280 nm was measured over 24 hours to monitor tryptophan release corresponding to the degradation of the GPSP hydrogels.

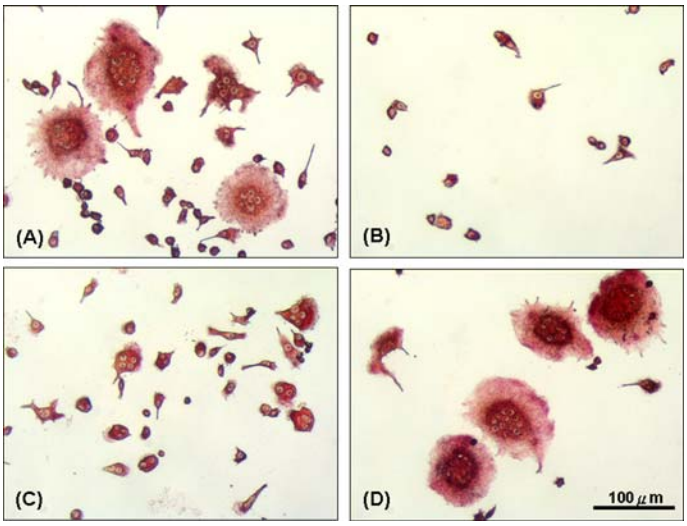

Figure 2. Isolated TRAP-positive dRAW264.7 osteoclasts by serum gradient. After differentiation in medium containing 30 ng/ml RANKL for 4 days, dRAW264.7 cells were combined with mono- and multi-nuclear cells (Figure 2A). After separation by serum gradient, the top fraction contained most of the mononuclear cells. The middle fraction of the gradient contained mixed groups of mononuclear and multinuclear cells. The majority of cells at the bottom fraction were multinuclear cells, which contained a very small portion of mononuclear cells (Figure 2B to D). The multinuclear cells collected at the bottom fraction were also stained TRAP positive, which indicted that they were activated osteoclasts. The bottom fraction of TRAP+ dRAW 264.7 osteoclasts were then used for hydrogel degradation studies.

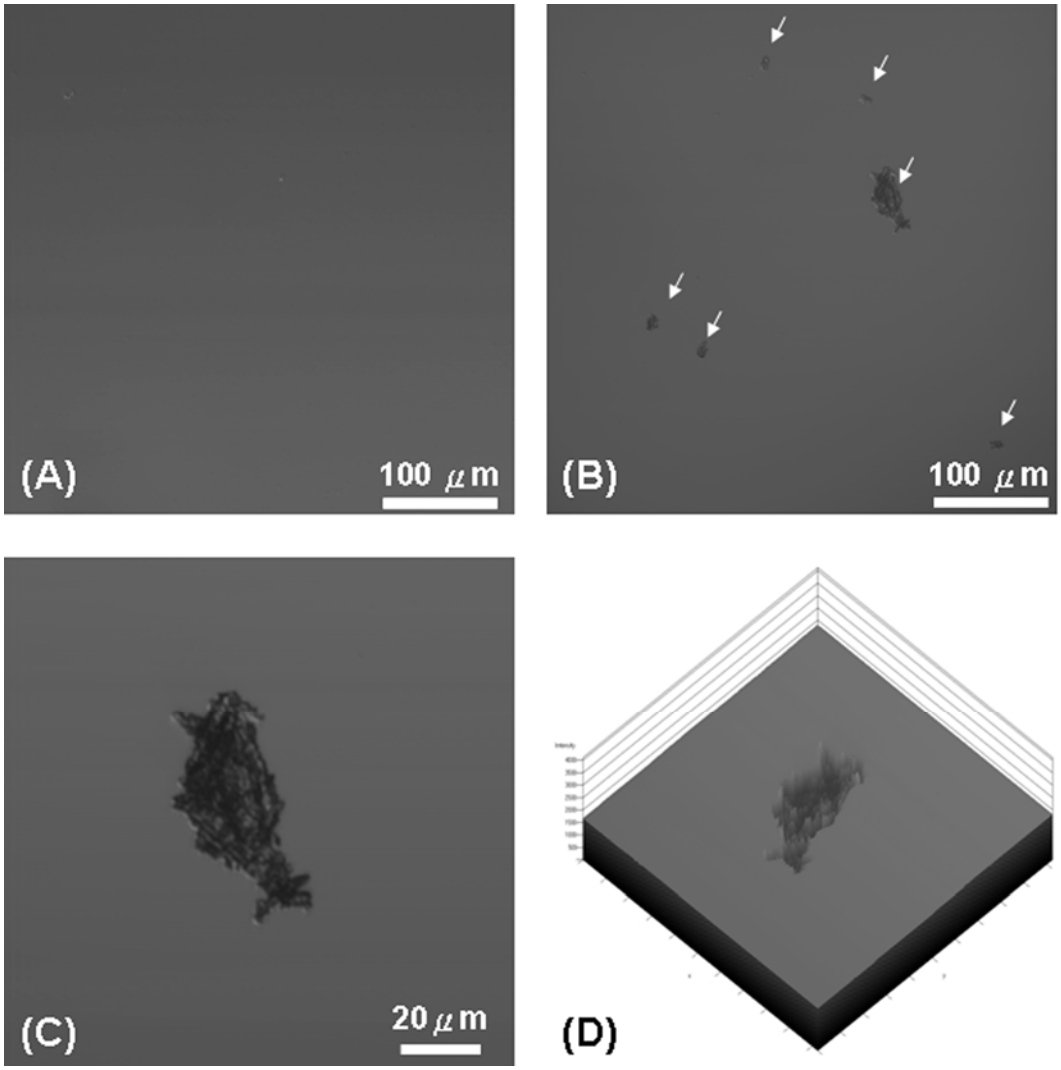

Figure 3. Differential interference contrast (DIC) images of GPSG hydrogel surfaces seeded with (A) dMC3T3-E1 osteoblasts and (B) dRAW264.7 osteoclasts. Cells were seeded on the hydrogels and cultured for 48 hours. Cells were detached with 20 mM EDTA and DIC images were obtained on a LSM LIVE 5 confocal microscope. No features were observed on gel surfaces seeded with osteoblasts (A). On the gel surface seeded with osteoclasts (B), several features can be identified after cells were detached. (C) and (D) show an enlarged image and an intensity profile of the feature, which suggests that the features on the surface were depressions.

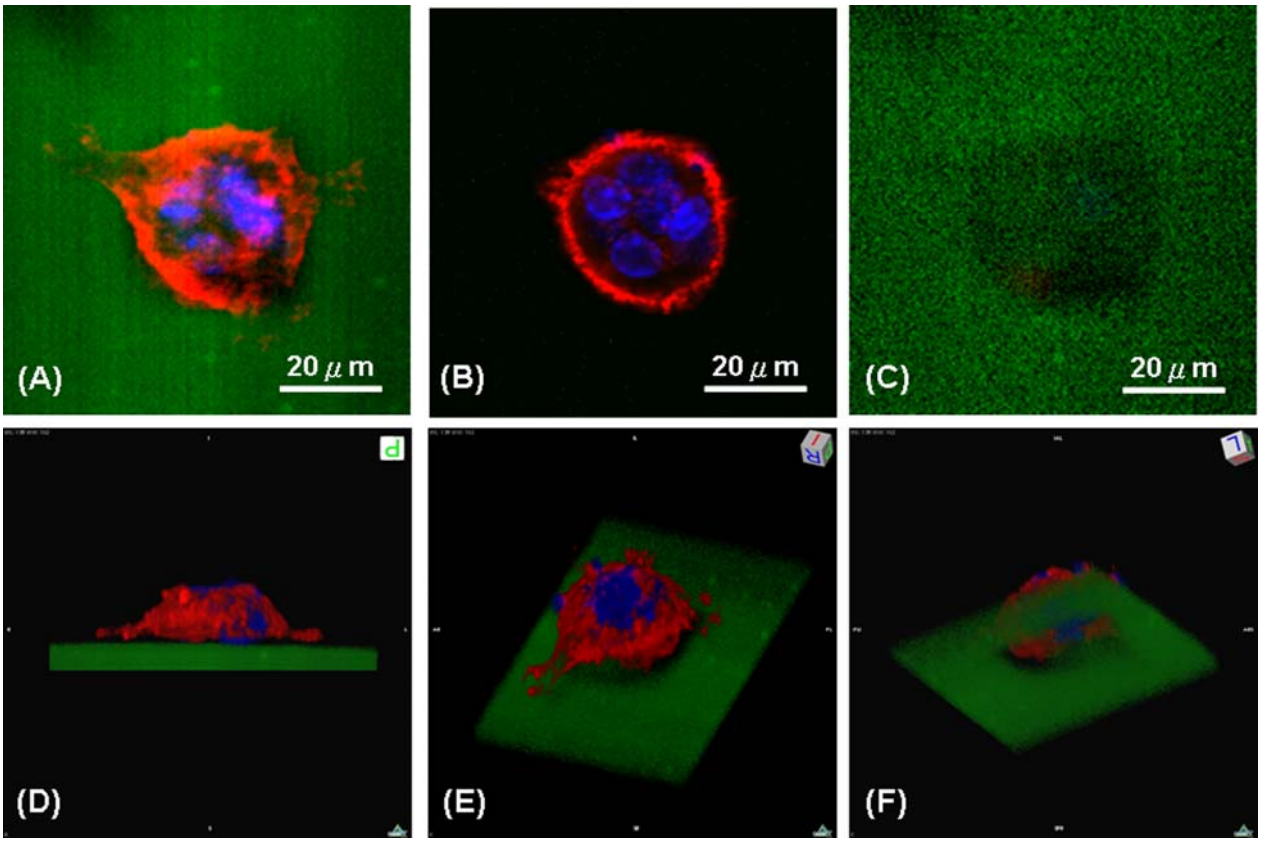

Figure 4. Three-dimensional fluorescent image reconstruction of an active osteoclast on the GPSG hydrogel surface. The GPSG hydrogel was labeled with Alexafluor 680 fluorophore (green), which is conjugated with the acryloyl-PEG-RGDS and incorporated into the hydrogel by photo-polymerization. The cells were fixed and permeabilized before staining the nuclei with DAPI (blue) and F-actin by rhodamine phalloidin (red) 48 hours after seeding. (A) Composed z-stack images of the osteoclast and hydrogel. (B) Sealing ring and multiple nuclei of the osteoclast. (C) GPSG hydrogel with fluorescent signal lost at middle. Z-stack Images were reconstructed using the volume renderings algorithm and presented from (D) side view, (E) orthogonal view from above, and (F) from bottom. The resorption site is located underneath the osteoclast, which was can be observed in the loss of the fluorescent intensity of Alexafluor 680. The resorption pit on the hydrogel surface can be clearly seen from different angles, suggesting that the GPSG hydrogel has been degraded by cathepsin K secreted by osteoclasts.

Assessing Mechanical Integrity of Spinal Fusion by in situ Endochondral Osteoinduction in the Murine Model

Ashvin K Dewan, Rahul A Dewan, Nathan Calderon, Angie Fuentes, Zawaunyka Lazard, Alan Davis, Michael Heggeness, John Hipp and Elizabeth Davis

Abstract

Historically, radiographs, micro-computed tomography (micro-CT) exams, palpation and histology have been used to assess fusions in a mouse spine. The objective of this study was to develop a faster, cheaper, reproducible test to directly quantify the mechanical integrity of spinal fusions in mice. Fusions were induced in ten mice using a previously described technique of in situ endochondral ossification, harvested with soft tissue, and cast in radiolucent alginate material for handling. Using a validated software package and a customized mechanical apparatus that flexed and extended the spinal column 150 degrees, the amount of intervertebral motion between adjacent vertebral discs was determined with static flexed and extended lateral spine radiographs. Micro-CT images of the same were also blindly reviewed for fusion. Mean intervertebral motion between control, non-fused, spinal vertebral discs was 6.1±0.2° during spine flexion/extension. In fusion samples, adjacent vertebrae with less than 3.5° intervertebral motion had fusions documented by micro-CT inspection. Measuring the amount of intervertebral rotation between vertebrae during spine flexion/extension is a relatively simple, cheap (<$100), and fast test for assessing the mechanical success of spinal fusion in mice that compared favorably to the standard, micro-CT.

Introduction

Spinal fusion is a common surgical procedure used to manage a variety of disorders. In 2001, over 50% of all inpatient lumbar spine operations, other than those for herniated discs, included a fusion procedure [1]. In 2001, $4.8 billion was spent on spine fusion surgery [1]. In 1992, lumbar fusion accounted for 14% of spending, but by 2003, fusion accounted for almost half of total spending on spine surgery [2].

Currently, the gold standard for spinal fusion involves a bone autograft from the pelvis [3]. This technique has several limitations. Donor site complications and morbidity have been estimated at 8% to 25% [4-7]. Donor site complications include pain, nerve and arterial injury, peritoneal perforation, sacroiliac joint instability, and herniation of abdominal contents through defects in the ilium [8]. Furthermore, the volume of bone extracted from the donor is often insufficient [7, 9] and pseudoarthrosis is a common result [10]. Given these shortcomings, recent research has focused on finding effective bone graft substitutes, such as bone morphogenic protein (BMP) based osteoinduction.

The feasibility of new technologies is commonly tested in small animal models first. The number of posterolateral fusion studies involving BMP osteodinduction in

rodents has exploded in the last decade [11-26]. Research to assess the effectiveness of these new technologies for promoting fusion is compromised however by the lack of a rapid, economical, validated test to determine if the treatment was successful. The recent validation of the rodent as a mechanical model of the human vertebral disc opens the door to new mechanical tests of the rodent spine that can be used to test efficacy, in addition to feasibility, of emerging spinal fusion strategies [27].

Historically, radiographs, micro-computed tomography (micro-CT) exams, palpation and histology have been used to assess fusions in a mouse spine. High-resolution micro-CT can reliably determine if a mechanical bridge has formed, but this is expensive, time consuming, and only reliable if the exam is very carefully assessed, since a fusion mass can get very close to a bone but remain separated by a thin layer of soft-tissue (Figure 1). The objective of this study is to develop a rapid and reproducible test to directly quantify the mechanical integrity of spinal fusions in mice. A validated test for fusion efficacy in the mouse spine would be used in many future studies of new biologic fusion technologies.

Figure 1: Spine micro-ct image examples with heterotopic bone formation

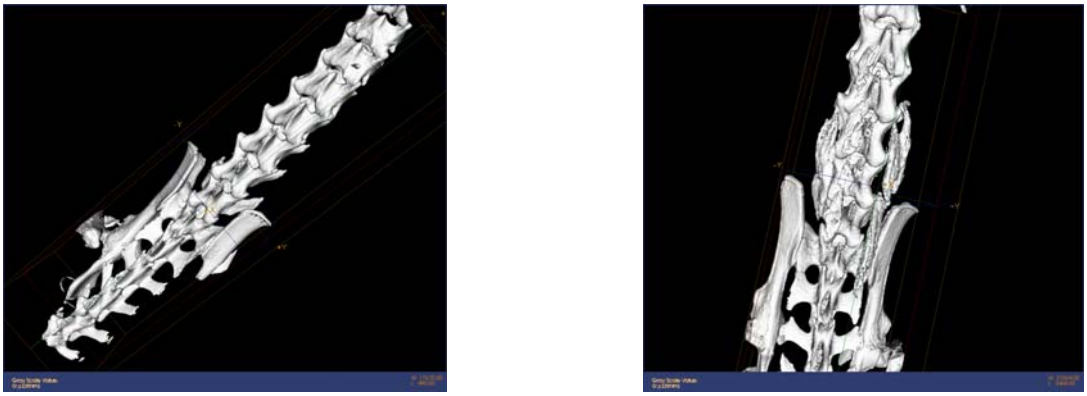

Materials and Methods

Cell Culture

Human diploid fetal lung fibroblasts (MRC-5) obtained from American Type Culture Collection (ATCC; Manassas, VA) were transduced with adenovirus encoding BMP-2 as described by Fouletier-Dilling, et al [28]. A control set was also prepared using the same cell line transduced with adenovirus without BMP-2 encoded. For implantation, the control and experimental cells were isolated from the growth medium and re-suspended at 5.6 x 10^6 cells/ml in saline medium.

Implantation

Male and female NOD/SCID mice (8-12 weeks old; Charles River Laoratories;

Wilmington, MA) were placed separately at five per cage and fed with an ad libitum diet and tap water in a 12 h day/night cycle according to our Institutional Animal Care and Use Committee protocols until ready for surgery. The backs of the mice were shaved and cleansed with alcohol. The senior spinal surgeon listed injected 500ul of the appropriate cell suspension prepared as described above unilaterally adjacent to the spinous process of the L4-L5 vertebrae in mice in the body of the paraspinous muscles in a 1cm track within the muscle body. Sutures were placed superior and inferior to mark the injection site. The animals were then returned to their respective cage for the remainder of the study.

A total of twenty animals were used for this experiment. Ten mice, 5 female and 5 male, received injections of the experimental cell suspension that produced encoded BMP protein. Ten mice, 5 female and 5 male, received an injection of the control culture that did not encode BMP protein. The mice were euthanized at 6 weeks.

Mechanical Testing

Following euthanasia, spines were harvested from the first lumbar to the first sacral vertebrae with all surrounding musculature and pelvis intact. The harvested spines were fixed and stored in formaldehyde until ready for testing. For mechanical testing spines were first cast in the center of a 2 x 1 x 4 cm block of dental Alginate impression material (Henry Schein, INC., Melville, NY). Next, spines were imaged on high resolution Xray in flexion, neutral, and extension using the custom crafted flexion and extension cells described below. The images were then analyzed using computer-assisted methods on Quantitative Motion Analysis (Medical Metrics, Houston, TX) that has been previously validated [29] and used to assess the mechanical integrity of spinal fusions in human patients. The computer-assisted analysis quantified the amount of intervertebral motion within $\pm 0.1^{o}$ that occurred in flexion and extension. Following the mechanical testing, the spine was imaged at 14 micron resolution using the micro-CT system. From the micro-CT data, three dimensional reconstructions of the vertebrae and any mineralized tissue were made (eXplore MicroView, v. 2.0, GE Healthcare, London, Ontario). A surgeon blindly reviewed the mouse spine CTs for fusions. Accuracy of spine fusion identification by CT was compared to the mechanical testing of the same spines.

Testing Apparatus

Three devices were constructed out of radiolucent polyethylene for flexing and extending the mice spines suspended in alginate at 60º, 110º, or 150º (see diagram below). Three 2 x 10 x 20 cm pieces were cut from polyethylene. Using a hack saw and electric sander arcs of 60º, 110º, or 150º were cut into the pieces. The arc cuts were made perpendicular to the 10 x 20 cm faces, 10 cm from the top of the long dimension

at the edge. A 10 x 23 cm frame to support the plastic pieces was constructed using 2 x 2 cm aluminum L brackets, with the L facing inwards along the longer dimension. Corners of the frame were fastened using separate 1 x 2 x 2 cm L brackets and bolts with nuts. The plastics pieces with the arcs cut into it were next secured to the frame using zip ties. Two 3 cm screws were placed through the frame and polyethylene 2 cm from the bottom edge of the frame to prevent the plastic from sliding out. Two springs 3.75 cm uncompressed length with spring constant __ were centered on the heads of the two screws supporting the corner L brackets such that an axial force was directed parallel to the long dimension of the plastic pieces.

Figure 2 : Custom designed apparatus for flexing/extending explanted spine

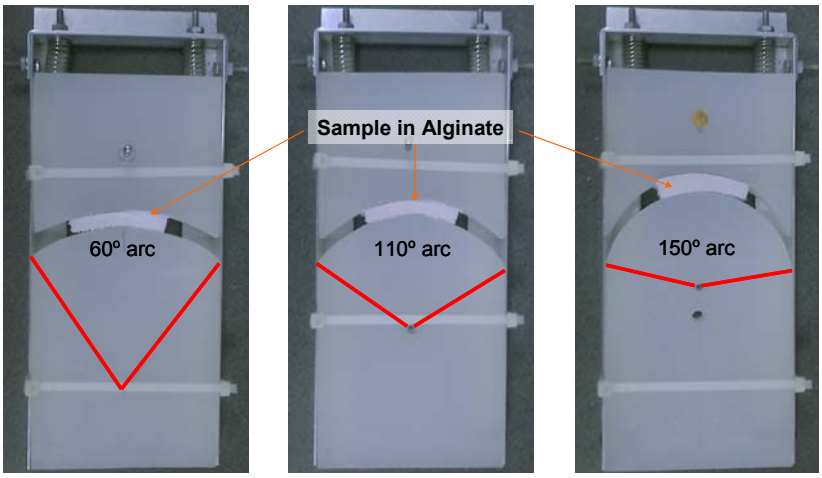

Palpation

Integrity of the fusions was qualitatively confirmed after removal of soft tissues with bleach and manual palpation. Sample spines were immersed in 90 cc bleach. After 45 minutes, 6lb fishing line was threaded through the spinal canal of the sample. Samples were then placed into a tray and covered before submerging in bleach again for 2 more hours. Bleach was replaced hourly. Samples with soft tissue remaining on the bones were submerged and monitored for additional 10 minute intervals until bone was completely cleaned. Bones were then photographed using a high resolution camera. Linking of adjacent vertebrae by fusion was documented when present.

Results

All mice tolerated surgery without any complications. Biomechanical characterization of untreated control spines was performed first to determine optimal spinal flexion/extension conditions for testing fusion integrity. Maximal intervertebral motion of untreated spines was observed at 150°of spinal flexion/extension. Intervertebral disc angle change of untreated mice followed normal distributions centered at means of 3.9±0.4°, 5.0±0.2°, and 6.1±0.2° per level for 60°, 110°, and 150°

of spinal flexion/extension respectively (Figure 3). The greatest variability in intervertebral motion was observed between the proximal lumbar discs of the harvested spine. In addition, mean intervertebral motion between distal lumbar vertebrae levels was slightly greater than mean intervertebral motion at proximal lumbar vertebrae levels (Figure 4), but not significant. Given the small magnitude of intervertebral motion observed at 60° flexion/extension of the untreated spines, subsequent fusion sample testing was conducted successively at only 110° and then 150° for maximal intervertebral disc angle change detection.

Injections of cells producing BMP-2 in the posterior paraspinal muscles resulted in situ endochondral ossification adjacent to vertebrae. Mineralized tissue of varying degrees was present by radiographic examination in all treatment animals at 6 weeks postoperatively. Distinguishing between bridged transverse processes and unbridged mineralized tissue was difficult with anterior-posterior and lateral radiographs. Untreated control animals did not demonstrate any osteoinduction by radiographic examination.

Microcomputed Tomography inspection of explanted spines exposed to BMP-2 was performed taking an average 5 hours/spine (including preparation, scanning, and examination). After 6 weeks of treatment, posterolateral osteoinduction bridging transverse processes of adjacent lumbar vertebral levels were observed in 9/10 treated spines. Fusion occurred at greater than two adjacent vertebrae for 5 of these spines. One such spine had 5 successive lumbar vertebrae, L1-L5, fused. The only spine that did not produce any fusion by micro-CT had a small amount of bone formation localized in the paraspinal muscle.

Biomechanical characterization of treated spines was performed at 110° and then 150° spinal flexion/extension. The intervertebral motion between lumbar discs neighboring the mineralized tissue masses decreased. A compensatory increase in intervertebral motion between lumbar discs away from the mineralized tissue was observed at both 110° and 150° testing. Two separate peaks of intervertebral disc angle change representing the linked and unlinked vertebrae from the pool of all the treated vertebrae were observed at both testing conditions (Figure 5). Mechanical data of fusions were correlated with CT findings next. Restriction of intervertebral motion by mineralized tissue neighboring the spine was variable. All adjacent vertebrae with less than 3.5 degrees of intervertebral disc angle change however had fusions documented by CT inspection.

Soft tissue envelopes of explanted spines were successfully dissolved using bleach. Segments of fused vertebrae in treated spines were palpated to confirm mechanical integrity. After 6 weeks of exposure to BMP-2, all 10 spines grossly exhibited linked vertebrae. Furthermore, 8 of these spines had greater than 2 adjacent linked vertebrae, with one spine exhibiting fusion from L1-L5 after bleach dissolution.

Levels coded as fused by palpation after BMP-2 exposure showed significantly decreased ($p<0.05$) intervertebral motion at 110° and 150° testing (2.4±0.3° and 4.2±0.4° respectively) compared to controls (Figure 7). Levels coded as fused by micro-CT after BMP-2 exposure also showed a significant decrease in intervertebral motion at 110° and 150° testing (3.1±0.3° and 3.5±0.4° respectively) compared to controls. Fusions identified by micro-CT however were relatively more stable compared to the fusions found by palpation. The lower rate of false positive fusions by the micro-CT relative to the palpation group might explain the decreased intervertebral motion observed. For both methods of identification, the percentage of intervertebral motion decrease from fusion was greater at 110° testing compared to 150° testing.

Conclusions

Measuring the amount of intervertebral rotation between vertebrae that occurs during flexion and extension is a relatively simple, cheap (<$100), and fast test for assessing the mechanical success of spinal fusion in mice. Existing methods of spinal fusion assessment such as micro-computed tomography (micro-CT) are time-consuming and cost prohibitive. Quantitative analysis of intervertebral rotation between flexion and extension can be used to reliably determine if adjacent vertebrae are fused, with all fused levels having under 3.5 degrees of intervertebral rotation. Given the emergence of new technologies for spinal arthrodesis developed in the rodent model, a method for quantifying spinal fusion integrity is important.

This is the first study to characterize the rodent spine in flexion-extension testing. Incorporating the same methodology used in human spine testing, we were able to assess spinal fusion in the rodent model. In humans, quality of spinal fusions is typically assessed through dynamic and static imaging studies [10, 29]. After performing spinal fusion, surgeons take radiographs of a patient's spine in flexion and extension. Based on the limitations in motion observed between two vertebrae after fusion, a surgeon can assess the quality of the fusion. Lately, software has become available that quantifies the degree of intervertebral motion between vertebral discs [29]. Using the same software and a simple, custom-designed, apparatus (Figure 2) to flex and extend the explanted rodent spines for radiographs, we were able to reliably measure interverteral motion in the rodent lumbar spine. Untreated lumbar mice spines behaved very similar to untreated human and rabbit lumbar spine described in literature [29, 30]. Mean intevertebral motion at L3-L5 of 5.7° reported during flexion and extension of the human spine is very similar to the mean intervertebral motion o f 6.1° demonstrated in flexion and extension of the mouse spine here [29]. Consistent with trends demonstrated in human and rabbit lumbar vertebrae, higher rodent lumbar levels also showed slightly less intervertebral motion compared to the lower lumber levels [31].

Defining normal intervertebral motion enabled us to objectively assess the fused rodent spines. The cut-off correlated with fusion by micro CT was within the 2°-4° range of cut-off reported for fusion in the literature [32, 33]. Characterization of fusion products revealed a great deal of variability in the quality of fusions, not detected by the existing fusion detection techniques. The induction of bone at a heterotopic site in the mouse did not necessarily imply the induction of directed formation of bone essential for spinal arthrodesis [10]. Often heterotopic bone bridging transverse processes of the vertebrae were not capable of restricting intervertebral motion during spinal flexion/extension. Grauer et al similarly identified differences in fusion quality not detected by palpation in flexion-extension testing of a rabbit model [30]. Furthermore, without a carrier, the location of the bony fusion mass induced was not precise. In cadavers Bono et al demonstrated that bridging at the intertranverse process was less mechanically stable than bridging at the interspinous processes [32]. The variability in fused domains can account for the variability in intervertebral motion observed. The success rates of fusion induced by BMP-2 determined by micro-CT and/or palpation reported in literature are 95-100% [11, 12, 14, 17-19, 21, 22, 24] and consistent with our findings.

A few authors have attempted to devise other quantitative biomechanical tests for assessing the integrity of spinal fusions in small animal models. Most of these published tests however require sophisticated equipment. In rabbits, uniaxial tensile mechanical testing of fusions has been performed [34]. The smaller scale of rodent model fusions however makes this technique prohibitive and tedious. Grauer et al developed a flexibility test for intervertebral motion in the rabbit [31]. Another group has compared displacement of fused rat spine in the sagittal plane with the application of a 3N force [13]. Generalizing the observations of these ex vivo tests to the clinical setting however can be trickier given that the same approaches are not used in the human.

Currently the most common methods for fusion assessment in the rodent model include histology, palpation, microcomputed tomography, and radiography. All of these techniques are qualitative with noteworthy limitations. Histology is accurate at evaluating bone formation and quality, but it is easy to miss bridging bone in out of plane sections when looking for fusions [16, 25]. Moreover static images of individual sections do not reveal how the newly mineralized tissue functions during physiologic motion of the spine. Palpation of interlocked segments is used to classify motion segments as fused or not fused. Although relative determinations of fusion strength can be made, this admittedly subjective technique [26] suffers from significant interobserver variation and unclear relevance to the clinical setting. Nonetheless, there are authors that believe palpation is the most sensitive and specific method of assessing spinal fusion [18, 25, 30]. Others consider micro-CT to be the gold standard for fusion determination [16]. On micro-CT bony bridging between adjacent transverse processes is considered fusion. CT is time consuming (5 hours/sample in this study) and

expensive. Moreover, determining the significance in the variability of fusions observed can be challenging. Consequently, some consider the combination of micro-CT and histology to be optimal [16]. Finally some studies use radiographic evidence of bony tissue along the margin of the spine to assess fusion. This is perhaps the most misleading however since adjacent and integrated mineralized tissue cannot be readily distinguished leading to overestimation of fusion [16]. There is no consensus about which technique is best for assessing fusion given each technologies limitations.

To date, rodents and other small animals such as rabbits have primarily been used to study the feasibility of bone graft substitutes [10]. The recent validation of the rodent as a mechanical model of the human vertebral disc however opens the door to new mechanical tests of the rodent spine that can be used to test efficacy, in addition to feasibility, of emerging spinal fusion strategies [27]. With the explosion in the number of studies using the rodent model for posterolateral fusion in the last few years [11-26], the development of a rapid, reproducible, biomechanical test for fusion assessment in rodents, such as the one described here, is essential.

Acknowledgements

Supported in part by an Alpha Omega Alpha Carolyn L. Kuckein Student Research Fellowship